NASA TECHNICAL NOTE

NASA TN D-2547

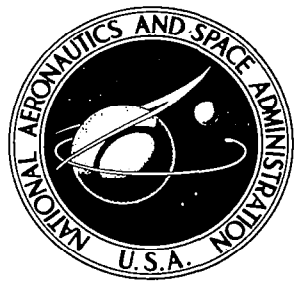

NASA TN D-2547

ENERGY TRANSFER FROM A LIQUID TO GAS BUBBLES FORMING AT A SUBMERGED ORIFICE

by M. R. L'Ecuyer and S. N. B. Murthy

Prepared under Grant No. NsG-140-61 *by*
PURDUE UNIVERSITY
Lafayette, Ind.
for

NATIONAL AERONAUTICS AND SPACE ADMINISTRATION • WASHINGTON, D. C. • JANUARY 1965

NASA TN D-2547

ENERGY TRANSFER FROM A LIQUID TO GAS BUBBLES FORMING AT A SUBMERGED ORIFICE

By M. R. L'Ecuyer and S. N. B. Murthy

Prepared under Grant No. NsG-140-61 by
Jet Propulsion Center
PURDUE UNIVERSITY
Lafayette, Indiana

for

NATIONAL AERONAUTICS AND SPACE ADMINISTRATION

For sale by the Office of Technical Services, Department of Commerce,
Washington, D.C. 20230 -- Price $5.00

ACKNOWLEDGMENTS

The authors are indebted to Professor M.J. Zucrow, Atkins Professor of Engineering, for his advice and counsel during the course of the investigation.

Special appreciation is also rendered to Professor C.F. Warner for his guidance in the initial phases of the research.

The subject investigation was sponsored by the National Aeronautics and Space Administration under Contract NsG-140-61.

TABLE OF CONTENTS

LIST OF TABLES

LIST OF FIGURES

ENERGY TRANSFER FROM A LIQUID TO GAS BUBBLES FORMING AT A SUBMERGED ORIFICE

By

M.R. L'Ecuyer and S.N.B. Murthy

ABSTRACT

An experimental and analytical investigation was conducted for determining the rate of energy transfer from a relatively hot liquid to a relatively cool gas injected into the liquid through a submerged orifice, resulting in the periodic formation of discrete gas bubbles at the orifice. A preliminary investigation indicated that a significant amount of energy transfer occurs during the time of formation of the bubbles. Consequently, the investigation reported herein is concerned with the determination of the energy transfer from the liquid to the gas bubbles during the period of formation of the bubbles at the orifice.

Experiments were conducted with dry nitrogen gas injected into distilled water and ethyl alcohol. The dry nitrogen gas was injected through single orifices having diameters of 0.159 and 0.079 cm, with dry nitrogen mass flow rates ranging from 2.25×10^{-3} to 12.7×10^{-3} gm/sec. The overall temperature difference between the liquid and the injected gas, which was produced by precooling the gas, was approximately 15°C. The change in temperature of the injected gas during the period of bubble formation was observed to be 55 to 90 per cent of the overall temperature difference.

Experimental measurements were employed to determine an average convective heat transfer coefficient for the bubble formation period based on a time integrated average surface area of the bubble and a log mean temperature difference. The heat transfer coefficient ranged from 2.4×10^{-3} to 5.3×10^{-3} cal/sec-cm^2-C. The rate of energy transfer to the bubble was found to be significantly influenced by the circulation of the gas within the bubble.

The effects of energy transfer upon the process of bubble formation at an orifice were also assessed by a comparison of the bubble formation characteristics in the presence of energy transfer with those in the absence of energy transfer.

In conjunction with the experimental investigation, a theoretical analysis was made of the formation process of a gas bubble assuming the bubble to be spherical in shape with complete mixing of the gas therein. The rate of growth of the bubble, the mean temperature, the mean pressure, and the volume

of the gas in the bubble were determined as a function of time during bubble formation. The analysis provided a means for predicting the effect of energy transfer upon the rate of growth of a bubble and for predicting the increase in the temperature of the gas in the bubble during formation, thereby providing a confirmation of the validity of the experimentally determined average heat transfer coefficient.

1. INTRODUCTION

A simple method of obtaining energy or mass exchange between two fluids is by the direct contact of the fluids by passing one of the fluids through the other. In particular, the transfer of energy from a hot liquid to a cool gas immiscible with the liquid can be accomplished by injecting the gas, through a submerged orifice, into the liquid. The natural disintegration of the injected gas stream into discrete gas bubbles enhances the process of energy transfer by producing a large surface area to volume ratio for the discrete phase. Such a process essentially becomes one of energy transfer from a hot liquid to the cool gas in the bubbles.

The energy transfer from a liquid to the gas in the bubbles may be considered as occurring during two distinct stages: (a) the energy transfer from the liquid to the gas during the period of formation of the bubbles at a submerged orifice and (b) the energy transfer from the liquid to the gas in the bubbles during the passage of the bubbles through the depth of the liquid. In addition to the fact that the first of those components, namely the energy transfer during the formation of a bubble, may be quite significant in magnitude, the actual mechanics of the heat transfer processes in the two stages differ significantly from each other.

The research reported herein is concerned with an experimental and analytical investigation[1] of the energy transfer to a gas bubble from the liquid surrounding it during the period of formation of the bubble at a submerged orifice. The experimental part of the investigation has in addition afforded an insight into the dynamics of gas and liquid motion during the formation period of the bubble.

The bubbling process has been employed frequently as an efficient means of energy transfer, as for example in the commercial production of ethylene by means of light hydrocarbon

[1] L'Ecuyer, M.R., "An Investigation of the Energy Transfer from a Liquid to a Gas Bubbling Through the Liquid," Ph.D. Thesis, August 1964, Purdue University.

pyrolysis (1).[1] It has also been suggested by Rom (2) that the bubbling process may be utilized for the heating of a rocket propellant gas by means of a molten core nuclear reactor. Such interest in the bubbling process as a means for direct energy transfer is one of the reasons which prompted the investigation discussed herein.

1.1 Review of the Literature

The study of the formation of gas bubbles in liquids by gas injection has been an important area for research in the broad field of intersurface phenomena because of the significance of the possible application of that process for the transfer of energy and mass between two fluids. Most of the investigations reported in the literature have been concerned with the fluid dynamic processes associated with the formation of gas bubbles, rather than with the phenomena involved in the transport of energy or mass between a liquid and the gas during the period of formation of the bubble.

In addition to the literature pertaining to the fluid dynamic aspects of the process of bubble formation, there is considerable information in the literature concerning the fluid flow associated with the steady translation of gas bubbles through liquids. Although such information is of particular importance in assessing the energy or mass transfer occurring during that stage of the bubbling process, it has little relevance to the unsteady process of bubble formation. Chao (3) has presented recently a summary of the significant theoretical developments in that area as well as a rigorous analytical treatment of the fluid flow both within and surrounding a spherical bubble translating through a continuous liquid. That aspect of the subject is not discussed herein.

The literature concerning the basic process of bubble formation, as related to energy or mass transfer applications, may be divided for convenience, into the following:

1. Literature pertaining to the fluid dynamic processes involved in the formation of a bubble.
2. Literature pertaining to to the transfer of energy or mass across an interface during bubble formation.

These are discussed separately in the following.

1.1.1 Fluid Dynamics of Bubble Formation

In any practical application of the bubbling process, it is, of course, of primary importance to have a knowledge of the size of the bubbles which are formed and which subsequently pass through

[1] Numbers in parentheses refer to references in the Bibliography.

the continuous liquid phase. Consequently, most of the investigations have been conducted with the emphasis primarily upon determining the terminal volume of the bubbles produced for specified conditions of gas injection.

When a gas issues from an orifice into a liquid there results, under certain conditions to be described presently, the formation of discrete gas bubbles at the orifice. The motion of the gas-liquid interface during the formation of a bubble can, in general, be considered to be governed by the fluid dynamic and interfacial forces due to

1. Momentum of the injected gas stream
2. Inertia of the displaced liquid
3. Drag on the interface associated with motion of the liquid relative to the bubble
4. Buoyancy
5. Interfacial tension

The system variables such as the gas injection rate, the liquid and gas physical properties, the liquid depth, the orifice size and shape, and the local acceleration due to gravitational action, which have been observed to influence the bubble formation process, derive their importance from their influence upon the aforementioned forces governing the motion of the interface. Because of the inherent instability (4) of the interface that is generated during the gas injection, the gas flow is periodically interrupted by the termination of the formation of one bubble, followed by the initiation of the formation of the succeeding bubble. It has been found (5,6) that the pulsating character of the flow imposed by the periodic formation of discrete bubbles produces an interaction or coupling of the bubble formation mechanism with the flow of gas. Thus, in addition to the variables directly associated with the forces governing the motion of the interface during the formation of a bubble, it has been found (5) that the fluid dynamic characteristics of the entire gas supply system up to the exit plane of the orifice can also have a significant influence upon the process of bubble formation. Such parameters include the L/D ratio of the orifice channel and the volume of the ante-chamber[1] supplying gas to the orifice.

An accurate evaluation of the dynamic forces acting at the interface, of course, requires an adequate knowledge of the flow of gas into the bubble. Unfortunately, the aforementioned coupling and the incomplete understanding of the interfacial phenomena involved have caused considerable difficulty in accurately defining the flow into a bubble for a given system. However, an

[1] The ante-chamber volume, though frequently not well defined, has been taken as the volume of the gas supply system from the orifice to the point where a large pressure drop occurs in the system and beyond which small pressure fluctuations (induced by bubble formation) are not transmitted.

attempt may be made to discuss the basic process of bubble formation in relation to the following.

1. Types of gas flow into the bubble
2. Effect of the gas flow rate on the formation mechanism
3. Effect of the physical properties of the liquid
4. Effect of the properties of the gas
5. Effect of motion of the liquid relative to the bubble
6. Effect of liquid depth
7. Effect of orifice size and shape

Types of Gas Flow. There are, in general, two types of flow during formation into a bubble, which may be reasonably well defined. One case, commonly referred to as the "constant gas flow rate" case, pertains, as the name implies, to bubble formation in which the rate of gas flow into a bubble is essentially constant. Such has been found (7) to be the case, for example, for bubble formation at the tip of a long capillary tube. The flow rate of gas is governed by the pressure drop in the capillary and, perhaps, some controlling device upstream of the capillary. Nevertheless, the pressure fluctuations at the tip (or orifice) of the capillary which result from bubble formation are not transmitted upstream. The flow is essentially independent of the bubble formation process and, as such, there is no coupling.

The other limiting case of flow, referred to as the "constant pressure supply" case, pertains to bubble formation at an orifice which is supplied with gas from an ante-chamber at constant pressure. That case is approximated, in practice when an orifice is supplied with gas by a very large ante-chamber. The rate of gas flow into a bubble for such a system has been found to vary throughout the formation period (7), apparently as the result of a variation of the pressure drop across the orifice. Such a system, though not entirely free from a coupling of the bubble formation and the flow, can be considered to be one for which the flow is practically independent of the ante-chamber volume. However, there still remains some uncertainty in determining both the pressure drop and the flow coefficient for such an orifice during the bubble formation period.

Any actual bubble formation system will probably operate under conditions in between the aforementioned limiting cases of flow and, therefore, will exhibit, to some extent, a coupling of the bubble formation mechanism with the gas supply system as well as a possible dependence of the process of bubble formation upon (a) the volume of the ante-chamber and (b) the L/D ratio of the orifice channel. A twofold increase in the ante-chamber volume, for a given mean gas flow rate, has been observed (8), for instance, to cause an increase in the terminal volume of the bubbles formed by as much as 50 percent, though

the effects were less pronounced the higher the mean gas flow rate. Unfortunately, a quantitative comparison of the available results becomes impractical in most cases since, as has been stated, much of the information in the literature concerning the formation of gas bubbles has been obtained with apparatuses that give rise to types of flow which fall between the aforementioned limiting cases. It has been found more fruitful to discuss the observed trends of the influence of the various varibles pertinent to the bubble formation process.

Hughes, et al (5) have derived two dimensionless groups to characterize the influence of the gas supply system upon bubble formation by considering the acoustical capacitance of the ante-chamber and the resistance to flow of the orifice channel. They are

$$N_c = \frac{g\,(\rho_L - \rho_g)\,V_c}{A_o\,\rho_g\,c^2}$$

$$N_R = L/D_o \qquad (1.1)^1$$

Values of the ante-chamber volume which make $N_c \ll 1$ approximate the condition of constant flow rate, whereas those which make $N_c \gg 1$ approximate the condition of a constant pressure supply. It has been observed (10) that an ante-chamber volume 10,000 times that of the bubble volume is required to approximate the condition of a constant pressure supply. The influence of the orifice channel, on the other hand, has been found (5,6,9) to be significant only when $N_R > 100$ or $N_R < 1$. Though not thoroughly tested, the parameters N_c and N_R have provided one means of characterizing the type of gas injection systems for at least the two limiting cases of flow.

Gas Flow Rate. In general, the terminal bubble volume, V_b, or the frequency of bubble formation, f, has been considered the principal variable in bubble formation studies. The most readily controlled independent variable is, of course, the rate of flow of gas through the system.[2] Because of the dependence of the forces due to liquid inertia, viscous drag, and buoyancy

[1] Refer to Appendix I for a definition of the notation.

[2] In many cases, the instantaneous rate of gas flow into a bubble is different from the mean rate of gas flow through the system and therefore also becomes, in such instances, a dependent variable. For convenience, reference hereafter to gas flow rate implies the mean gas flow rate if there exists such a difference.

upon the volume or the volumetric growth rate of the bubble, the volumetric gas flow rate has been employed consistently in the literature for describing the rate of gas injection. The influence of the volumetric gas flow rate, $\dot{q}_i$, hereinafter referred to simply as the "gas flow rate", upon the terminal bubble volume can be divided (5,11,12,13,14) into three regimes characterizing the operative forces; namely, (a) static, (b) dynamic (or unsteady), and (c) the so-called turbulent interaction.

At very low gas flow rates ($\lesssim$ 1 cm^3/sec) the bubble formation process is essentially static, with the terminal volume of the bubbles being determined by a balance between the static forces due to buoyancy and surface tension. Thus,

$$V_b = \frac{\pi D_o \sigma}{g (\rho_L - \rho_g)} \qquad (1.3)^1$$

For a given orifice and liquid, V_b is reported to be essentially independent of variations in gas flow rate (8,10,13,14) although the value that has been measured is somewhat different from that predicted by equation 1.3. Next, it may be observed that, by assuming that the gas density is practically constant, one obtains

$$V_b \cdot f = \dot{q}_i \qquad (1.4)$$

and, therefore, the frequency of formation, f, varies linearly with the gas flow rate in the static regime.

As the gas flow rate is increased, the dynamic forces become operative in governing the rate of growth of a bubble and its terminal volume. Thus, in the dynamic regime, there is a range of gas flow rate for which both V_b and f increase with the flow rate (13,14,15). At some value of gas flow rate, the frequency becomes approximately constant[2] and a further increase in $\dot{q}_i$ results in a linear increase in V_b, as indicated by equation 1.4. Both the static and the dynamic regimes may be said to yield regular bubble formation, that is, the periodic formation of bubbles of approximately equal volume for a given flow rate.

---

[1] It has been assumed that the liquid perfectly wets the orifice material, the bubble is spherical, and surface tension is the same for both static and dynamic interfaces.

[2] The approximately constant value of the frequency of bubble formation is referred to as the "maximum frequency".

In the dynamic regime, the occurrence of a constant frequency of formation above a particular value of the gas flow rate has been attributed as largely due to viscous retardation (12) and/or coalescence of the bubbles at the orifice (6,16). In very viscous liquids (e.g., castor oil), the constant frequency condition occurs (12) at much lower frequencies than in relatively inviscid liquids (e.g., water). The recent theoretical work of Walters and Davidson (16) shows that the occurrence of the maximum frequency in relatively inviscid liquids corresponds to a gas flow rate above a value

$$\dot{q}_i \geq 28\, g^{1/2}\, R_o^{5/2} \qquad (1.5)$$

When the gas flow rate is increased above the values mentioned above, the formation of bubbles is characterized by a randomness both in the size as well as in the frequency of formation. The cause for this is attributed to a much greater interaction between the liquid and the high velocity gas jet such as may be obtained with a turbulent gas jet (17). It is that regime of flow that has been referred to as the turbulent regime. It has been found (17,18) that the distribution of the mean diameter of the different size bubbles can be approximated reasonably well, under those circumstances, by a logarithmic normal-probability function. It also appears that the maximum size of the bubbles produced can be approximately predicted (18) by the application of Rayleigh's theory (19) concerning the instability of fluid jets. Such predictions indicate (17,18) that, for the so-called turbulent regime, the size of the bubbles produced and the frequency of formation are entirely independent of the orifice size and the gas and liquid properties.

Of course, the lines of demarcation between the static, dynamic, and turbulent regimes are not sharp, and the actual flow rates at which transitions occur from one regime to another are apparently dependent upon the liquid physical properties and the orifice size (12,15,19,20).

Liquid Physical Properties. The physical properties of the liquid which influence the bubble formation process are the density, the surface tension, and the dynamic viscosity. In the static regime, the terminal bubble volume should vary inversely with the liquid density (since $\rho_L >> \rho_g$) as indicated by equation 1.3. That trend has been verified (9,11,14) within the limitation of some variation of other properties of the liquid in addition to the density.

The buoyant force acting on a bubble, of course, increases with the liquid density, tending to produce smaller bubbles in more dense liquids. However, in the dynamic regime, the liquid

inertia force, which is proportional to the liquid density, tends to retard the bubble at the orifice thus increasing the final bubble volume. The net effect of those two opposing trends has been experimentally observed (7,8,20) to cause the terminal bubble volume to vary approximately as ρ_L^{-n}, where n varied from 1/10 to 1/3. Thus, experimental data for wide ranges of gas flow rate indicate that density effects are small where observed (21). It has been found (7), however, for very viscous liquids that the dynamic inertia force does not come into play as early as the viscous drag force; and consequently, in such liquids, V_b can vary as $\rho_L^{-3/4}$ for low gas flow rates in the dynamic regime.

The surface tension force on the bubble is particularly important in the static regime, and it has been found (11) that V_b varies directly with σ as would be expected from equation 1.3. There are, however, indications (12,22,23) of an even stronger dependence ($V_b \propto \sigma^3$) which apparently have not been fully investigated.

In the dynamic regime, the surface tension force is of secondary importance; and consequently, experimental data indicate (21,23) that surface tension effects are small, with V_b increasing only slightly with increasing σ (20). It has been found, however, (7,25) that surface tension can have a significant influence upon both the pressure in the gas supply system and the rate of flow of gas into a bubble.

The influence of the liquid viscosity arises from the occurrence of a viscous drag force acting on the interface. Obviously, there should be no influence of viscosity on the terminal bubble volume in the statis regime, and that fact has been demonstrated (9,11,14,22). The influence of liquid viscosity upon the terminal bubble volume for formation in the dynamic regime has also been shown (8,9,11,13,14,16,20,21,24) to be very small for liquids of relatively low viscosity ($\mu \leq 200$ cp). Some correlations (20,21) of the bubble volume data, for liquid viscosities in that range, indicate that V_b varied as μ^m where m varied from 1/12 to 1/50. In an analysis of the formation of a bubble in relatively inviscid liquids, Davidson and Schuler (25) entirely neglected viscous forces in their theoretical model. The approximate agreement of theory and experiment obtained by them indicates that, in such liquids, the predominant dynamic force acting at the interface is probably that due to the inertia of the liquid. However, for bubble formation in liquids having viscosities of the order of 500 to 1000 cp, it has been observed by the same authors that viscosity does have a significant influence on the terminal bubble volume. In their analysis of such bubble formation, Davidson and Schuler (7) considered the liquid inertia and viscous drag forces to be of equal

importance, and their experimental and analytical results indicate that V_b varied as μ^m where m had a value ranging from 2/3 to 3/4.

Gas Properties. The influence of the physical properties of the gas upon the bubble formation process has received only limited attention. It has been shown that the use of nitrogen gas (13) and hydrogen gas (9) resulted in the formation of bubbles the same size as were obtained with air, other conditions being the same. Davidson and Schuler (7) predicted, analytically, an increase in the terminal bubble volume of approximately 1 percent for changing the injected gas from CO_2 to air. Their experimental observations indicated an increase of 1.8 percent. Such effects were attributed to the differences in (a) the gas momentum for the two cases and (b) the effect of gas density upon the orifice discharge coefficient. However, effects of such magnitude are generally considered negligible. The dimensionless parameter, N_c, defined in equation 1.1 indicates that the gas density and the acoustic speed of the gas may be important in characterizing the type of flow into the bubbles resulting for a given system. It should be noted that, for a perfect gas,

$$\rho_g \cdot c^2 = \gamma p_c$$

and, therefore, N_c is only dependent upon the specific heat ratio for the gas and the pressure of the gas in the antechamber.

Liquid Motion. The forces acting on the bubble as a result of motion of the liquid relative to the bubble can arise from induced or forced liquid motion. Considering, first, a liquid essentially at rest with respect to the orifice, there is motion of the liquid which is induced as a result of the growth and rise of the gas bubbles. Of course, an infinite liquid bath would minimize the effect of such induced liquid motion. In the use of liquid containers of finite dimensions, it has been found (14) that there was no significant change in the size of the bubbles formed for container diameters greater than approximately 8 bubble diameters. The effect of the induced liquid motion upon the bubble volume was observed to be significant (7) when the orifice projected upwards into the liquid bath. The liquid consequently could move upwards in that case at the base of the bubble, causing an additional force on the bubble which tends to reduce the terminal bubble volume by as much as 10 percent. When the orifice was surrounded with a ring of a diameter 1.5 times that of the bubble diameter, it was found (7) to reduce the effect of induced liquid motion to a minimum, and the ring therefore acted as an anti-circulation device. In most analytical treatments, the effect of the induced liquid

motion is not taken into account simply because of the difficulty of predicting such flow. Hence, its actual effect is little understood. As one might expect, the influence of such induced liquid motion has reportedly been more significant in liquids of relatively low viscosity (7,25).

Another type of liquid motion, namely the forced liquid motion relative to the orifice, has been observed to reduce the terminal bubble volume for a given gas flow rate. It has been found (12) that, in the dynamic regime, the bubble diameter varied approximately inversely with increasing tangential velocity of the liquid relative to the orifice. The reduction of bubble diameter with increasing liquid velocity is less pronounced the higher the gas flow rate. In the so-called turbulent regime, it has been found (18) that the diameter of the largest bubbles varied inversely with the relative liquid velocity to the 1/2 power.

Liquid Depth. It has been shown in numerous instances that the depth of the liquid does not influence the bubble volume or frequency provided the depth is at least equal to 2 or 3 bubble diameters (7). The liquid depth would of course influence the pressure in the gas supply system which is of little significance, on the whole, in view of the very small influence of the gas properties.

Orifice. The size, shape, and orientation of the orifice used for gas injection have been important variables of interest in the formation of bubbles. For the most part, vertically oriented, circular orifices have been utilized, though there is some limited data (24) concerning the use of triangular and slot shaped orifices. In an investigation of round-edged and sharp-edged orifices (17), the flow coefficient for air discharging into air was compared with that for air discharging into water. The sharp-edged orifice for the air-water system exhibited a larger flow coefficient (10 to 15 percent) than that for the air-air system. That may have been a result of disruption of the vena contracta by the formation of the bubbles and the subsequent increase in the effective orifice area. The flow coefficient for a round-edged orifice was nearly the same for the air-water and air-air systems, since the vena contracta was located near the throat and apparently less disturbed by bubble formation. As mentioned previously, there still remains some uncertainty in determining the effective pressure drop across a bubbling orifice (24). There are indications (5) that the dynamic forces may cause pressure differences considerably different from those predicted merely on the basis of static surface tension effects.

The influence of the orifice diameter upon the terminal bubble volume, in the static regime, has been found (11) to

follow the trend indicated by equation 1.3 wherein V_b varies linearly with D_o. However, there is also some indication (9) that V_b may vary as $D_o^{3/2}$ in the static regime. Regular bubble formation has been observed (9) up to orifice diameters of 0.5 cm and in some cases (6) for orifices as large as 1.6 cm in diameter.

Some experimental data for bubble formation in the dynamic regime (14,20,25) indicate that the influence of the orifice diameter upon the terminal bubble volume is insignificant. However, the data from other sources (6,15,21,24) indicate that V_b varies as D_o^n, where n is approximately 1/3 to 1/2. The magnitude of the maximum frequency in the dynamic regime has been found to increase with a decrease in orifice diameter; $f_{max} \alpha D_o^{-m}$, where m varies from 1/3 to 1/2, (6,15,20).

Even though the trends of influence of the variables pertinent to bubble formation seem, as illustrated above, to show reasonable agreement among the variety of sources in the literature, it should be mentioned that no systematic variation of the several parameters has been attempted. The current theories on the mechanism of bubble formation which have to take into account both the unsteady nature of the flow processes involved and the interaction of the fluid dynamic and interfacial forces are, therefore, largely subjective in their relation to the limited experiments considered by individual researchers. It might be expected that the success of any attempt to describe such phenomena in terms of overall or mean quantities would be limited. Davidson and Schuler (7,25) have presented, perhaps, the most significant analytical treatment of the bubble formation process considering both of the aforementioned limiting cases (constant flow rate and constant pressure supply) for the flow of gas into the bubbles. Based upon the assumption of a spherical bubble growing about a point source of gas, they were able to predict the terminal bubble volume for a given orifice, liquid, and gas flow condition. In the case of constant gas flow rate, the flow rate was, of course, the independent variable. In the case of a constant pressure supply, the ante-chamber pressure was chosen as the independent variable, while the flow rate into the bubble as well as the terminal bubble volume were considered dependent variables. For the analysis of bubble formation in a viscous liquid, the vertical motion of the spherical bubble about the point source was determined by a balance of buoyant, liquid inertia, and viscous (Stoke's) forces.[1] In the analysis of bubble formation in an

[1] The liquid inertia force was omitted in the consideration of small (0.3 - 2.5 cm^3/sec) gas flow rates.

inviscid liquid, only buoyant and liquid inertia forces were included. Closed form solutions were obtained only for the case of constant gas flow rate. Those were

(viscous liquid-low gas flow rate)

$$V_b = 8.04 \left(\frac{\mu}{\rho g} \dot{q}_i\right)^{3/4} \tag{1.6}$$

(inviscid liquid)

$$V_b = 1.378 \frac{\dot{q}_i^{6/5}}{g^{3/5}} \tag{1.7}$$

The aforementioned authors obtained agreement between the predicted and the experimental values of the terminal bubble volume within 10 percent, in most cases, for the case of bubble formation in a viscous liquid for both types of (limiting) flow considered. Similarly, they obtained reasonable agreement for the case of formation in an inviscid liquid for a constant gas flow rate. Considering that their analysis is the first to enable the prediction of the terminal bubble volume for arbitrarily specified conditions on the gas flow rate, orifice size, and liquid properties, the results are encouraging. The analysis provides an added insight into the regimes of importance of the dynamic forces which govern the motion of the gas liquid interface. However, the comparison of theory and experiment solely on the basis of the terminal bubble volume does not permit one to assess the adequacy of the representation of the governing forces at each instant during the formation period of the bubble. A knowledge of the forces acting on the bubble interface and the fluid surrounding the bubble at each instant during the growth of the bubble is essential for the understanding of the energy and mass transfer processes where they occur.

1.1.2 Energy Transfer During Bubble Formation

A great majority of the investigations which have been reported in the literature concerning the energy or mass transfer to bubbles or drops pertain to the period of their passage through a continuous liquid phase and not the period of formation. Though there are some features of similarity in the transfer processes themselves, the data obtained during the passage of the bubble has very limited application to the analysis of energy or mass transfer during bubble formation. The unsteady nature of the processes involved during bubble formation and the complexity of analyzing the various interactions

during that period have hindered investigations in that area, and, as such, the information in the literature is very meager.

For the most part, the investigations reported in the literature pertaining to interfacial transport phenomena have been concerned with mass transfer across an interface. In addition, much of the data concerning the energy or mass transfer between the continuous and the discrete fluid phases pertain to transfer between a continuous liquid and a liquid drop. However, in view of the analogy between the energy and mass transfer processes and the similarity, in some limited respects, between bubbles and drops, much of the available information can be applied to the understanding of the phenomenon of energy transfer to bubbles. The following discussion considers that information in relation to the process of energy transfer during bubble formation.

Numerous investigators (26,27,28,29,30,31) concerned with the energy or mass transfer to bubbles or drops as a function of the distance of travel through a continuous liquid have reported "end effects", and they have been commonly attributed to the transfer of energy or mass during the formation period or immediately thereafter. An estimate of the amount of energy or mass transfer during the formation period has frequently been made on the basis of experimental data for the amount of transfer as a function of the depth of the liquid by extrapolating such data to a zero liquid depth. The validity of such an extrapolation is based on the assumption that the heat (or mass) transfer increases linearly during the rise time of the bubble. There is some evidence which indicates that the transfer varies nonlinearly during the rise time (32) and, therefore, that such an assumption may be highly inaccurate (33). However, it provides some basis for an estimate of the maximum amount of transfer that may occur during the formation period. For the case of liquid vapor transfer to air bubbles, Calderbank (28) has estimated that the bubbles may be as high as 80 percent saturated during the period of bubble formation. Investigation of the mass transfer for cases controlled by both gas-phase resistance and liquid-phase resistance indicated (28) that the transfer during the bubble formation period ($\gtrsim$ 40 percent) was equally as significant as that during the time of passage of the bubbles through the liquid.

The present author has applied the same technique (extrapolation to zero liquid depth) to the data of McDowell and Myers (34) for energy transfer to liquid drops and found that the change in drop fluid temperature during the time of formation may have been as much as 12 to 30 percent of the available overall temperature difference. Other experiments (35,36,37) concerned with the rate of mass extraction from droplets have also indicated that as much as 5 to 40 percent of the extraction

may occur during drop formation. All such information seems to emphasize the significance of the energy or mass transfer during the bubble or drop formation period in relation to the transfer for the overall process of continuous and discrete fluid contact.

Linquist (38) and Garner and Skelland (29) have conducted investigations specifically concerned with mass transfer during bubble and drop formation, respectively. Linquist observed that, for the case of water vapor transfer to dry nitrogen bubbles during formation, the saturation of the bubbles varied from 40 to 65 percent as the vapor pressure of the liquid was increased. Furthermore, the mass transfer coefficient was found to decrease with time during the formation period, but it was shown that the degree of saturation of the bubbles at the end of the formation period could be analytically computed by employing an average mass transfer coefficient for the entire formation period. Although there was no significant variation of the molecular diffusivity of the gas-vapor combination, the results indicated that the average mass transfer coefficient varied as $D_g^{1/2}$. Such a trend compares reasonably well with that observed by Calderbank (28), who showed that the transfer rate during bubble formation varies as $D_g^{2/3}$ for nearly a threefold variation of D_g.

The decrease of the mass transfer coefficient with time during the formation period has also been observed in connection with extraction from drops by Garner and Skelland (29) and Coulson and Skinner (39). Such variation has been attributed to a decrease with time of the mixing of the fluid within the bubble or drop. Just as in the case of bubbles or drops passing through the liquid, the circulation of the fluid in a droplet may be expected to have a predominant influence upon the rate of energy or mass transfer. In support of this, two facts may be stated. Firstly, Garner and Skelland (29) have observed that the rate of extraction from drops during the period of formation of the drops at an orifice was strongly influenced by the agitation within the drops. They observed (40) that the flow from the orifice traveled down the central axis of the drop and circulated back along the interface. An increase in the rate of feed from the orifice caused an increase in the rate of circulation. Furthermore, the rate of extraction during formation was found to be increased as much as 50 percent by increasing the velocity of flow from the orifice, although there were indications that the increase in bubble or drop size during formation also had a strong influence upon the circulation therein.

Secondly, theoretical predictions (29) of the mass transfer coefficient, assuming a stagnant drop, have been found to

be an order of magnitude smaller than the values determined experimentally. Experimental values of the mass transfer coefficient for the drop formation period also indicated that the velocity of circulation was substantially greater than that during the passage of the drops through the liquid.

Whether the effect of internal circulation upon the rate of energy or mass transfer to a bubble is merely the result of an increase in the effective area of transfer as suggested by Harriott (41), or the result of eddy diffusion as postulated by Handlos and Baron (26) is not yet known. Nevertheless, the importance of that phenomenon is well established.

The circulation within a bubble which may be present while passing through a liquid bath, may probably be the result of the transfer of viscous shear across the interface; the circulation within a bubble during the formation period, on the other hand, arises from the momentum associated with the fluid stream entering the bubble. The interfacial phenomenon may also exercise during the latter period some influence on the decay of the circulation by the viscous transfer of momentum out of the bubble. The internal circulation during formation and its apparent decay with time should, however, be closely related to the viscous dissipation in the fluid within the bubble. An indication of such an effect has been observed by the author from some experimental data for energy transfer to droplets (34). An estimate[1] of the drop fluid temperature change during formation indicated that as much as 30 percent of the available temperature change may have occurred during the formation of kerosene and xylene drops in water, whereas only a 12 percent change in temperature was indicated for the case of viscous oil drops formed in water. In view of the relatively low viscosity of the more common gases employed in bubble experiments, the circulation in gas bubbles could be large. It may be expected that the kinematic as well as the thermal properties of the gas will have an influence upon the energy transfer during formation.

The experimental data of Linquist (38) regarding mass transfer during bubble formation indicate, on assuming an analogy between heat and mass transfer, that the energy transfer coefficients range from 3.5×10^{-3} to 7.0×10^{-3} cal/sec-cm^2-C.

Recent investigations (42,43) in connection with boiling heat transfer have indicated coefficients of heat transfer, between water and injected steam, that are several orders of

[1] By extrapolation of the fractional transfer as a function of liquid depth to zero liquid depth.

magnitude greater than the aforementioned values for immiscible fluids. There is evidence in such cases (43), however, that the presence of an inert gas in the injected steam appreciably reduced the heat transfer coefficient. It may be expected that such cases involving, primarily, latent energy transfer are considerably different from the energy transfer associated with the contacting of immiscible fluids.

In summary, a review of the literature indicates that the amount of energy or mass transfer occurring during the formation of a bubble may be a significant portion of the total transfer for the overall bubbling process. In developing an understanding of the fluid dynamic, interfacial and transport processes associated with the energy transfer to a gas bubble during formation, the following aspects of the problem remain open for further investigation:

1. In view of the apparent interaction of the fluid dynamic and energy transfer processes, there is a need, first, for a detailed consideration of the fluid dynamic and interfacial forces that govern the rate of growth of a bubble throughout the period of formation. Such a study should encompass the formulation of an analytical representation of those dynamic forces as well as an experimental evaluation of the influence of the several parameters (mean flow rate, liquid properties, apparatus parameters) upon the instantaneous rate of gas flow into a bubble.
2. In order to understand the mechanism of energy transfer between the liquid and the gas in the bubble there is a need for quantitative information concerning the pattern of the circulation of the gas in a bubble and its variation with time during the formation period as influenced by fluid dynamic and interfacial forces.
3. Finally, there is a need for a detailed consideration of the interfacial phenomena that give rise to the periodic formation of discrete bubbles. That aspect of the problem requires a consideration of (a) the conditions necessary for the initiation of the formation of a bubble and (b) the stability of that bubble interface under the combined action of the dynamic forces acting thereon in order to determine the length of the formation period of a bubble.

1.2 Preliminary Diagnostic Study

The information in the literature concerning the energy or mass transfer to a bubbling gas is principally concerned with the transfer occurring during the passage of the gas bubbles through the liquid. Though there is sufficient indication that the energy transfer occurring during the formation of the

bubbles may be quite significant, there has not been any quantitative data reported to indicate which part of energy transfer, if either, is the more important. Consequently, an exploratory investigation was conducted to determine the relative importance of the energy transfer occurring during (a) the formation of the bubbles and (b) the passage of the bubbles through the liquid. The relative importance of the energy transfer occurring during bubble formation and bubble motion was investigated by measuring the overall change in the temperature of the injected gas for varying depths of the liquid phase.

The apparatus utilized for the preliminary investigation is illustrated schematically in Fig. 1. A cylindrical tank, 20.3 cm in inside diameter, was employed to contain the liquid phase. Air was injected into the liquid through a 0.159 cm diameter orifice in the base of the liquid tank. The air was supplied to the orifice from a high pressure supply via a pressure regulator, precision flow meter, needle valve, and ante-chamber.

The liquid phase was heated by means of an electrical immersion heater. A Dow Corning silicone liquid (DC 710R), which permitted liquid temperatures up to 232C,[1] was used as the continuous phase. The upper portion of the ante-chamber was surrounded by a water-cooled manifold to prevent heat conduction through the base of the liquid tank from preheating the air.

The gas inlet temperature was measured by means of an iron-constantan thermocouple mounted just to the side of and 0.6 cm below the orifice. The liquid temperature was measured by means of an iron-constantan thermocouple located radially, 5 cm from the orifice axis and midway in the liquid depth. It was found that the stirring action of the gas bubbles eliminated both radial and axial temperature gradients in the liquid.

The stream of gas bubbles rising through the liquid was collected at the surface of the liquid by means of a cylindrical tube (open at both ends), 5 cm in inside diameter.[2] The cylindrical collector was supported by a movable rack which permitted the location of the collector at the liquid surface, regardless of the liquid depth. The lower end of the collector projected into the liquid ($\sim$ 0.3 cm) to insure collection of the gas bubbles. The outlet temperature of the gas stream was measured by means of iron-constantan thermocouples positioned, radially, at the center of the collector. Three thermocouples, with a

---

[1] Vapor pressure of 1.5 mm Hg at 232C.

[2] An inverted funnel collector was found to be unsatisfactory because of excessive liquid splashing of the thermocouples.

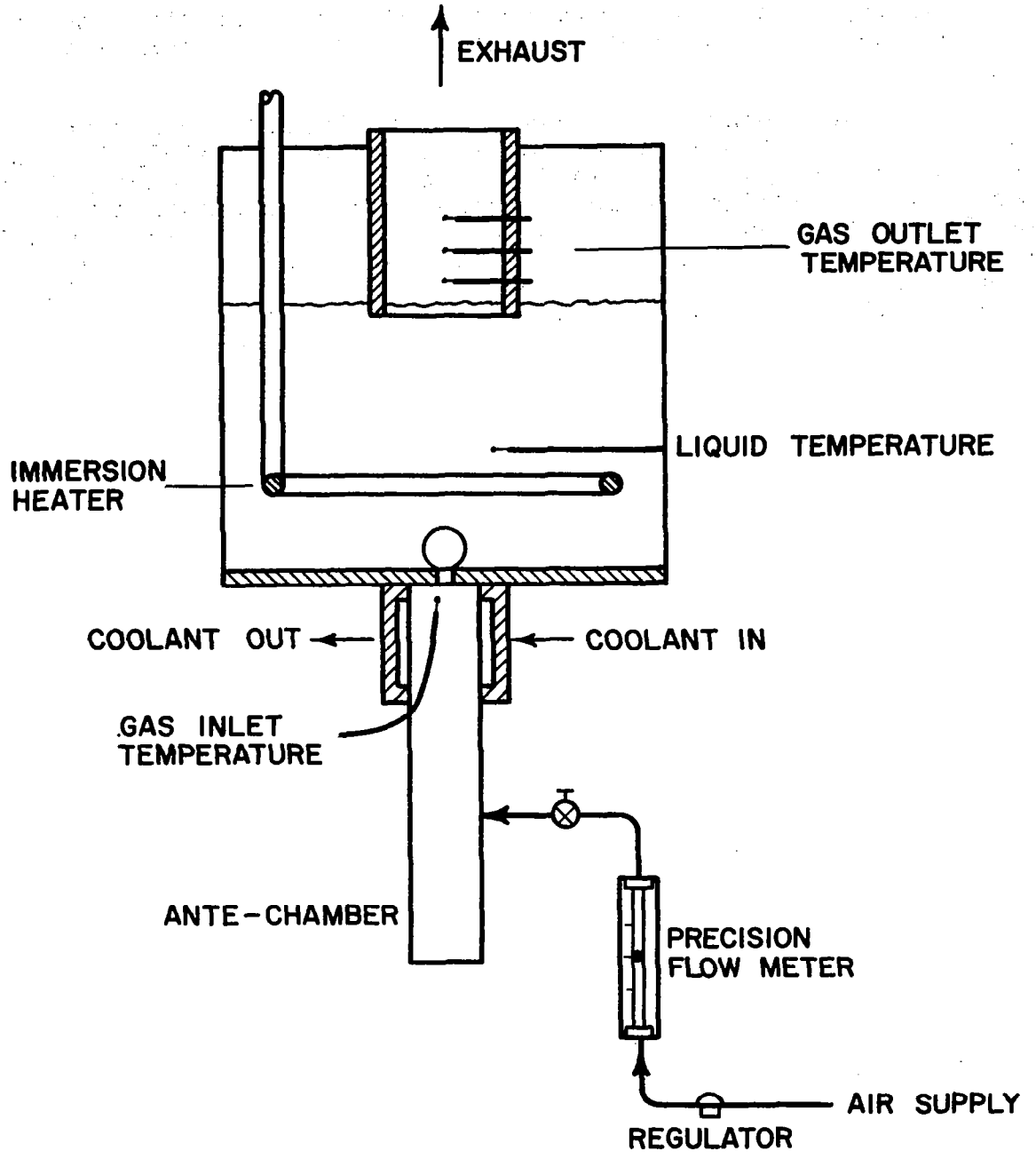

FIG. 1 PRELIMINARY APPARATUS

vertical separation of 1.2 cm were employed to obtain a measurement of the gas temperature independent of the splash of the liquid.

In the exploratory experiments, the liquid and gas inlet temperatures were maintained constant at approximately 17°C and 27°C, respectively. The relative importance of the energy transfer occurring during bubble formation and bubble motion was investigated by measuring the outlet gas temperature as a function of the depth of the liquid. Liquid depths of 2.8, 5, and 7.6 cm were employed. Liquid depths below 2.8 cm were not used in order to avoid alteration of the bubble formation process. The mean gas flow rate was varied over the range from 3.4×10^{-3} to 10.2×10^{-3} gm/sec, resulting in regular bubble formation at frequencies from 8 to 20 per second.

The experimental determination of the outlet gas temperature showed that the outlet gas temperature was essentially uninfluenced by the variations in the depth of the liquid or in the gas flow rate, and was approximately equal to the temperature of the liquid.

Such results should be viewed accounting for the inherent difficulties of the technique employed for measuring the outlet gas temperature. Collection of the stream of gas bubbles at the surface of the liquid resulted in a very turbulent mixing of the gas and splashing liquid. Consequently, it is highly probable that such mixing could have resulted in additional energy transfer to the gas before it reached the thermocouples measuring the outlet gas temperature. In addition, the very low mass flow rate of the gas required to produce regular bubbling increased the possible error in the measurement of the true outlet gas temperature due to energy transfer between the collector and the gas.[1] On the other hand, it is probable that the errors due to such effects were approximately the same regardless of the depth of the liquid. Therefore, the absence of a noticeable dependence of the measured gas outlet temperature upon the depth of the liquid did seem to indicate that the energy transferred to the gas bubbles during the first 2.8 cm of contact with the liquid must have been quite significant. It was also found that the results obtained were consistent with the unpublished experimental observation of Myers.[2]

---

[1] The temperature of the collector had a noticeable influence upon the measured gas outlet temperature.

[2] Myers, J.E., Professor of Chemical Engineering, Purdue University, private communication.

In a practical system, the use of many closely spaced streams of gas bubbles and larger overall temperature differences would, perhaps, result in a more pronounced influence of liquid depth upon the gas outlet temperature, nevertheless, the energy transfer during bubble formation remains an important stage in the overall bubbling process.

1.3 Scope of the Present Investigation

The research discussed herein was concerned with the energy transfer from a liquid to gas bubbles during their period of formation at a single submerged orifice. The investigation consisted of both an experimental and analytical study.

The experimental investigation was conducted to obtain quantitative information regarding the variables that govern the transfer of energy from a liquid to gas bubbles in the process of formation at a single submerged orifice. Measurements were made for the determination of the change in the temperature of the gas in a bubble due to energy transfer from the liquid as the bubbles were formed. In addition, data were obtained for determining the rate of transfer of energy to the bubbles during their period of formation. The effects of the gas flow rate, the orifice size, and the liquid physical properties upon the energy transfer during the formation period were investigated. Some information regarding the effect of energy transfer on the basic process of bubble formation was also obtained.

The analysis developed herein applies to the dynamic growth of an idealized gas bubble under the combined influence of gas injection through an orifice and energy transfer from the surrounding liquid. The bubble is assumed to be spherical in shape with complete mixing of the gas therein. The analysis provides a means for determining the effect of energy transfer upon the rate of growth of the bubble and for calculating the increase in the temperature of the gas in the bubble during a formation period of specified length.

2. EXPERIMENTAL INVESTIGATION

When a gas is injected into a liquid through a submerged orifice, there results, under certain conditions, the periodic formation of discrete gas bubbles. If the liquid is hot, relative to the temperature of the injected gas, there occurs energy transfer from the liquid to the gas in the bubble. The experimental investigation was concerned with obtaining quantitative data regarding the energy transfer that occurred as the bubbles

were formed at the orifice. Transparent liquids were employed to permit the use of high speed photography for recording the sequence of bubble formation. A difference between the temperature of the liquid and the temperature of the gas entering the bubble was produced by precooling the gas while the liquid was maintained at ambient temperature. This was necessary to minimize the transfer of liquid vapor into the bubbles so that the effects of heat transfer could be isolated.

Measurements were made for determining the mean temperature of the gas in the bubble at the termination of the bubble formation period when the bubble detached from the orifice. In addition, measurements of the average surface area of the bubbles and the time of formation were made for determining an average convective heat transfer coefficient for the bubble formation period.

The operating variables for the investigation were the orifice diameter, the properties of the liquid, and the mean mass flow rate of the gas. A considerable range of bubble size, formation time, and flow rate into the bubble were investigated by selected variation of those variables.

In support of the analytical investigation described in Section 3, an auxiliary investigation was also conducted to determine the actual instantaneous rate of mass flow into a bubble. Several interesting facts regarding the details of the mechanism of bubble formation were also obtained.

2.1 Description of Apparatus and Experimental Method

2.1.1 Principal Apparatus

General Description. Figure 2 illustrates schematically the principal experimental apparatus utilized for the periodic formation of gas bubbles by the injection of a gas into a liquid. The apparatus consisted of a liquid container bonded to a flat disc base. A submerged orifice for the injection of gas was provided by a circular hole in the cylindrical orifice body which was mounted in the base of the container. The submerged orifice was supplied with gas from a small reservoir or ante-chamber attached to the orifice body projecting below the base of the liquid container. The liquid container with the orifice assembly was mounted atop a wide-mouth vacuum flask which served as a support for the liquid container and also as a gas-to-fluid heat exchanger below the orifice assembly. The heat exchanger was employed to control (in this case to reduce) the temperature of the gas injected into the liquid in order to produce a condition for heat transfer. Gas was supplied to the ante-chamber

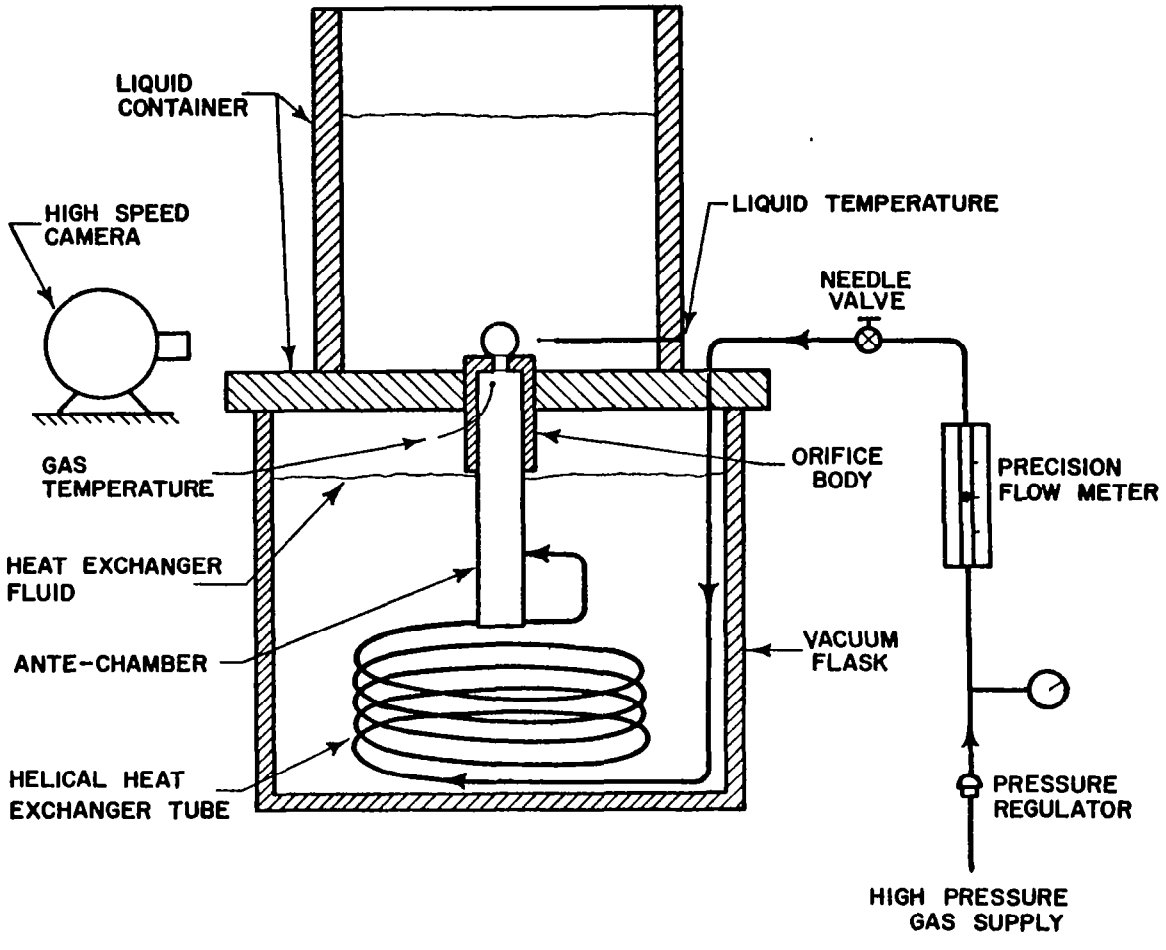

FIG. 2 PRINCIPAL APPARATUS

for injection into the liquid from a high pressure source through a precision flowmeter, a needle valve, and the helical tubing of the heat exchanger. The ante-chamber volume was kept as small as possible in order not to lose the difference in temperature produced by the heat exchanger. It is realized that the ante-chamber volume is a parameter that influences the formation of the bubbles, and therefore, the use of a single ante-chamber size may imply a particular class of bubbles (5).

The apparatus enabled the periodic formation of gas bubbles for mean volumetric gas flow rates up to 30 cm^3/sec. However, it was found that flow rates below approximately 10 cm^3/sec (0.6 in^3/sec) resulted in the regular formation of bubbles of approximately equal volume; and, consequently, the investigation was confined to flow rates in that range.

Both distilled water and ethyl alcohol were used as the liquid bath in which gas bubbles were formed. Dry nitrogen gas was used for injection into the liquid throughout the investigation.

Ethyl alcohol was selected because it was found that its lower surface tension enabled the production of gas bubbles considerably smaller than those produced in water under similar conditions. In addition, the fact that the thermal conductivity of ethyl alcohol is approximately one-third that of water aided in the consideration of the importance of the thermal resistance of the liquid phase in determining the rate of transfer of energy to the gas bubbles.

In the experiments conducted to obtain data regarding bubble formation with heat transfer, the gas was precooled prior to entering the orifice such that there was a significant difference between the temperature of the liquid and the temperature of the gas entering the bubble. In such experiments, liquid nitrogen (b.p. ~ 77K at 1 atm.) was used as the heat exchanger fluid which provided an orifice inlet temperature of approximately -129C (-200F). With the liquid phase maintained at approximately 21C (16C for ethyl alcohol), an overall temperature difference of approximately 150C (270F) was obtained.

In the experiments conducted to obtain data regarding bubble formation without heat transfer, the temperature of the gas entering the bubble was maintained the same as the temperature of the surrounding liquid. This was accomplished by using water at approximately 21C as the heat exchanger fluid thus controlling the temperature of the gas entering the orifice at 21C, (16C for ethyl alcohol).

High speed motion pictures of the bubble formation process, taken at the level of the orifice, provided a technique for investigating the details of the formation of a gas bubble. Frame-by-frame projection of the photographs enabled an accurate determination of the bubble volume, the bubble surface area, and the time of formation of the bubble.

Detailed Description. The liquid container was fabricated from transparent plexiglass tubing 8.9 cm inside diameter by 0.635 cm wall. The cylindrical portion of the container was bonded to a plexiglass base 20 cm in diameter.

The orifice body consisted of a cylindrical tube, 1.9 cm in outside diameter, closed at one end, with an orifice of the desired size drilled in the closed flat end. The outside of the orifice body was threaded to facilitate the mounting of the body in the base of the liquid container with the axis of the orifice vertically oriented. It was found that the wettability of the orifice material had a significant influence on the size of bubble formed and the time of formation. Consequently, orifices made of plexiglass (wetting for water) and teflon (non-wetting for water) were used in the investigation. The entire orifice body was machined from bar stock of the desired material with a very smcoth finish on the closed end. A hole of the desired size was drilled in the center of the closed end of the orifice body to provide a round, sharp-edged orifice. Orifices of 0.159 cm and 0.0795 cm in diameter and with an L/D ratio of approximately 2 were used in the investigation.

The cylindrical ante-chamber supplying gas to the orifice was 1.11 cm in inside diameter and 21.6 cm long and was mounted with the upper end sealed inside the orifice body.

Prior to entering the ante-chamber, the gas was passed through a helical heat exchanger tube (0.476 cm x 0.076 cm wall, 21.3 m long) suspended from the liquid container base.[1] The heat exchanger facilitated the control of the temperature of the gas entering the orifice. The vacuum flask provided a well insulated container for the heat exchanger fluid as well as a support for the liquid container. The level of the fluid in the flask was maintained approximately at the lower end of the orifice body to minimize the change in the temperature of the gas as it flowed up the ante-chamber to the orifice.

A 16mm Fastax camera was used to obtain the high speed motion pictures (2500 frames per second) of the bubble formation process. The orifice body was mounted in the liquid container base such that the surface of the orifice was 0.6 cm above the

[1] The effective volume of the ante-chamber and helical tube combination was approximately 57.4 cm^3.

base, permitting photographs at the orifice level. The Fastax camera was equipped with a 60 cycle timing light which enabled an accurate determination of the time associated with any event recorded on the film.

The temperature of the gas entering the orifice was measured by means of an iron-constantan thermocouple mounted to the side and 0.3 cm below the entrance to the orifice. An iron-constantan thermocouple projecting radially through the liquid container 0.3 cm above the surface of the orifice facilitated the measurement of the temperature of the liquid in the proximity of the orifice. It was found that the stirring action of the gas bubbles rising through the liquid bath prevented the occurrence of significant radial or axial temperature gradients in the liquid; and, consequently, the thermocouple used for measuring the liquid temperature was located radially 4 cm away from the orifice so as to avoid any interference with the formation of the bubbles.

2.1.2 Auxiliary Apparatus

An auxiliary investigation was conducted, in support of the analytical investigation presented in Section 3, to determine the actual rate of mass flow into a bubble as it formed under given conditions. Several other interesting facts regarding the mechanism of bubble formation were also obtained.

The auxiliary apparatus utilized for the investigation, similar to the principal apparatus previously described, is illustrated schematically in Fig. 3. A plexiglass orifice with a diameter of 0.159 cm and an L/D ratio of 4 was employed. The principal and auxiliary apparatuses differed primarily in the ante-chamber employed to supply gas to the orifice. As shown in Fig. 3, the ante-chamber of the auxiliary apparatus consisted of a cylindrical tube 1.11 cm inside diameter and 19 cm long. At the base of the ante-chamber, an O-ring sealed coupling enabled sealing of the chamber by means of a removable plug or variation of the ante-chamber volume by the addition of another length of tubing. With the plug in place the standard ante-chamber volume was 21.7 cm^3. Addition of a 17.8 cm length of tube at the sealed junction gave an ante-chamber volume of 39.8 cm^3.

Near the upper end of the cylindrical ante-chamber, immediately below the orifice body, a small chamber 2.86 cm inside diameter was connected to the ante-chamber by means of a tube 1.11 cm inside diameter by 1.9 cm long. The small chamber was used to house a pressure microphone which was employed to measure the transient pressure of the gas in the ante-chamber during the formation of a bubble. By knowing the variation in the ante-chamber pressure with time it was possible to determine the time

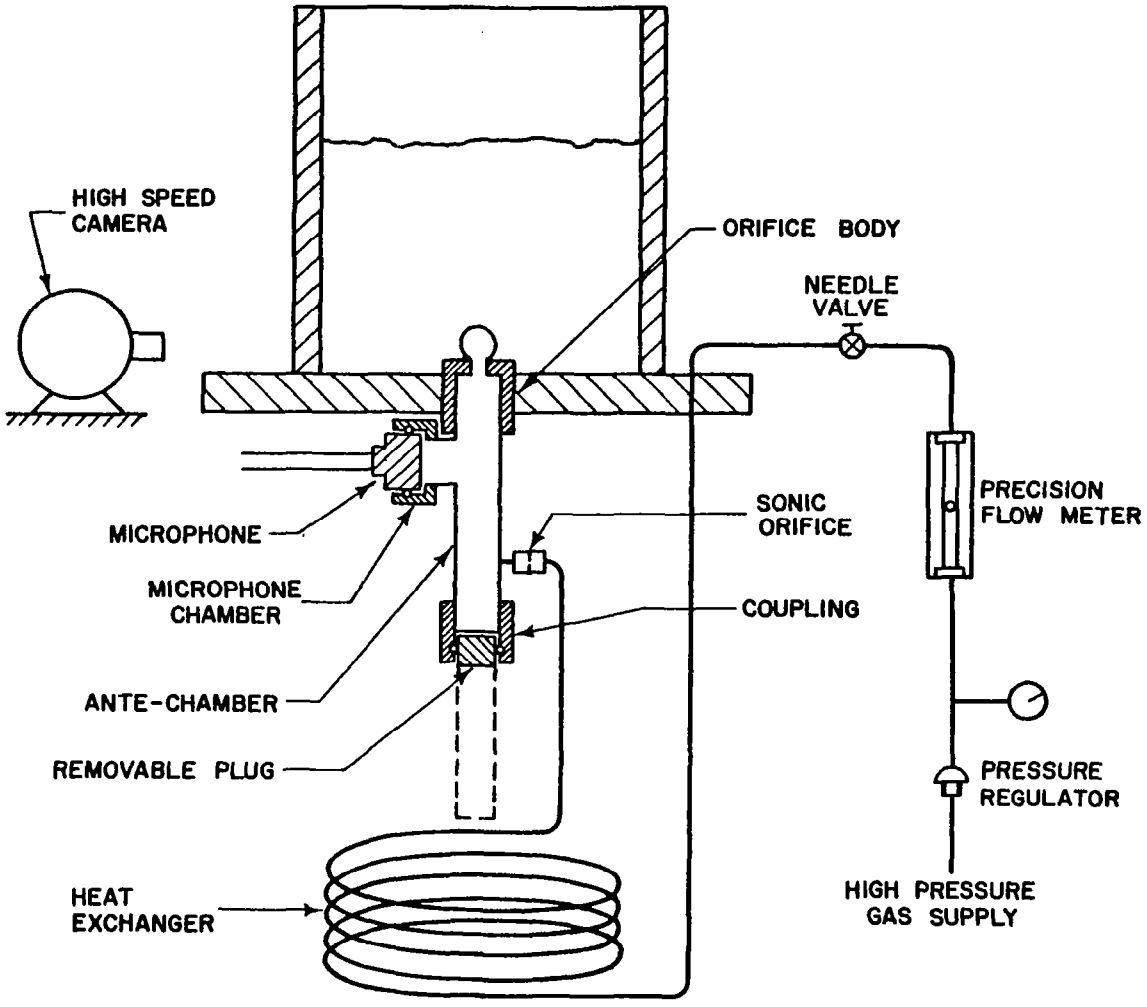

FIG. 3 AUXILIARY APPARATUS

rate of change of mass stored in the ante-chamber and, therefore, to determine the rate of mass flow into the bubble. Details of the microphone instrumentation and calibration are discussed in Appendix II.

The steady state mass flow rate of the gas into the system was controlled by means of a sonic orifice located at the entrance to the ante-chamber. A gas pressure of 3 atm was maintained on the upstream side of the sonic orifice to insure sonic flow. The purpose of the sonic orifice was to isolate the ante-chamber supplying the orifice from all other components (tubing, etc.) involved in supplying gas to the ante-chamber, thus ensuring that the steady state mass flow rate of the gas into the system was not affected by the periodic bubble formation. The effective volume of the ante-chamber was, therefore, the true volume of the chamber supplying the orifice. Sonic orifices were constructed to enable operation at four different steady state gas flow rates ranging from 1.5 to 5.2 cm^3/sec.

All experiments were conducted using distilled water and nitrogen gas which were maintained in thermal equilibrium by means of the heat exchanger as described in Section 2.1.1.

High speed motion pictures taken at the orifice level were again employed as a means for determining the bubble volume and the timing of events in the bubble formation process. The output of the pressure microphone was displayed on an oscilloscope and recorded by means of a polaroid camera. Synchronization of the ante-chamber pressure record and the high speed motion pictures enabled a correlation of the photographed events with corresponding points on the pressure record.

2.1.3 Experimental Method

In the investigation of the effect of energy transfer upon the formation of a gas bubble, the primary objective was the determination of the change in the temperature of the gas in a bubble which resulted from energy transfer to the bubble as it was formed. It was apparent that any direct means of measuring the bubble gas temperature would not be feasible because (a) as with any interfacial phenomenon, penetration of the interface would completely alter the processes involved, and (b) the mass of gas in a bubble was too small (10^{-3} gm) to activate common sensing devices. Consequently, it was necessary to devise a technique for indirectly determining the temperature of the gas in a bubble.

Because of the apparent axial symmetry of a bubble forming at a smooth, vertically oriented orifice, it was found that the volume of the bubble could be calculated from a two-dimensional

picture of the bubble. High speed motion pictures taken at the orifice level provided a means for recording the sequence of the formation of a bubble. A frame by frame projection of such pictures enabled one to obtain a picture of the bubble at the instant of detachment from the orifice. By calculating the volume of the bubble from one such picture and determining the mass of gas in the bubble from mean flow measurements, it was possible to determine, by means of the perfect gas law, the average temperature of the gas in the bubble assuming that the pressure within the bubble could be approximated by the static pressure due to the liquid head and the surface tension.

The procedure for computing the volume of a bubble from a two dimensional picture is illustrated in detail in Appendix III. The volume and surface area of the bubble at the instant of detachment from the orifice are referred to as the terminal bubble volume and terminal bubble surface area, respectively.

The procedure for computing a mean temperature of the gas in a bubble from the calculated volume of the bubble required an accurate determination of the mass of the gas in the bubble. The mass of gas injected into the bubble through the orifice could be adequately determined from mean flow measurements provided it was assumed that the amount of liquid vapor transferred into the dry bubble was negligible. Linquist (38) showed that the transfer of liquid vapor into a dry gas bubble during its period of formation was appreciable under certain conditions. However, it was also shown that for water at temperatures below 27C (80F) the volume of liquid vapor transferred to a bubble was less than 2 percent of the volume of the gas in the bubble. Consequently, the investigation was restricted to water temperatures below 27C, and the mass transfer from the liquid was considered to be negligible. In the case of ethyl alcohol, which has a relatively larger vapor pressure, operating temperatures were restricted to values below 16C.

The high speed motion pictures of the periodic formation of gas bubbles revealed that the process of formation of a given bubble may be divided, for convenience, into the following two stages, each characterized by a certain period of time:

1. Beginning with the instant of detachment of a certain bubble, there was a period of time, referred to hereinafter as the "lapse time," during which there was gas flow into the reservoir or ante-chamber which supplied the orifice but no bubble (or convex interface) being formed at the orifice. The pressure in the ante-chamber increased during that time until a level was reached which initiated the formation of

the bubble under consideration.[1]

2. During what has been termed the "total formation time" the gas bubble increased in volume as gas flowed from the orifice into the bubble until it was detached from the orifice. The "total formation period" was therefore defined as the interval of time between the instant when the meniscus became visible above the orifice and the instant when the bubble was visibly detached from the orifice.

The total time associated with the formation of a given bubble is the sum of the lapse time and total formation time and is, of course, the reciprocal of the bubble frequency. The timing marks on the high speed motion pictures enabled an accurate determination of the lapse and total formation times for any given bubble.

It was found that for steady state operating conditions at a fixed mean gas flow rate, the frequency of formation of gas bubbles was reasonably constant, though small variations in the lapse time and total formation time of successive bubbles were observed ($\lesssim \pm 2\%$). The variation was probably due to small random changes in the motion of the liquid surrounding the bubbles as they formed and ascended from the orifice. An average of the lapse times and the total formation times for a series (usually 5) of consecutive bubbles was computed as representative of the particular steady state operating conditions. Reference hereafter to lapse time and total formation time should be taken to indicate the average values for a given run unless stated otherwise. In a few cases where the random variation of lapse and total formation times was large ($> \pm 5\%$), the average was computed for 10 consecutive bubbles. At higher mean gas flow rates ($\gtrsim 10$ cm^3/sec in water), an ordered variation of the lapse and total formation times, sometimes referred to as doubling and tripling (5,6) was observed. In such cases, there was a cyclic process of forming bubbles of two or three distinct types. For example, in the case of doubling, a bubble referred to as type 1 would be formed followed by a bubble of type 2 and then type 1 and so on. The lapse time and total formation time of a given type of bubble exhibited only a small, random variation about some average as previously mentioned in regard to the formation of a single type of bubble. Average values of the lapse and total formation times for each type of bubble were computed. Overall averages for the lapse and total formation times were also determined with equal weighting of each type of bubble. When such doubling or tripling occurred the overall average values were taken as representative of the particular steady state

[1] The termination of the lapse time has been defined as the instant when the meniscus first becomes visible above the orifice plane as observed on the high speed photographs. That definition is somewhat arbitrary because of the difficulty in detecting a minute motion of the meniscus.

operating conditions. However, care was taken in the choice of the operating conditions such that a single type of bubble was formed in most cases.

Since the mass flow rate of gas through the system was held constant for a given experiment and all of the gas entering the system was injected into the bubbles, the average mass of gas in a bubble was computed as the product of the mean mass flow rate of gas and the average total bubble time. The significance of the total formation time in regard to bubble formation with heat transfer was for determining the rate of energy transfer to a bubble.

Experiments for measuring all quantities pertinent to bubble formation were conducted both with and without heat transfer. Bubble formation with heat transfer, referred to hereinafter as "non-isothermal" bubble formation, was characterized by the existence of a significant difference between the temperature of the liquid, T_L, and the temperature of the gas entering the bubble, T_i ($T_L > T_i$). Bubble formation without heat transfer, referred to as "isothermal" bubble formation, was obtained by maintaining thermal equilibrium between the liquid and the gas entering the bubble ($T_L = T_i$). The results of the analysis in Section 3 show that the fact that T_L equals T_i does not ensure that the temperature of the gas in a bubble is constant during its formation. In fact, it is further shown that the strict attainment of the condition of isothermal bubble formation requires a certain amount of energy transfer to and from the gas in a bubble in accordance with the work done by or on the bubble as it forms. However, the magnitude of such energy transfer is small, and the net energy transfer for the entire formation period is essentially zero. Consequently, from the experimental point of view, bubble formation under the condition of overall thermal equilibrium, $T_L = T_i$, was assumed to be isothermal and, for all practical purposes, without heat transfer.

An experimental run was conducted as follows:

1. The heat exchanger was filled with the fluid appropriate for the type of bubble formation to be observed. (Liquid nitrogen for the non-isothermal case; water for the isothermal case)
2. The mass flow rate of gas through the system was set at a predetermined value which remained constant throughout the run.
3. The liquid container was filled with the desired liquid to a depth of 5 to 8 cm above the orifice.
4. Allowing a short interval of time to ensure steady state operation, the values of the gas mass flow rate, orifice inlet temperature, liquid temperature, and liquid head were recorded simultaneously while taking high speed photographs of the bubble formation process.

Experiments were conducted at selected values of gas mass flow rate over the maximum range giving steady, periodic bubble formation. The variation of the gas mass flow rate provided a range of the size of bubble produced. The use of orifices of 0.159 cm and 0.0795 cm in diameter and the use of plexiglass and teflon for constructing the orifices also provided a variation in the average total formation time. Such variation was considered essential since it was expected that the energy transferred to a bubble would be significantly influenced by the size of the bubble, the total formation time, and the rate of mass flow into the bubble.

For a given experimental run, the recorded data enabled the determination of:

1. T_L = liquid temperature
2. T_i = orifice inlet temperature
3. $\dot{W}_i$ = steady state mass flow rate of gas
4. t_l = average lapse time[1]
5. t_f = average total formation time[1]
6. $t_t = t_l + t_f$ = average total bubble time
7. $m_b = t_t \times \dot{W}_i$ = average terminal bubble mass
8. $p_b = p_{atm} + p_{hydrostatic} + p_{surface\ tension}$ = static bubble pressure
9. V_b = average terminal bubble volume

isothermal:
$$V_b = \frac{m_b \bar{R} T_L}{p_b}$$

non-isothermal: 1

In the case of the non-isothermal experiments, those primary quantities were used to calculate the mean temperature of the gas in the bubble at the end of the bubble formation period. Thus,

$$T_b = \frac{p_b V_b}{m_b \bar{R}} = \text{mean terminal bubble temperature.} \qquad (2.1)$$

[1] From the high speed motion pictures for five consecutive bubbles.

The fraction of the overall temperature difference remaining after bubble formation, referred to as the "unaccomplished temperature ratio", was determined as

$$Y_e = \frac{T_L - T_b}{T_L - T_i} \qquad (2.2)$$

The amount of energy transferred to a bubble during the time of formation was calculated by means of the following equation, derived in Appendix III,

$$E = m_b \, c_p \, (T_b - T_i) \qquad (2.3)$$

where c_p = constant pressure specific heat of the gas.
It is fully recognized that such an expression is based on the assumption that the energy transferred to the gas as it flows through the orifice is negligible. The amount of energy transferred to the gas as it flows through the orifice may be estimated on the basis of a heat transfer coefficient for the entrance region of a tube. It can be shown (44) that the increase in gas temperature in flowing through the orifice ($T_{\text{bubble in}} - T_i$) may be as much as 10C for most conditions, and possibly as high as 30C for the extremely low gas flow rates. Such temperature changes are really not of negligible magnitude. However, in view of the uncertainty in predicting the entrance region heat transfer coefficient, a correction for the change in gas temperature in flowing through the orifice was not introduced. Care was taken to minimize the length of the orifice channel ($\sim 2\ D_o$) consistent with the requirement that no liquid leak back into the ante-chamber. The orifice wall temperature was also kept at a minimum by maintaining the level of the liquid nitrogen around the base of the orifice body. The energy transfer to the gas in the bubble computed by means of equation 2.3 is referred to hereinafter as the "heat transfer during bubble formation" while recognizing the aforementioned limitation.

An average heat transfer coefficient for the bubble formation period was computed using equation 2.3 for the amount of energy transferred, a time-integrated average bubble surface area, and a log-mean temperature difference. Figure 4 illustrates one such plot from which a time-integrated average surface area, $\bar{A}$, was calculated. For each non-isothermal run, the average heat transfer coefficient was calculated by

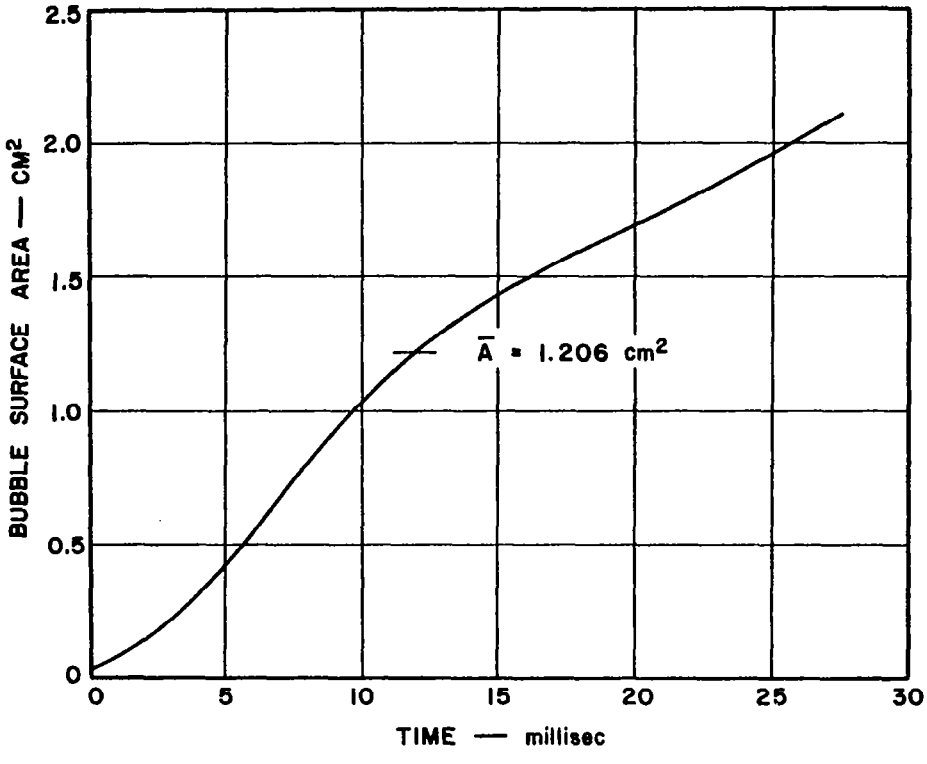

FIG. 4 BUBBLE SURFACE AREA DURING FORMATION

$$\bar{h} = \frac{m_b\, c_p\, (T_b - T_i)}{t_f\, \bar{A}\, \dfrac{(T_L - T_i) - (T_L - T_b)}{\ln \dfrac{T_L - T_i}{T_L - T_b}}}$$

which readily simplifies to

$$\bar{h} = \frac{m_b\, c_p\, \ln\left(\frac{1}{Y_e}\right)}{t_f\, \bar{A}} \qquad (2.4)$$

It was mentioned previously that experimental data were obtained for bubble formation under isothermal conditions and non-isothermal conditions. The experimental results for each type of bubble formation are presented individually in the two sub-sections that follow. A complete discussion of the results is presented in Section 4.

The experimental data pertaining to the details of bubble formation are presented individually in Section 2.4 and also discussed in Section 4.

2.2 Results for Isothermal Bubble Formation

In order to be able to isolate the effects of heat transfer on the bubble formation process, it was considered essential to determine initially the general bubble formation characteristics of the apparatus without any significant heat transfer to the gas bubbles. Such a condition could be obtained by maintaining thermal equilibrium between the liquid and the gas entering the bubble, ($T_L = T_i$), previously referred to as "isothermal" bubble formation. The bubble formation characteristics of a specific apparatus depend upon (a) the gas flow rate, (b) the physical properties of the liquid, (c) the orifice size, and (d) the volume of the ante-chamber (see Section 1.1.1). A convenient method of representing the bubble formation characteristics for a given liquid, orifice size, and ante-chamber volume is by means of the terminal volume of the bubbles formed as a function of the mean volumetric gas flow rate (the gas density does not significantly influence the process of bubble formation; see Section 1.1.1). It is necessary, in addition, to provide information regarding the total formation time and the lapse time; and those are also presented in the foregoing as functions of the steady state gas flow rate.

The physical properties of the liquid, particularly the viscosity and surface tension, can have an influence on the terminal volume of the bubbles produced for a given mean flow rate (7,25). However, with the operating temperature of the liquid being the same for both the isothermal and non-isothermal cases in the present investigation, the physical properties of the liquid phase remained constant for each liquid; and their effect on the bubble formation process was expected to be essentially the same for both the isothermal and the non-isothermal cases.[1]

As was mentioned previously, experimental data were obtained using distilled water and ethyl alcohol as liquids and dry nitrogen as the gas, while employing orifices made from plexiglass and teflon. The various combinations of operating conditions employed both in the isothermal and the non-isothermal cases are presented in Table 1. The isothermal bubble formation characteristics of the various systems are discussed individually in the remainder of this section.

Table 1

Systems for Bubble Formation

System	Liquid	Gas	Orifice	D_o	L/D_o
I	Dist.water	N_2	plexiglass	0.159 cm	2
II	Dist.water	N_2	teflon	0.159 cm	2
III	Ethyl Alcohol	N_2	teflon	0.159 cm	2
IV	Dist.water	N_2	plexiglass	0.0795 cm	2

Figure 5 illustrates the formation of a bubble under isothermal conditions, employing system I (see Table 1), as observed by means of high speed photography. Figure 6 shows a plot of the bubble volume as a function of the normalized formation time obtained from the photographs illustrated in Fig. 5. The case illustrated was for $\dot{q}_i = 3.2$ cm³/sec.

[1] Such would not be the case where an overall temperature difference for heat transfer was produced by heating the liquid.

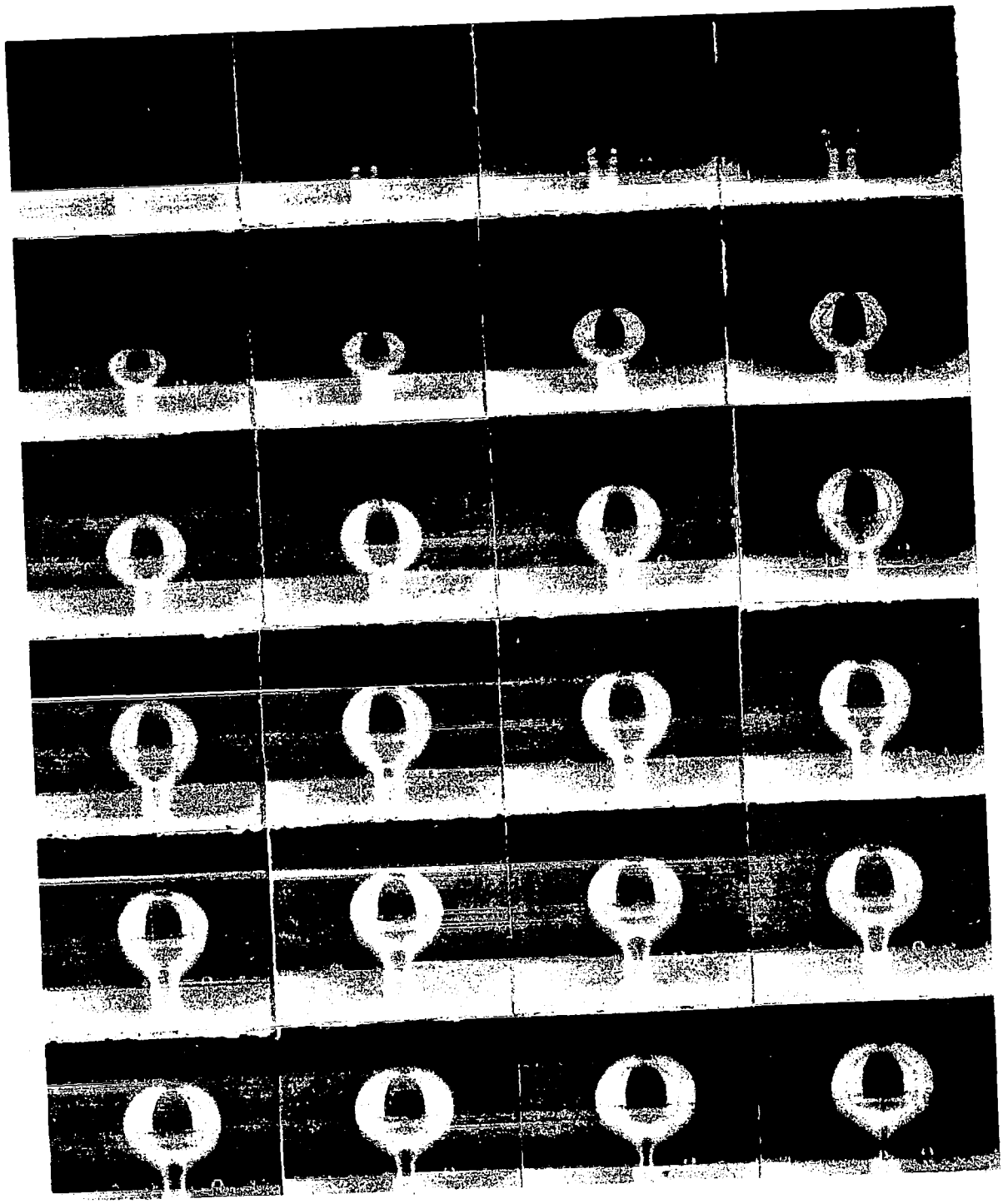

RUN I-14 2820 FR/SEC

FIG. 5 PHOTOGRAPHIC RECORD OF ISOTHERMAL BUBBLE FORMATION

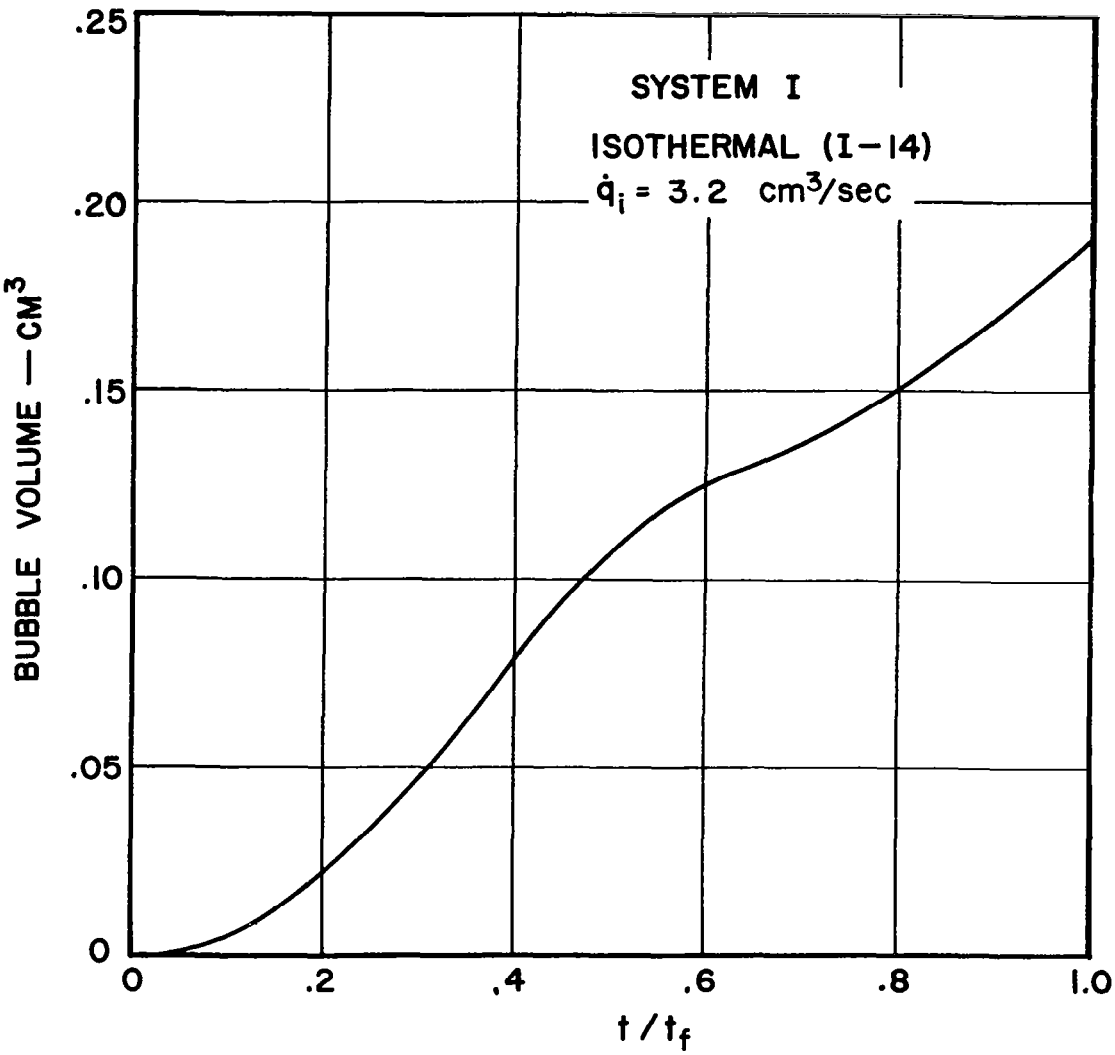

FIG. 6 ISOTHERMAL BUBBLE GROWTH (SYSTEM I)

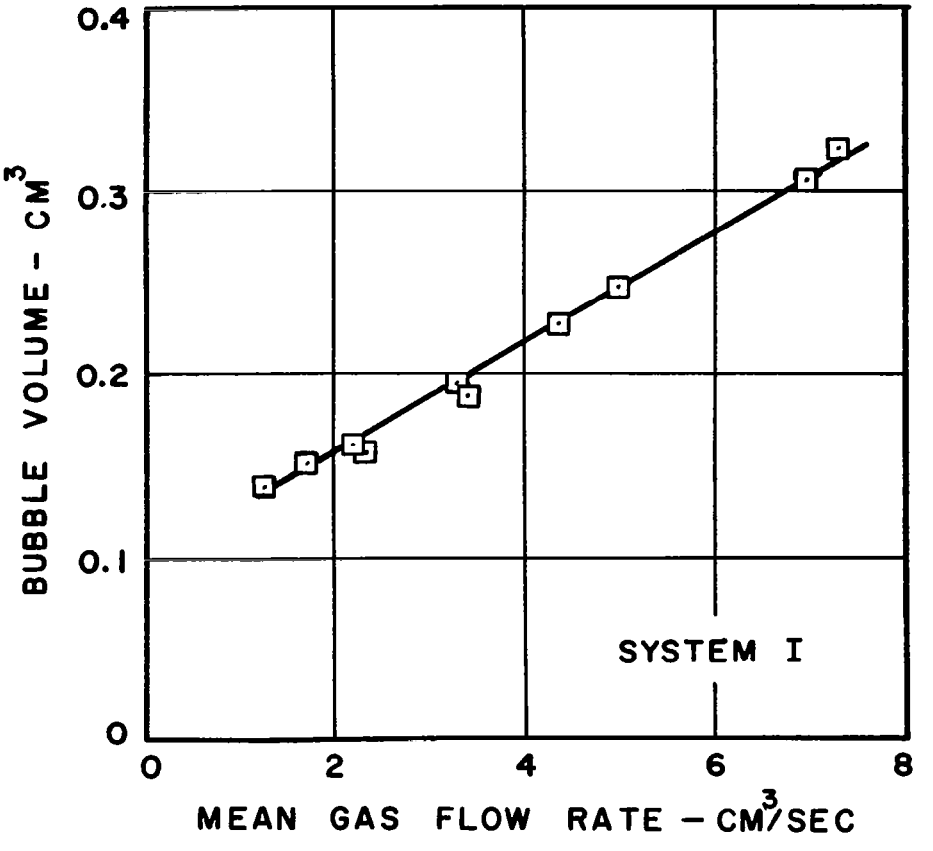

FIG. 7 TERMINAL BUBBLE VOLUME FOR ISOTHERMAL FORMATION (SYSTEM I)

Figure 7 illustrates a plot of the average terminal bubble volume, V_b, as a function of the mean volumetric gas flow rate, $\dot{q}_i$, for the isothermal bubble formation employing System I. As can be seen, there existed a linear relationship between V_b and $\dot{q}_i$ over the range of flow rates which was found to result in the steady, periodic formation of a single type of gas bubbles. Above a flow rate of approximately 8.5 cm³/sec an alternate formation of two distinct types of bubbles (doubling) was observed. The investigation was restricted to the range of $\dot{q}_i$ wherein a single type of bubble was formed.

The bubble formation characteristics of the aforementioned system (I) are further illustrated in Figs. 8 and 9 which present the average total formation time, t_f, and the average lapse time, t_l, as functions of the mean gas flow rate. It is interesting to note that t_f was very nearly constant, decreasing slightly with increasing $\dot{q}_i$. Surprisingly, the terminal volume of the bubbles produced was essentially independent of the time required for the formation of the bubbles as seen by a comparison of Figs. 7 and 8. For the range of flow rate of 2 to 7 cm³/sec, the terminal bubble volume increased by 94%, whereas the total formation time decreased by less than 11%.

As previously defined, the lapse time, t_l, depicts the interval of time during which the pressure in the ante-chamber increased to a level sufficient to initiate the formation of a bubble. Consequently, t_l is plotted as a function of the mean mass flow rate of the gas, $\dot{W}_i$, since the increase in the ante-chamber pressure was dependent upon the mass of gas stored therein. If one considers the isothermal flow of a perfect gas into the "closed" ante-chamber,[1] the rate of change of

$$\frac{dp_c}{dt} = \frac{\bar{R}T}{V_c} \frac{dm}{dt}$$

Since the mass flow into the system was constant,

$$\frac{dp_c}{dt} = \frac{\bar{R}T_c}{V_c} \dot{W}_i = \text{constant}$$

From the preceding expression it is apparent that the time required to increase the ante-chamber pressure to the level sufficient to initiate bubble formation is given by

[1] Since there was no bubble forming during the lapse time the ante-chamber was essentially closed to outflow during that time.

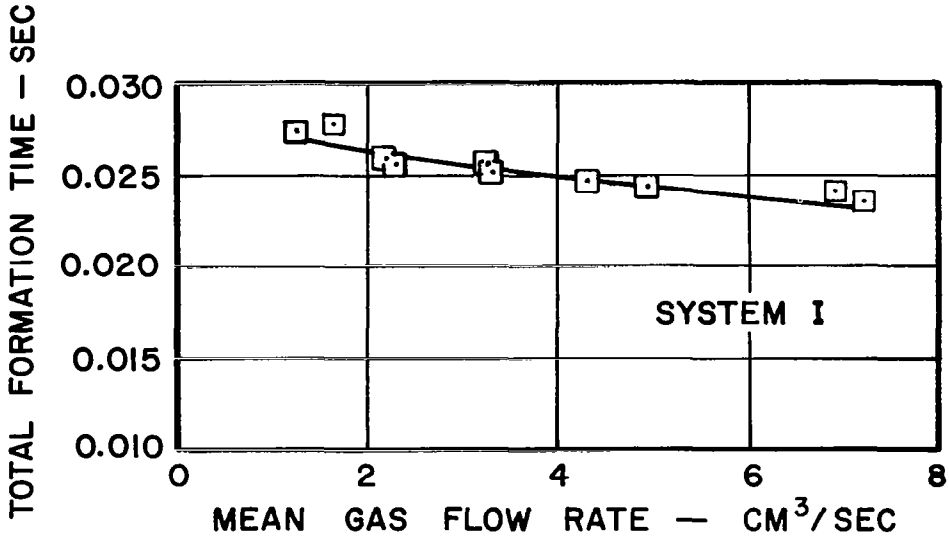

FIG. 8 TOTAL FORMATION TIME FOR ISOTHERMAL FORMATION (SYSTEM I)

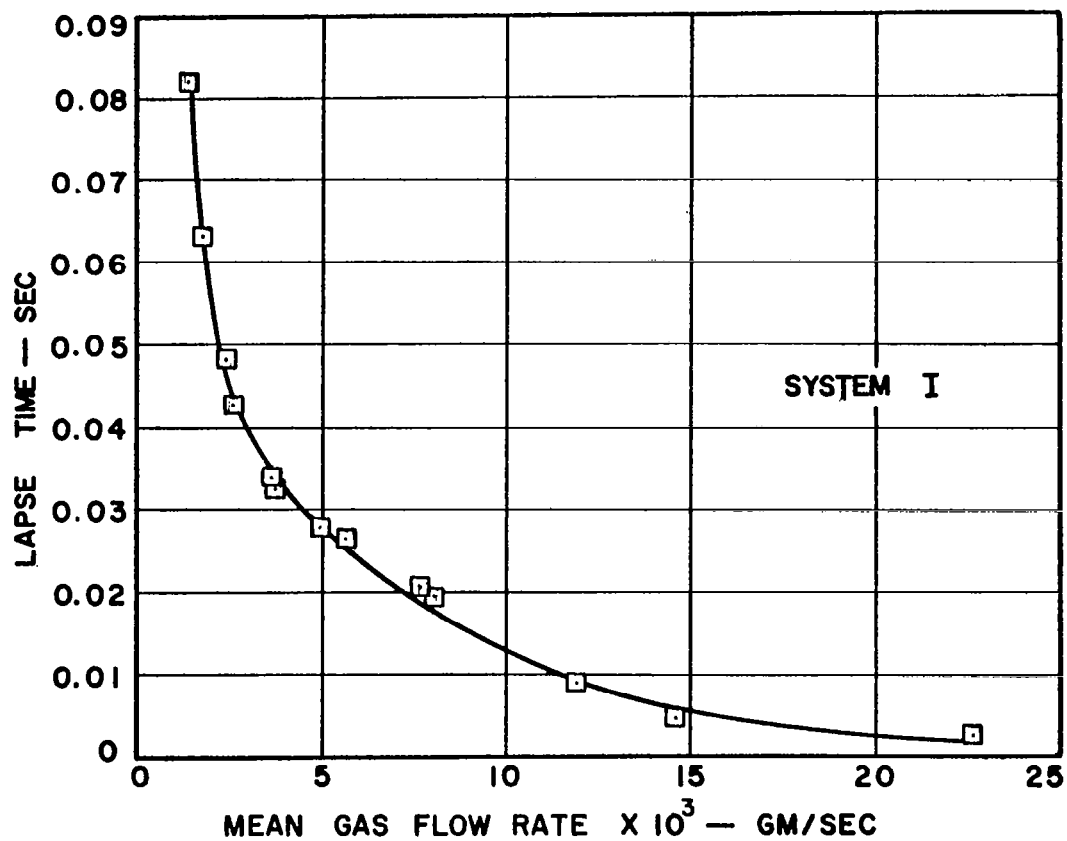

FIG. 9 LAPSE TIME FOR ISOTHERMAL FORMATION (SYSTEM I)

$$t_l = \frac{V_c}{\bar{R}T_c} \quad \frac{p_f}{\dot{W}_i} \tag{2.5}$$

where

p_f = increase in ante-chamber pressure required to initiate bubble formation

$\dot{W}_i$ = steady state gas mass flow rate

V_c = volume of the ante-chamber

T_c = temperature of gas in the ante-chamber

$\bar{R}$ = gas constant

From equation 2.5, one expects the lapse time for a given system to vary according to

$$t_l \propto \frac{p_f}{\dot{W}_i} \tag{2.6}$$

The inverse dependence of t_l on $\dot{W}_i$ is illustrated in Fig. 9. Additional data for flow rates beyond the range of interest ($\dot{W}_i > 9 \times 10^{-3}$ gm/sec) have been included to illustrate that t_l decreased nearly to zero as $\dot{W}_i$ was increased. It should be pointed out that p_f would be expected to depend upon the liquid being used in relation to its wetting characteristics, the orifice size, and, perhaps, the mean gas flow rate.

Figures 10, 11, and 12 similarly illustrate the isothermal bubble formation characteristics for System II (see Table 1). Figure 10 shows that the range of $\dot{q}_i$ for which there was a linear relationship between V_b and $\dot{q}_i$ was approximately 3 to 6.5 cm^3 sec. Above a flow rate of approximately 6.5 cm^3/sec the alternate formation of different types of bubbles (doubling) was observed. A comparison of Figs. 7 and 10 illustrates that the difference in the material with which an orifice was constructed resulted in as much as a 25 percent change in V_b; however, the change of V_b with $\dot{q}_i$ was essentially the same.

It can be observed in Fig. 11 that the total formation time for System II exhibited a much stronger dependence upon $\dot{q}_i$ than was observed for System I. The purpose of employing orifices constructed of different materials was indeed to enable such variation in the types of bubble formation observed.

The inverse dependence of the lapse time, t_l, upon the steady state mass flow rate, $\dot{W}_i$, was again observed as illustrated in

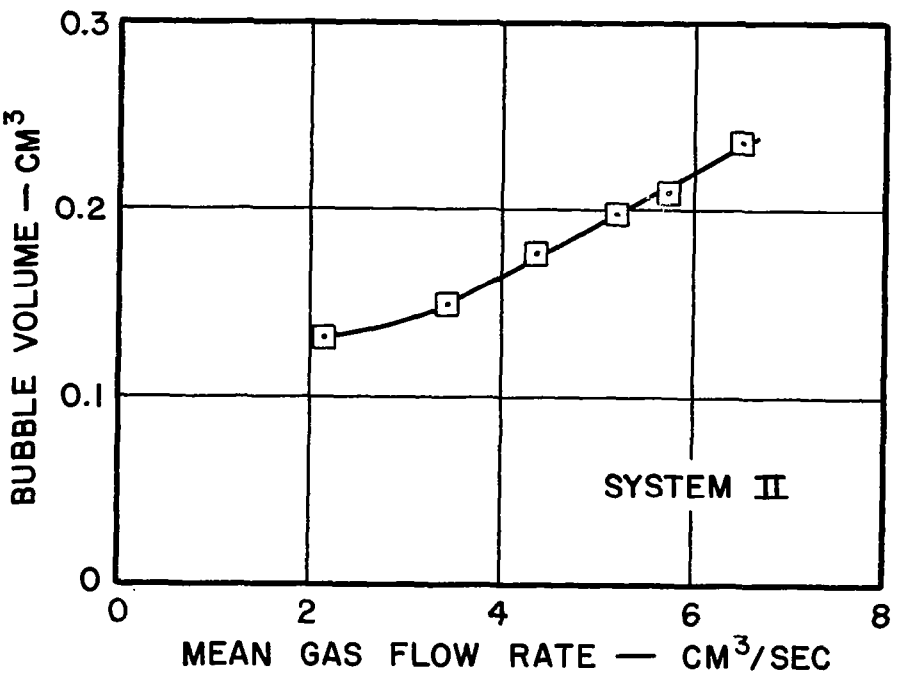

FIG. 10 TERMINAL BUBBLE VOLUME FOR ISOTHERMAL FORMATION (SYSTEM II)

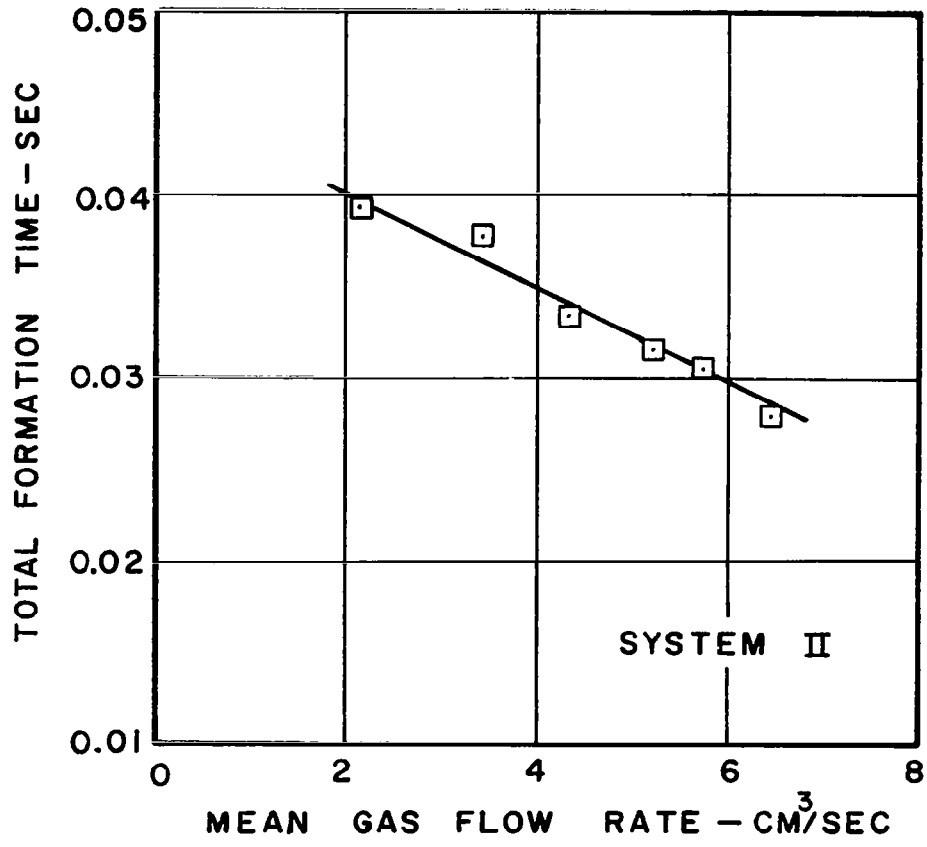

FIG. 11 TOTAL FORMATION TIME FOR ISOTHERMAL FORMATION (SYSTEM II)

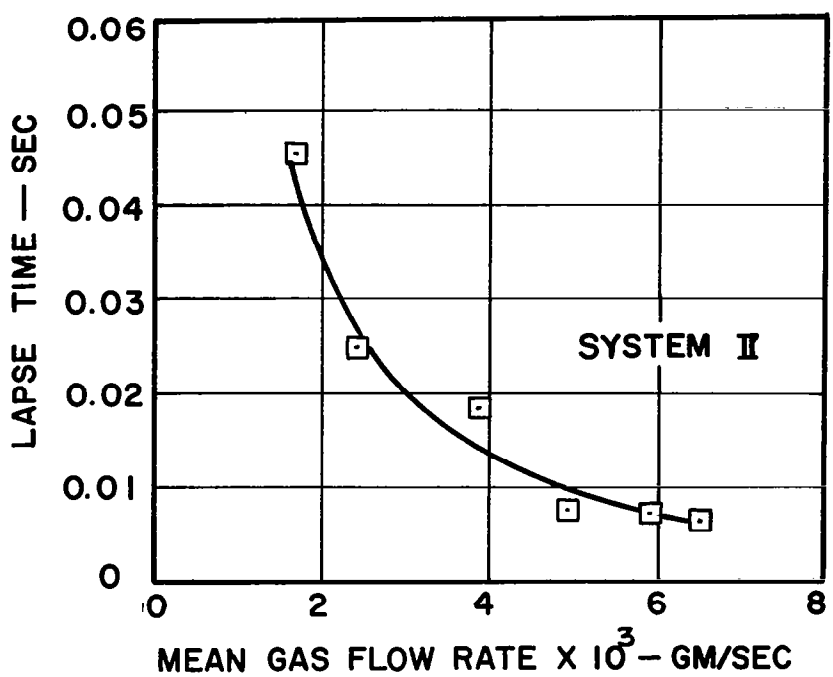

FIG. 12 LAPSE TIME FOR ISOTHERMAL FORMATION (SYSTEM II)

Fig. 12. Comparing Figs. 9 and 12, it is observed that the magnitude of t_l for a given W_i also depended upon the orifice material through its influence on the increase in ante-chamber pressure required to initiate bubble formation. The teflon orifice, which apparently was not wetted by water, resulted in a p_f smaller than that for the plexiglass orifice (apparently wetted). (see discussion in Section 2.4.2).

Further variation in the type of bubble formation was obtained by employing System III (see Table 1). Because of the relatively higher vapor pressure of ethyl alcohol, the isothermal experiments were conducted with the liquid and gas maintained at 16C in order to insure a negligible transfer of liquid vapor to the gas bubbles. In general, the process of bubble formation in ethyl alcohol was much less regular than that in water. The variation of t_f for the individual bubbles from the average value of t_f was less than ± 2 percent in ethyl alcohol, which was comparable to that observed for the previous systems with water. However, the variation of t_l for the individual bubbles from the average value of t_l was as high as ± 20 percent. Such characteristics may probably be attributed to the low value of surface tension for ethyl alcohol.

Figure 13 illustrates the variation of the average terminal bubble volume with the flow rate. The variation, as may be observed, is linear similar to the relation for the other systems. The alternate formation of different types of bubbles (doubling) was observed at a flow rate as low as 3.4 cm^3/sec.

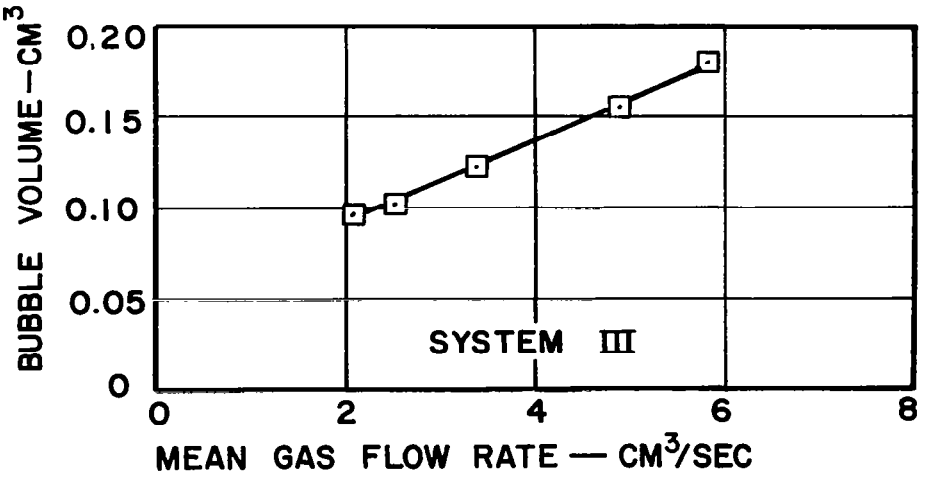

FIG. 13 TERMINAL BUBBLE VOLUME FOR ISOTHERMAL FORMATION (SYSTEM III)

Figure 14 shows that the bubble formation performance of System III was markedly different from that of System II (Fig. 11) due to the different liquid employed. For System III, t_f was practically constant over the range of 1 to 5.8 cm^3/sec. Upon comparison of Figs. 8 and 14, one observes that the values of t_f for the teflon orifice in ethyl alcohol (System III) were nearly equal to those for the plexiglass orifice in water (System I). One may perhaps attribute that to the fact that ethyl alcohol, with its low surface tension, may have wetted teflon in the same manner as water wetted plexiglass.

Figure 15 shows the inverse dependence of the lapse time, t_l, on the mean gas mass flow rate for System III. Overall average values of t_l are plotted, but as previously mentioned there was considerable variation from bubble to bubble.

The general bubble formation characteristics of the apparatus employing a 0.0795 cm diameter orifice, System IV (see Table 1), are not presented, but the quantitative heat transfer data obtained with that orifice are included in Section 2.3.2. The experimental data for isothermal bubble formation presented illustrate the characteristics of the apparatus for forming bubbles for the three different systems. These data will be used as the norm for comparison with similar data obtained under non-isothermal conditions to determine the effect of heat transfer on the formation of gas bubbles.

2.3 Results for Non-Isothermal Bubble Formation

The primary purpose of the investigation was to determine what effect the non-isothermal conditions had upon the temperature of the gas in the bubble and upon the general formation of the bubble. The mean temperature of the gas in a bubble was determined by employing the technique described in Section 2.1.3. Since the gas bubbles formed under non-isothermal conditions were formed using the same apparatus as that for obtaining the isothermal data reported in Section 2.2, and since the liquids utilized for obtaining the non-isothermal bubble formation data had the same physical properties as those utilized for obtaining the isothermal bubble formation data, the differences between the bubble formation characteristics for non-isothermal and isothermal bubble formation were attributed entirely to the heat transfer to the bubbles.[1] All of the different types of bubble formation

[1] As noted in Section 1.1.1, the difference between the temperature of the gas in the ante-chamber for the isothermal and non-isothermal cases does not affect the characteristics of the apparatus.

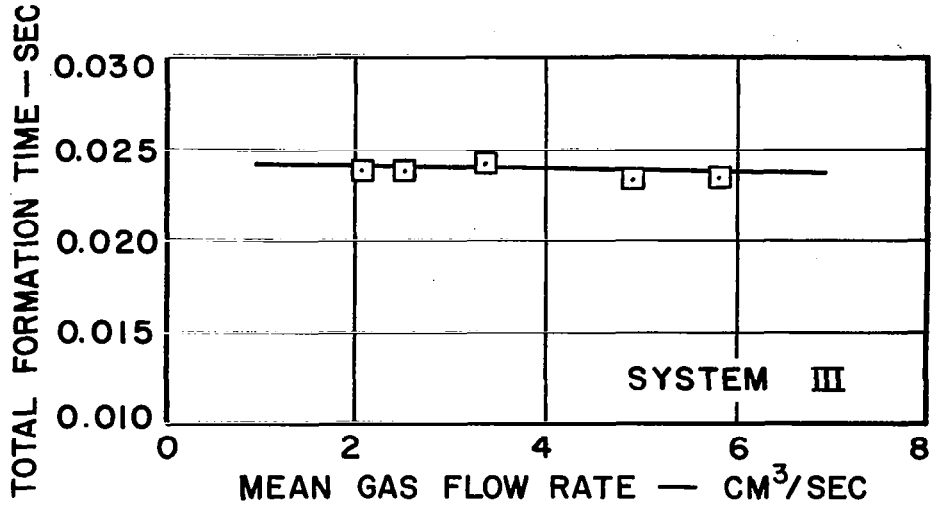

FIG. 14 TOTAL FORMATION TIME FOR ISOTHERMAL FORMATION (SYSTEM III)

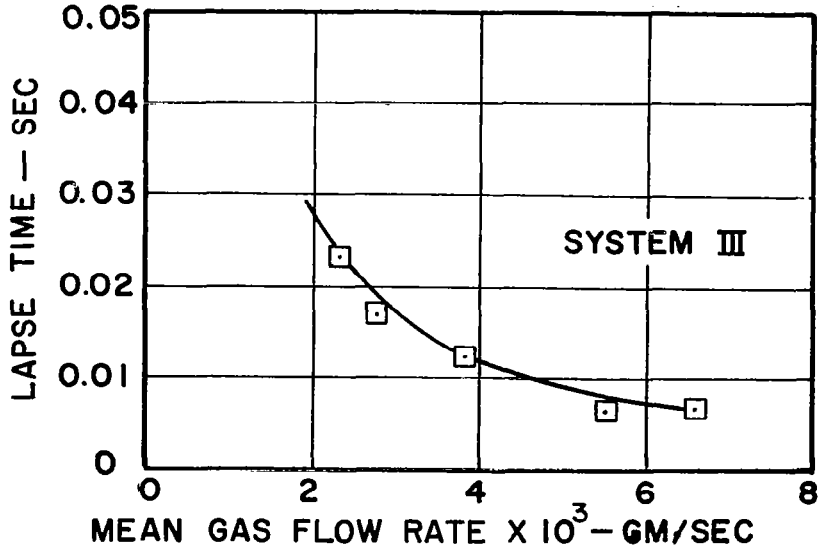

FIG. 15 LAPSE TIME FOR ISOTHERMAL FORMATION (SYSTEM III)

conditions, as described in Section 2.2, Table 1, were investigated under non-isothermal conditions to determine the influence on the heat transfer to the bubbles of the parameters pertinent to the processes occurring within the bubbles.

The experimental results for the investigation of non-isothermal bubble formation are presented in two parts: (a) the general bubble formation characteristics which, when compared with the results in Section 2.2, indicate the effect of heat transfer upon bubble formation, and (b) the quantitative heat transfer data indicating the change in temperature of the gas in the bubble during formation and the rate of heat transfer to the bubble as it formed.

2.3.1 General Bubble Formation Characteristics

Figure 16 presents a plot of the average terminal bubble volume, V_b,[1] as a function of the mean volumetric gas flow rate, $\dot{q}_i$, for the case of the non-isothermal formation with System I (see Table 1). The mean volumetric gas flow rate was based on the temperature (~ 150K) of the gas entering the orifice. With the water maintained at 21 C, the overall temperature difference (T_L-T_i) was approximately 144C (260F). The dotted line in Fig. 16 represents the experimental data obtained with System I under isothermal bubble formation (Fig. 7); and, as can be seen, V_b was considerably larger for the non-isothermal case. The linear relationship between V_b and $\dot{q}_i$ was still present in the non-isothermal case, with the bubble formation being regular and the bubbles very nearly of spherical shape over the entire range of flow rates considered. Figure 17 illustrates the formation of a bubble under non-isothermal conditions as observed by means of high speed photography. Figure 18 shows a plot of the bubble volume as a function of the normalized total formation time obtained from the photographs illustrated in Fig. 17. The case illustrated was for $\dot{q}_i = 3.1$ cm^3/sec.

At this point it is interesting to consider the volume which the bubbles obtained during the non-isothermal formation would occupy if there had been no heat transferred to the gas bubbles as they formed (i.e., no thermal expansion). The value of the "unheated" bubble volume is calculated, for example, as the volume that a given bubble mass would occupy if there was no change in the temperature of the gas in the bubble during the time of formation.[2] Thus,

$$V_i = V_b \frac{T_i}{T_b} \qquad (2.7)$$

---

[1] Obtained by means of high speed photography as described in App. III.

[2] It was assumed that there was no change in the gas temperature in flowing through the orifice.

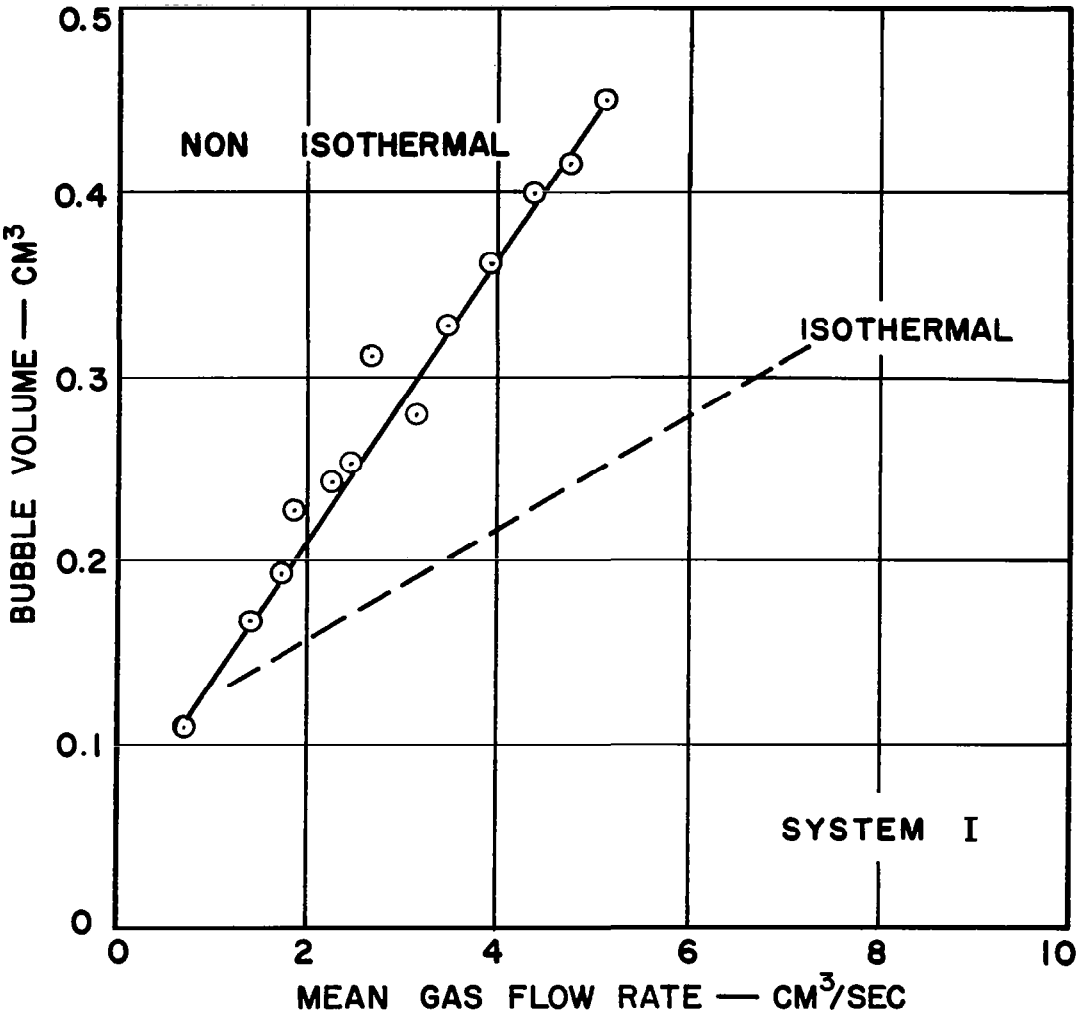

FIG. 16 TERMINAL BUBBLE VOLUME FOR ISOTHERMAL AND NON-ISOTHERMAL FORMATION (SYSTEM I)

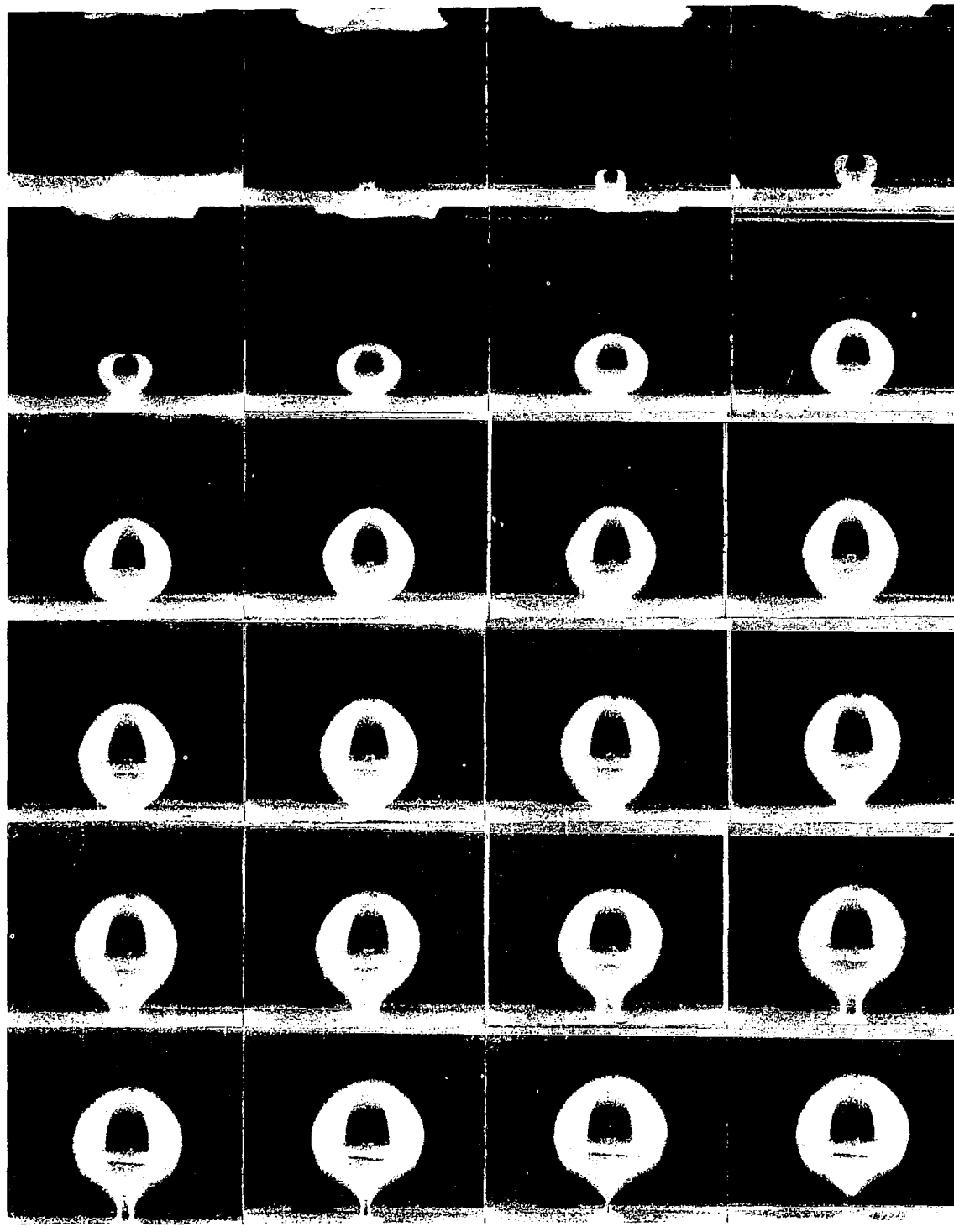

RUN H-18 2880 FR/SEC

FIG. 17 PHOTOGRAPHIC RECORD OF NON-ISOTHERMAL BUBBLE FORMATION

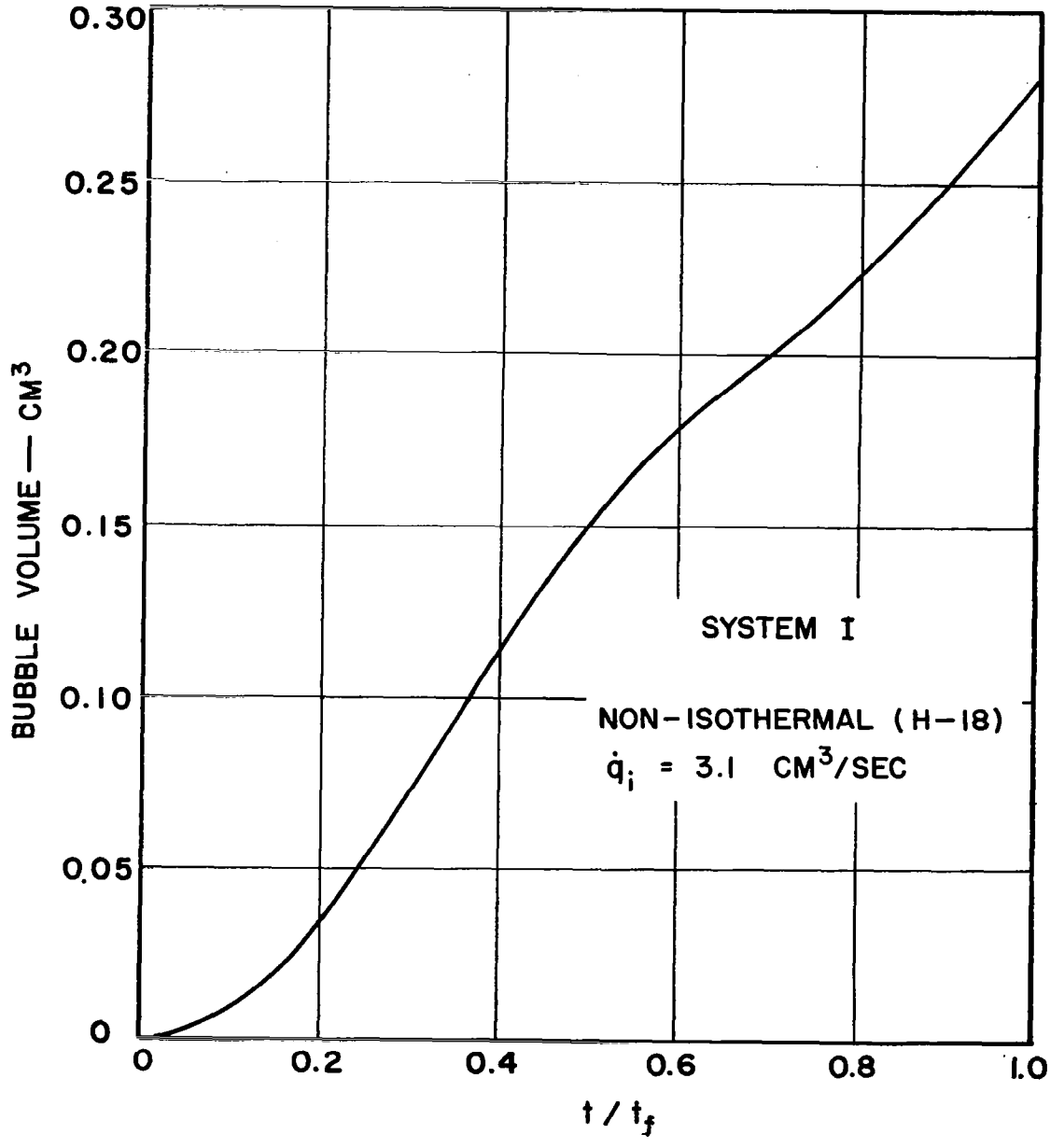

FIG. 18 NON-ISOTHERMAL BUBBLE GROWTH (SYSTEM I)

where

V_i = "unheated" bubble volume

V_b = terminal bubble volume obtained for non-isothermal formation

T_i = absolute temperature of gas entering the orifice

T_b = calculated mean temperature of the gas in V_b (see equation 2.1)

A plot of the calculated "unheated" bubble volume, V_i, as a function of $\dot{q}_i$ is presented in Fig. 19. The actual experimental data obtained under the isothermal conditions given earlier in Fig. 7 are also shown in Fig. 19. As can be seen, the calculated unheated bubble volume for a given value of mean volumetric gas flow rate was not markedly different from that obtained under isothermal conditions. Below a flow rate of approximately 3.2 cm^3/sec, the calculated values for V_i were less than the isothermal values for V_b by as much as 35 percent at the lowest flow rate. For flow rates above 3.2 cm^3/sec, V_i was somewhat larger but was within 10 percent of $V_{b_{iso}}$. Thus, the volume of gas passed through the orifice into the bubbles in the non-isothermal case was not markedly different from the volume of gas passed into the bubbles in the isothermal case for sufficiently large volumetric flow rates.

At the point of intersection of the two curves in Fig. 19 ($\dot{q}_i \sim 3.2$ cm^3/sec), the volume of gas passed from the ante-chamber into the bubbles in the non-isothermal case was exactly equal to the volume of gas passed into the bubbles in the isothermal case. It was then assumed that at a mean gas flow rate of approximately 3.2 cm^3/sec, the instantaneous volumetric rate of gas flow into the bubbles was also approximately the same for both the non-isothermal and isothermal cases. The experimentally determined value of bubble volume as a function of time during formation for isothermal and non-isothermal formation were given in Figs. 6 and 18, respectively, for a mean volumetric gas flow rate of approximately 3.2 cm^3/sec. Those data are presented together in Fig. 20 for convenience. The difference between the instantaneous values of the bubble volumes in Fig. 20 can therefore be attributed to thermal expansion due to heat transfer in the non-isothermal case.

The average total formation time with System I is presented as a function of $\dot{q}_i$[1] in Fig. 21. The dotted curve represents the data obtained for the same system under isothermal conditions

[1] Evaluated at the temperature of the gas entering the orifice.

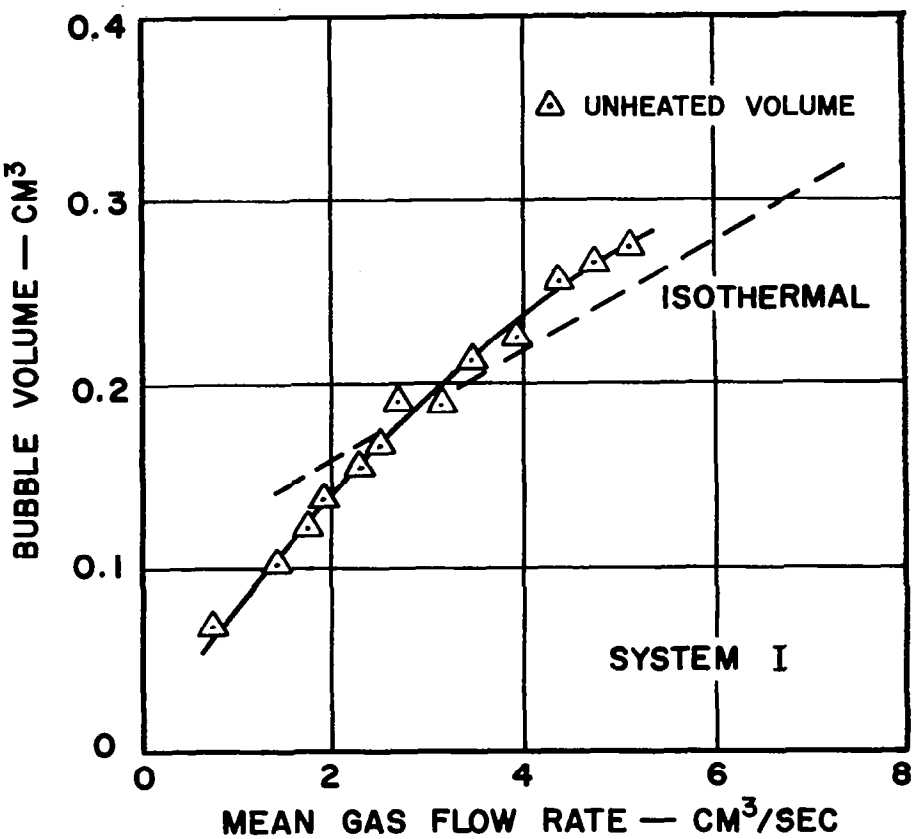

FIG. 19 COMPARISON OF UNHEATED AND ISOTHERMAL BUBBLE VOLUME (SYSTEM I)

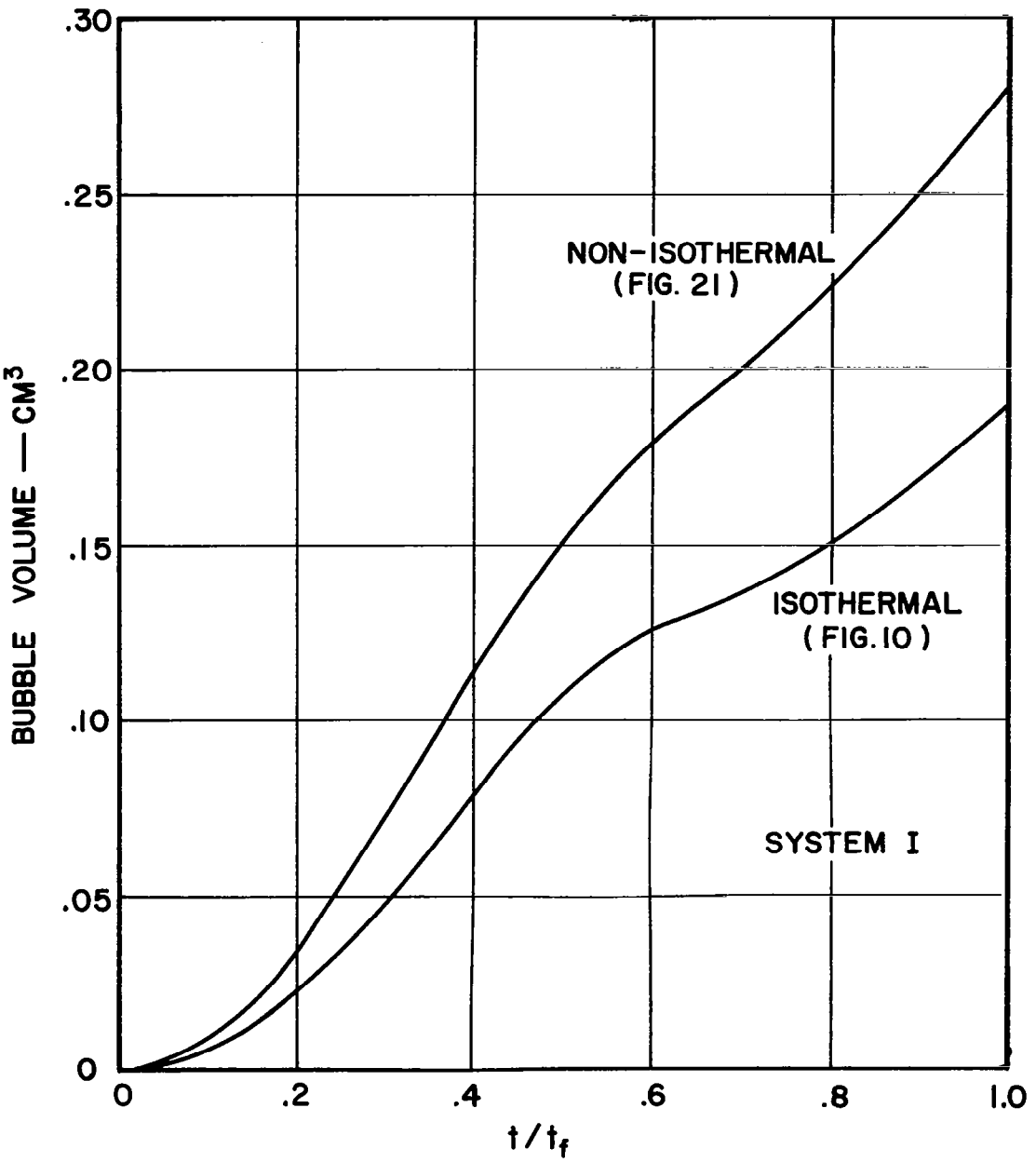

FIG. 20 COMPARISON OF ISOTHERMAL AND NON-ISOTHERMAL BUBBLE GROWTH (SYSTEM I)

(see Fig. 8). It is apparent that the total formation time for the non-isothermal conditions was approximately 7 to 10 percent larger than for the isothermal conditions, while decreasing slightly with increasing $\dot{q}_1$.

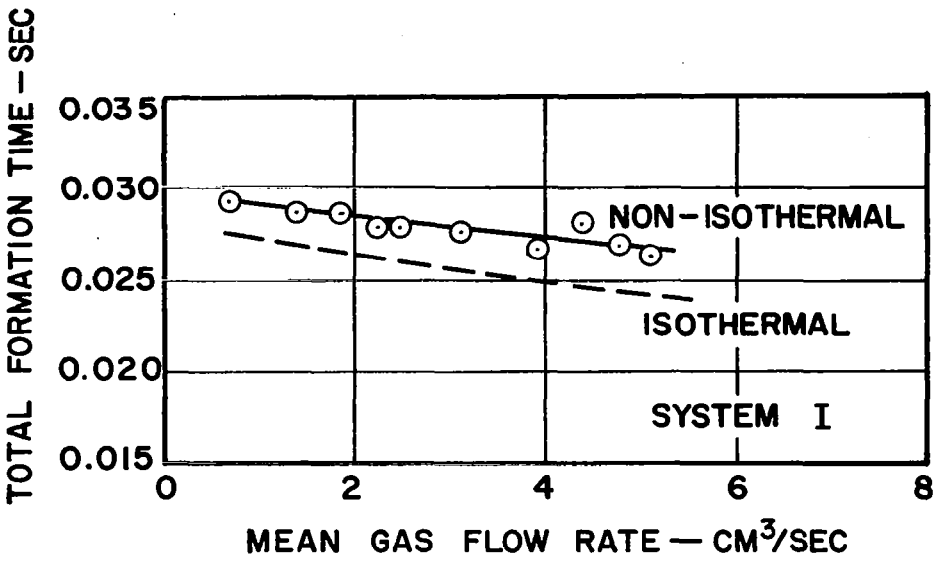

FIG. 21 TOTAL FORMATION TIME FOR ISOTHERMAL AND NON-ISOTHERMAL FORMATION (SYSTEM I)

Figure 22 demonstrates qualitatively that the lapse time was dependent upon changes in the ante-chamber pressure. The dotted line again represents the data for isothermal formation (Fig. 9). The difference between the values of the lapse time, for a given mean mass flow rate, for the non-isothermal and the isothermal cases is, of course, due both to the changes in the pressure in the ante-chamber and to the different absolute temperatures of the gas in the ante-chamber. Note that the gas in the non-isothermal case was precooled about 144C (260F) below the temperature of the gas for the isothermal case.

Results similar to those just discussed for System I were also obtained for the two other bubble formation systems, II and III, (see Table 1).

Figures 23 and 24 present the data obtained for the non-isothermal formation employing System II ($T_i \sim 122K$; $T_L \sim 21C$), with an overall temperature difference of approximately 172C (310F). The terminal bubble volume, V_b, is presented as a function of the mean volumetric gas flow rate, $\dot{q}_i$,[1] in Fig. 23. The data obtained for isothermal bubble formation (from Fig. 10) as well as the "unheated" bubble volume, V_i, are also illustrated for comparison. As before, the terminal bubble volume for the non-isothermal case was considerably larger than that obtained for the isothermal case for a given value of $\dot{q}_i$. The linear relationship between V_b and $\dot{q}_i$ is apparent. However, the calculated values of the "unheated" bubble volume were considerably less, by as much as 41 percent at the lowest flow rate, than the values of V_b obtained under isothermal conditions for most of the range of $\dot{q}_i$. Furthermore, it was observed that above a flow rate of approximately 4.5 cm^3/sec (7 cm^3/sec for the isothermal case) an alternate formation of two types of bubbles (doubling) occurred.

Figure 24 illustrates the total formation time, t_f, as a function of $\dot{q}_i$ for both the non-isothermal and isothermal (Fig. 11) cases for System II. Each case exhibits the same general trend of variation of t_f with $\dot{q}_i$; however, t_f for the non-isothermal case was consistently 9 percent (approximately) smaller than that for the isothermal case, a trend opposite to that for System I.

The results for the non-isothermal formation of nitrogen bubbles in ethyl alcohol, System III (see Table 1), are presented in Figs. 25 and 26. In that case, an overall temperature difference of approximately 150C (270F) was obtained with an orifice inlet temperature of $T_i \sim 139K$ and a liquid temperature of $T_L \sim 16C$.

As in the previous cases, Fig. 25 shows that the terminal bubble volume for non-isothermal bubble formation in ethyl alcohol was considerably larger than that obtained under isothermal conditions (from Fig. 13), apparently due to the thermal expansion in the former case. Again, it was found that in the non-isothermal bubble formation the flow rate at which the alternate formation of two types of bubbles commenced was lower than that for the isothermal case. Doubling was observed at $\dot{q}_i \sim 2$ cm^3/sec in the non-isothermal case. In general, the non-isothermal bubble formation in ethyl alcohol was very irregular compared to that in water, as mentioned in Section 2.2. It is also shown in Fig. 25 that the calculated "unheated" bubble volume was consistently less than the isothermal bubble volume by as much as 10 to 25 percent.

---

[1] Based on the temperature of the gas entering the orifice.

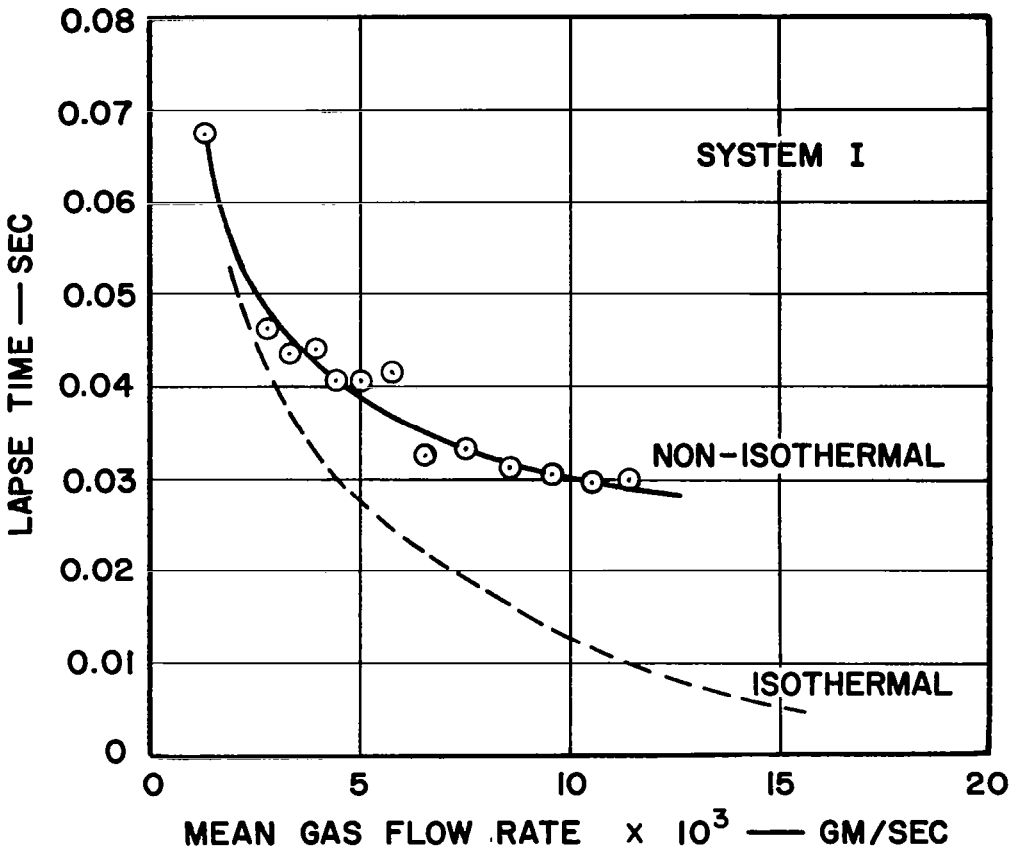

FIG. 22 LAPSE TIME FOR NON-ISOTHERMAL AND ISOTHERMAL FORMATION (SYSTEM I)

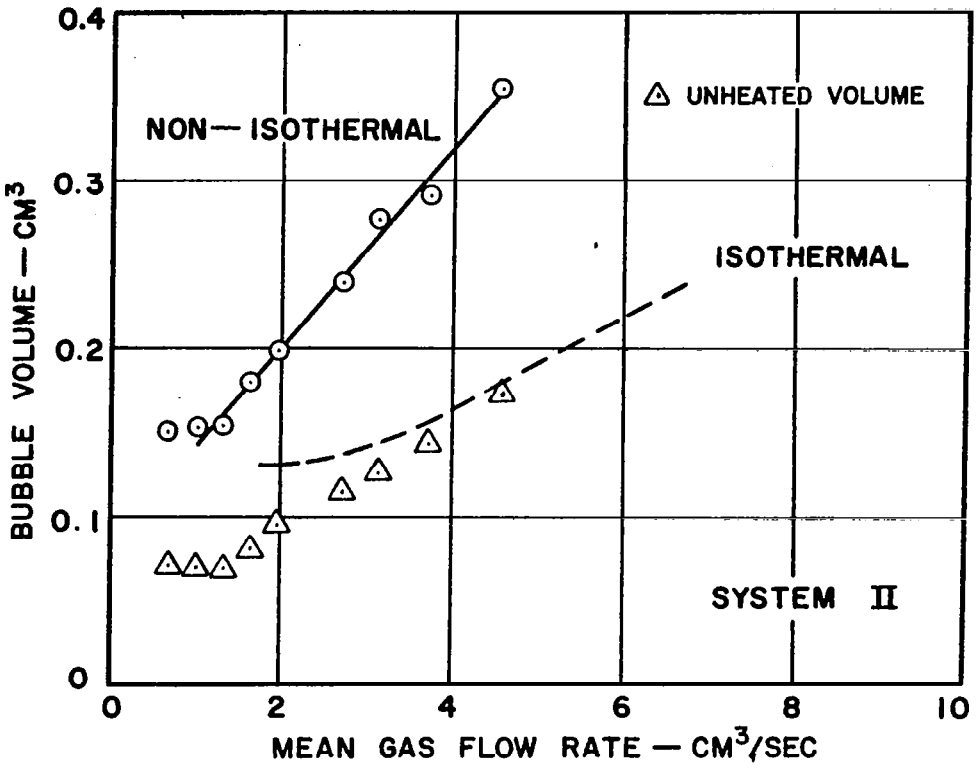

FIG. 23 COMPARISON OF BUBBLE VOLUME FOR NON-ISOTHERMAL AND ISOTHERMAL FORMATION (SYSTEM II)

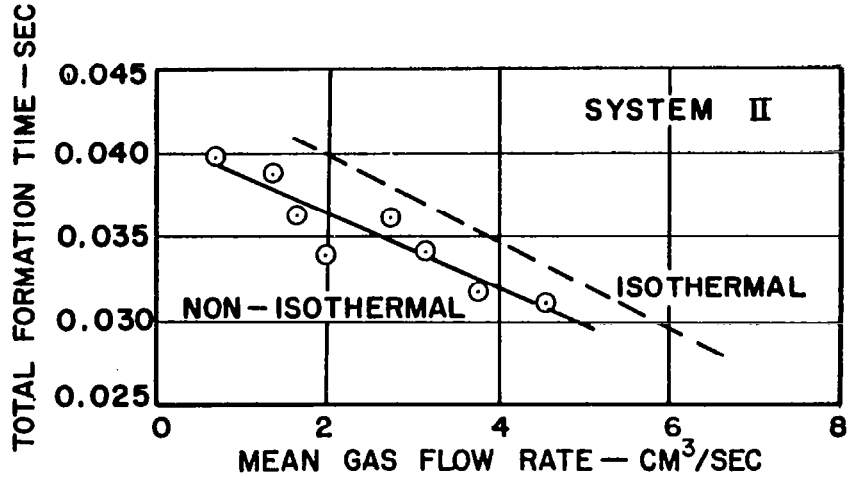

FIG. 24 TOTAL FORMATION TIME FOR ISOTHERMAL AND NON-ISOTHERMAL FORMATION (SYSTEM II)

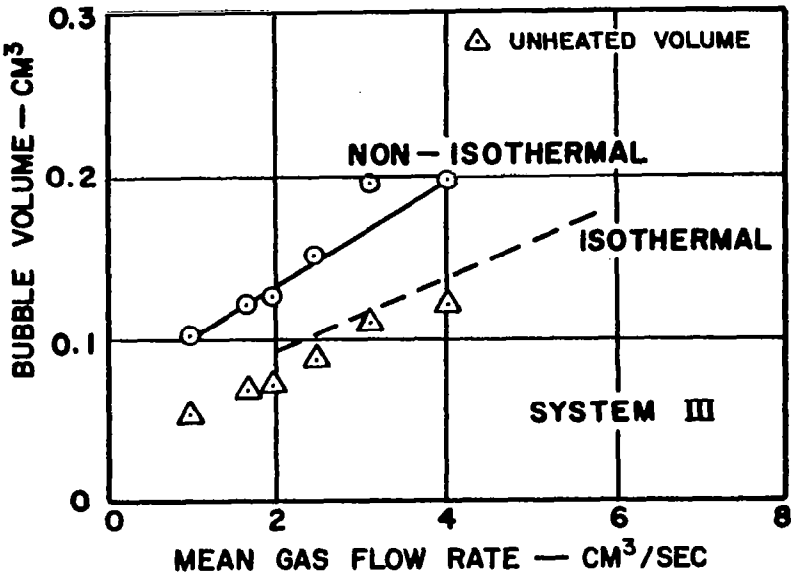

FIG. 25 COMPARISON OF BUBBLE VOLUME FOR NON-ISOTHERMAL AND ISOTHERMAL FORMATION (SYSTEM III)

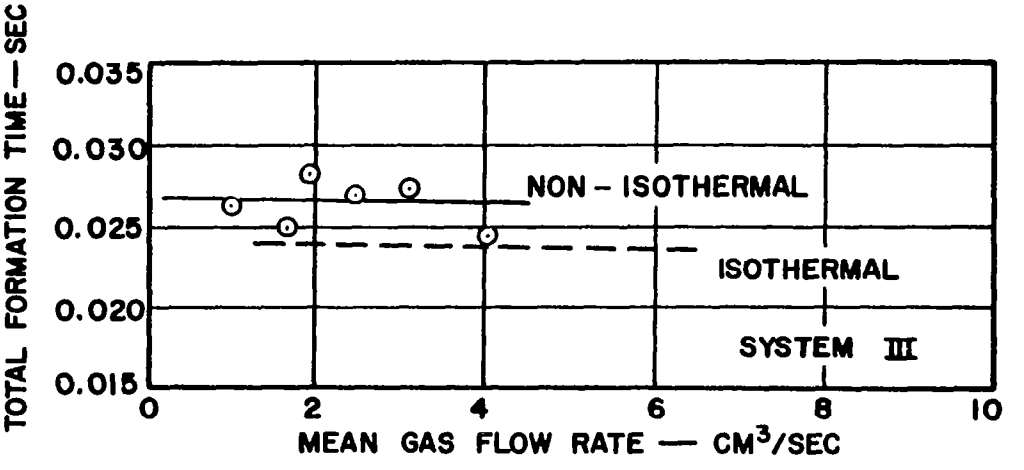

FIG. 26 TOTAL FORMATION TIME FOR NON-ISOTHERMAL AND ISOTHERMAL FORMATION (SYSTEM III)

Figure 26 illustrates that the average total formation time for the non-isothermal bubble formation remained approximately constant throughout the range of $\dot{q}_i$, as for the isothermal case (from Fig. 14), and was approximately 6 to 7 percent higher. The same trend was observed in System I.

The general bubble formation characteristics of the apparatus employing a 0.0795 cm diameter orifice, System IV (see Table 1), are not presented; but the quantitative heat transfer data obtained with that orifice are included in Section 2.3.2.

The aforementioned results pertaining to the general characteristics of non-isothermal bubble formation for the three systems considered indicate the following differences between non-isothermal and isothermal bubble formation while the apparatus characteristics were held substantially identical in the two cases.

1. The thermal expansion of the gas in a bubble as a result of heat transfer during bubble formation in the non-isothermal case increased the effective volumetric rate of growth of the bubble above that in the isothermal case. Irregularities in the bubble formation process occurred at lower values of mean volumetric gas flow rate in the non-isothermal case than in the isothermal case.
2. The calculated volume of gas passed through the orifice into the bubbles under non-isothermal conditions was less than the volume of gas passed into the bubbles under isothermal conditions at low mean volumetric gas flow rates and approached the values observed under isothermal conditions at the higher gas flow rates.
3. The total bubble formation time under non-isothermal conditions was found to be approximately 5 to 10 percent larger than that under isothermal conditions using Systems I and III. It was approximately 10 percent less for the non-isothermal case using System II.

2.3.2 Heat Transfer Data

The quantitative results pertaining to the heat transfer to a gas bubble during the period of formation are presented in terms of (a) the change in temperature of the gas in a bubble during the time of formation and (b) an average convective heat transfer coefficient for the period of bubble formation. The average convective heat transfer coefficient was particularly useful for the analytical calculations presented in Sections 3.3.3 and 3.4.2.

Figure 27 illustrates the order of magnitude of the change in bubble gas temperature during bubble formation observed for the Systems I, II, and III previously discussed. The accomplished temperature ratio $X = T_b - T_i / T_L - T_i$, representing the change in the bubble gas temperature during formation as a fraction of the overall temperature difference, is plotted as a function of the mean volumetric gas flow rate (based on T_i). As can be seen, the three systems exhibited the same general trend, with X reaching a maximum at a low value of $\dot{q}_i$ and then decreasing with increasing $\dot{q}_i$ to an approximately constant value. It is apparent that the change in the temperature of the gas in a bubble during bubble formation was as high as 85 percent of the overall temperature difference available and in all cases considered was at least 55 percent of the overall temperature difference. Thus, for overall temperature differences of approximately 140 to 165C, the energy transfer to the bubbles during the period of bubble formation was quite significant.

The value of X at the large flow rates was approximately 10 to 15 percent higher for System II than for Systems I and III. That may have been due to the fact that the total formation time for the bubbles produced with System II was larger (10 percent or more) than that of the other two systems (see Figs. 21, 24, and 26).

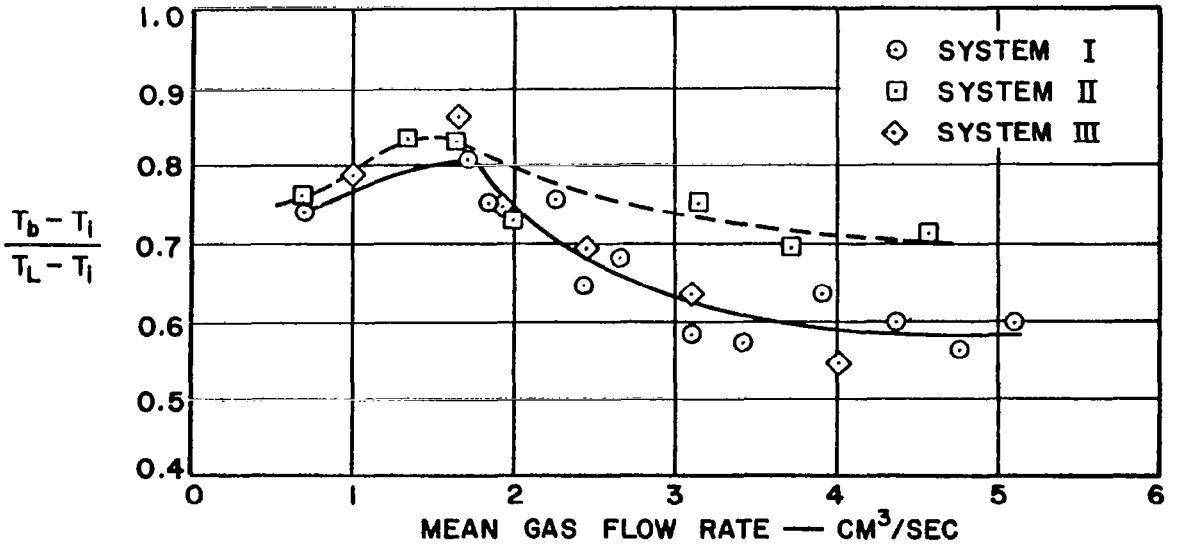

FIG. 27 TEMPERATURE INCREASE DURING NON-ISOTHERMAL BUBBLE FORMATION

The results presented in Fig. 27 in terms of the mean volumetric gas flow rate for a given bubble formation system are also presented in terms of parameters pertinent only to the bubbles in Fig. 28. The heating of a gas bubble during its period of formation at an orifice was considered somewhat analogous to the transient heating of a submerged object. Consequently, Fig. 28 illustrates the "unaccomplished temperature ratio", $Y = T_L-T_b/T_L-T_i$, for the bubbles, as a function of the dimensionless Fourier modulus

$$Fo = \frac{\alpha\, t_f}{R_m^2}$$

where

α = thermal diffusivity of the gas in the bubble

R_m = mean bubble radius for the bubble formation period.

Because of the significant variation of the density of the gas in the bubble with temperature, α was evaluated at a mean temperature, $T_m = \frac{T_b+T_i}{2}$. The radius of the bubble, R, of course varied throughout the bubble formation period due to the mass addition through the orifice and the thermal expansion of the gas in the bubble as a result of the heat transfer. Consequently, it was convenient to introduce a mean bubble radius, R_m, to characterize the size of bubble formed. The mean bubble radius was taken as the radius of an equivalent sphere of volume equal to the unheated volume, V_i.[1] Thus, R_m characterizes the "unheated" volume of gas passed through the orifice into the bubble. This representation makes it possible to employ the present data to estimate the change in the temperature of the gas in a bubble during the period of bubble formation knowing only the "unheated" bubble volume and the total formation time. The unheated bubble volume can, of course, be readily determined from a knowledge of the mass of gas per bubble and the gas inlet temperature.

Figure 28 includes data obtained for Systems I, II and III and also for System IV (see Table 1). Those systems represent a considerable variation in bubble size, total formation time, and flow into the bubble. There was considerable scatter of the data which was probably the result of employing a mean radius to characterize the continuously varying size of the bubbles.

[1] $R_m = (\frac{3}{4\pi} V_i)^{1/3}$

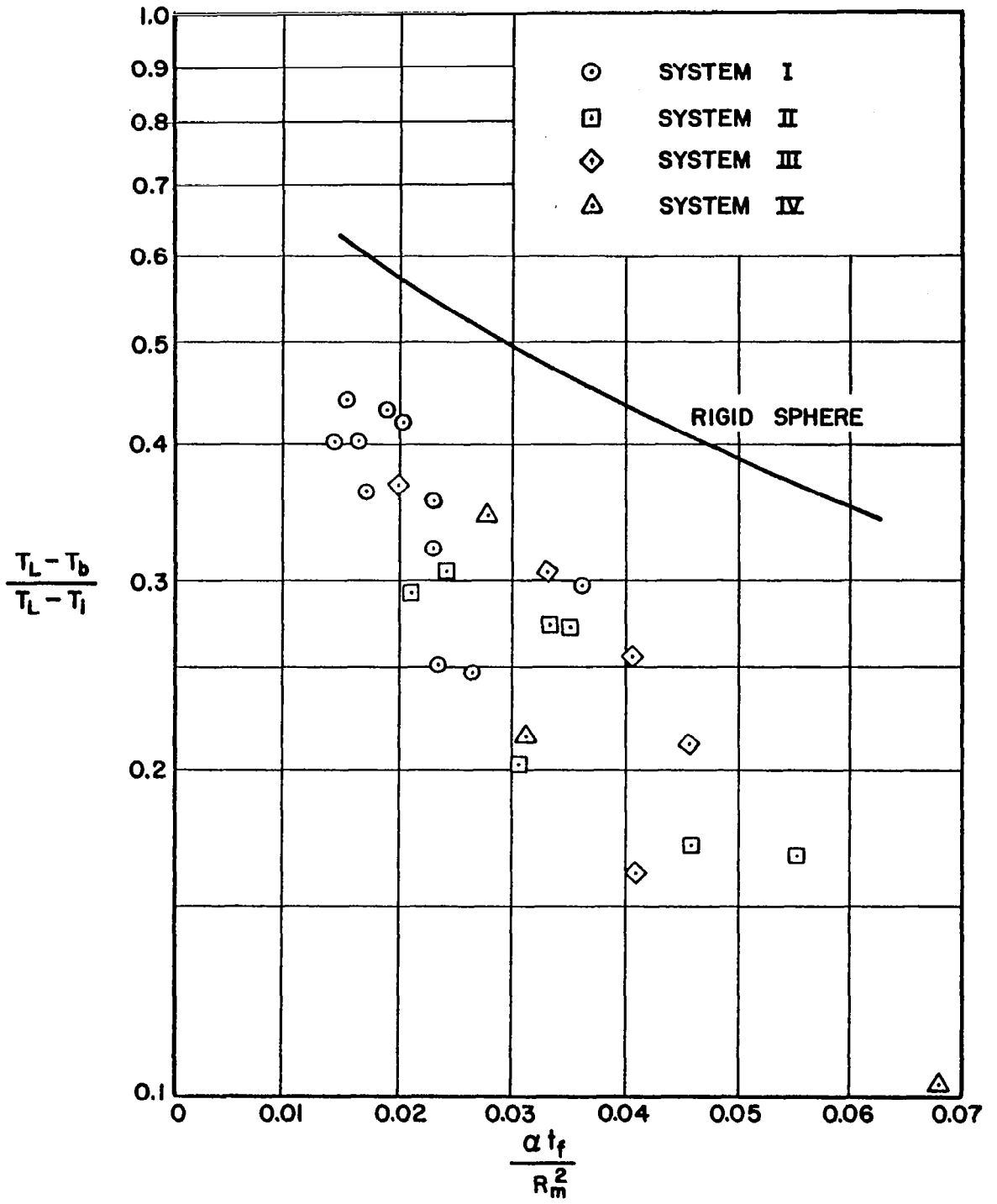

FIG. 28 UNACCOMPLISHED TEMPERATURE RATIO VERSUS FOURIER MODULUS

The solid line presented in Fig. 28 represents the analytical solution for Y as a function of Fo for the transient heating of a rigid sphere with negligible external resistance. As can be seen, the unaccomplished temperature ratio for the gas bubbles was considerably less than that predicted for a rigid sphere, which appears to indicate that circulation of the gas in the bubbles must have had a significant influence upon the rate of energy transfer to the bubbles.

The use of ethyl alcohol, with a thermal conductivity one-third that of water, did not significantly influence the heating of the gas bubbles. One would expect that the gas-side thermal resistance was the controlling factor.

An average convective heat transfer coefficient for the bubble formation period was determined in the manner described in Section 2.1.3, equation 2.4. For the various bubble formation systems and gas flow rates employed, $\bar{h}$ was found to vary from 2.4×10^{-3} to 5.3×10^{-3} cal/sec-cm^2-C (18 to 39B/hr-ft^2-F), while the overall energy transfer rate to the bubbles during formation was of the order of 0.25 cal/sec.[1] Such rates of energy transfer were still sufficient to cause a significant change in the temperature of the gas in a bubble during the period of formation due to the small energy capacity of the gas bubbles formed.

The values of the average heat transfer coefficient for the bubble formation period may be correlated in terms of the following variables:

$\bar{h}$ = average convective heat transfer coefficient for the bubble formation period.

$\bar{m}$ = mass velocity (M/L^2T) of the gas stream entering the bubble.

L = characteristic dimension of the bubble

μ_g = dynamic viscosity of the gas

c_{p_g} = constant pressure specific heat of the gas

k_g = thermal conductivity of the gas

Since $\bar{h}$ was determined as an average for the total bubble formation time, all other parameters were represented by mean values

[1] The heat transfer coefficient was of the same order as that indicated by analagous mass transfer data. See Section 1.1.2.

for the same period. The rate of mass flow into the bubble was found to vary throughout the period of bubble formation. Consequently, a mean value of the mass velocity of the gas stream entering the bubble was determined by

$$\bar{m} = \frac{m_b}{t_f A_o} \tag{2.8}$$

where

m_b = terminal bubble mass

t_f = total formation time

A_o = orifice cross-sectional area

Similarly a mean value for the characteristic dimension of the bubble was determined for convenience by

$$L = 2R_m = d_m = 2\left(\frac{3}{4\pi} V_i\right)^{1/3} = \text{diameter of an equivalent spherical bubble of volume equal to the "unheated" bubble volume.}$$

The variables $\bar{m}$ and d_m characterized the degree of mixing of the gas within the bubble which was a result of the momentum of the gas stream entering the bubble.

The conduction of energy within the bubble was considered to be negligible in view of the mixing therein, except in a thin layer adjacent to the gas-liquid interface. The thermal conductivity of the gas was included since, as mentioned earlier, it was expected that the gas-side thermal resistance was the controlling factor.

The aforementioned variables were combined into the following groups by standard dimensional analysis techniques:

$$\pi_1 = \left(\frac{\bar{h}}{\bar{m}\ c_{p_g}}\right)$$

$$\pi_2 = \left(\frac{\bar{m}\ d_m}{\mu_g}\right)$$

$$\pi_3 = \left(\frac{\mu_g \, c_{p_g}}{k_g}\right)$$

These dimensionless groups represent the familiar Stanton, Reynolds, and Prandtl numbers. Thus,

$$\pi_1 = \frac{Nu}{Re \; Pr} = St$$

$$\pi_2 = Re$$

$$\pi_3 = Pr$$

Figure 29 illustrates a plot of St as a function of Re, including the experimental data for Systems I, II, III, and IV (see Table 1). The effect of the Prandtl number is not clearly demonstrated, since, with the use of nitrogen gas throughout the experiment, there was no significant variation in Pr. Despite the scatter of the data, it is significant to note that all the heat transfer results are correlated with ± 25 percent by the expression

$$\frac{Nu}{Re \; Pr} = 26.9 \; Re^{-0.884} \qquad (2.11)$$

Figure 29 includes data obtained with

1. orifices 0.159 cm and 0.0795 cm in diameter
2. orifices made of plexiglass and teflon
3. distilled water and ethyl alcohol
4. mean gas flow rates varying from 2.25×10^{-3} to 12.7×10^{-3} gm/sec.

The reasonable correlation of the data, obtained from such a variety of conditions, by equation 2.11 indicates the feasibility of presenting the heat transfer data in terms of parameters pertinent only to the bubble formed and the flow into it.

The effect of the degree of mixing within the bubble upon the average heat transfer coefficient is illustrated by equation 2.11, noting that

$$\bar{h} \; \alpha \; \frac{(\bar{m})^{0.12}}{d_m^{0.88}}$$

For a bubble of a given mean size (d_m = constant), one would expect the mixing within the bubble to increase as the mass velocity into the bubble increased; and, accordingly, the preceding expression shows that $\bar{h}$ increases as $\bar{m}$ increases (more mixing). Similarly, for $\bar{m}$ = constant, the smaller the bubble,

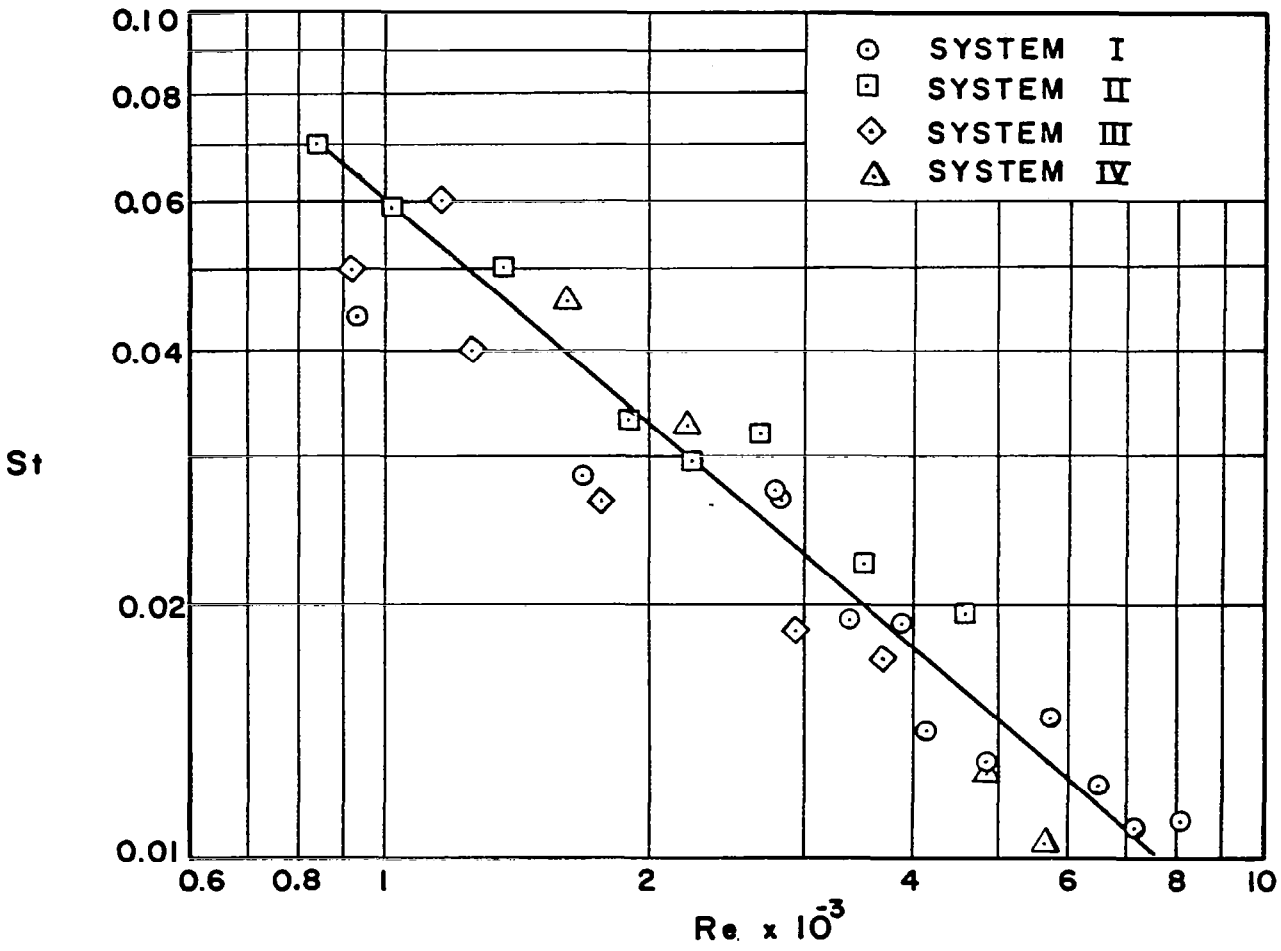

FIG. 29 STANTON NUMBER VERSUS REYNOLDS NUMBER FOR NON-ISOTHERMAL FORMATION

or d_m, the better the mixing and the larger the $\bar{h}$, as shown by the preceding expression.

Equation 2.11 was employed for determining an average heat transfer coefficient for the bubble formation period used in the analytical computation discussed in Section 3.4.2. Such computations enabled a prediction of the change in the temperature of the gas in a bubble during the bubble formation period for selected non-isothermal conditions.

2.4 Details of Bubble Formation

An auxiliary investigation of the process of bubble formation was conducted utilizing the apparatus described in Section 2.1.2. The primary purpose of the investigation was to determine the actual non-steady rate of mass flow into a bubble formed at an orifice supplied by a given ante-chamber for a given mean gas flow rate (see also Section 3.3.1, equation 3.13). The investigation also provided some information concerning the increase in the ante-chamber pressure prior to the initiation of the formation of successive bubbles and the effect of the volume of the ante-chamber on the terminal volume of the bubbles produced.

2.4.1 Mass Flow into a Bubble

The instantaneous rate of mass flow into a bubble was determined by a mass balance on the ante-chamber supplying gas to the bubble via the orifice. Thus,

$$\left(\begin{matrix}\text{mass flow rate} \\ \text{into the bubble}\end{matrix}\right) = \left(\begin{matrix}\text{mass flow rate in-} \\ \text{to the ante-chamber}\end{matrix}\right) - \left(\begin{matrix}\text{time rate of change of} \\ \text{mass in the ante-chamber}\end{matrix}\right)$$

Assuming that the gas is ideal, that the flow of gas through the ante-chamber is isothermal, and that the dimensions of the ante-chamber are such that the pressure is uniform throughout, the mass balance can be expressed as follows:[1]

$$\frac{dm}{dt} = \dot{W}_i - \frac{V_c}{\bar{R}\, T_c} \frac{d\, p_c}{dt} \qquad (2.12)$$

where

m = instantaneous mass of the bubble

$\dot{W}_i$ = mass flow rate into the ante-chamber

[1] Equation 2.12 is identical to equation 3.13, Section 3.3.1.

V_c = volume of the ante-chamber[1]

T_c = temperature of the gas in the ante-chamber

$\bar{R}$ = gas content

p_c = pressure of the gas in the ante-chamber

Since a sonic orifice was employed at the inlet to the ante-chamber, the ante-chamber volume, V_c, was then the entire and only reservoir supplying gas to the bubble. Equation 2.12 was evaluated by the measurement of $p_c(t)$ for given conditions of mean flow and ante-chamber volume.

The transient pressure $p_c(t)$ in the ante-chamber was measured by means of a microphone mounted therein as described in Section 2.1.2. A plot of the ante-chamber pressure, referred to the pressure at the beginning of a cycle, $(p_c(t) - p_c(0)$, is presented as a function of time in Fig. 30. The origin of the time scale was chosen arbitrarily. Each cycle of the periodic function was associated with the formation of a bubble.

High speed motion pictures of the bubble formation process were obtained simultaneously in synchronization with the measurement of the transient ante-chamber pressure. Thus, it was possible to correlate points on the pressure curve with events observed on the motion pictures. In particular, it was found that the detachment of a bubble from the orifice corresponded to the point of discontinuity in the slope of the pressure curve. Figure 31 illustrates one cycle of $p_c(t)$ (from Fig. 30) with the lapse time and the total formation time clearly indicated for a bubble. It should be apparent that the transient pressure function used for evaluating equation 2.12 was that for the total formation time, for, by definition, there was no bubble visibly forming during the lapse time. By obtaining the slope of the pressure curve, $(\frac{dp_c}{dt})$, during the total formation time, the rate of mass flow into the bubble could be calculated from equation 2.12.

It should be pointed out that the analysis in Section 3 considers the growth of a bubble during the interval of time between the instant when the bubble is a hemisphere of radius equal to that of the orifice ($R_{bubble} = R_o$ at $t_{theory} = 0$) and the instant

[1] From the sonic orifice to the orifice at which the bubbles were formed.

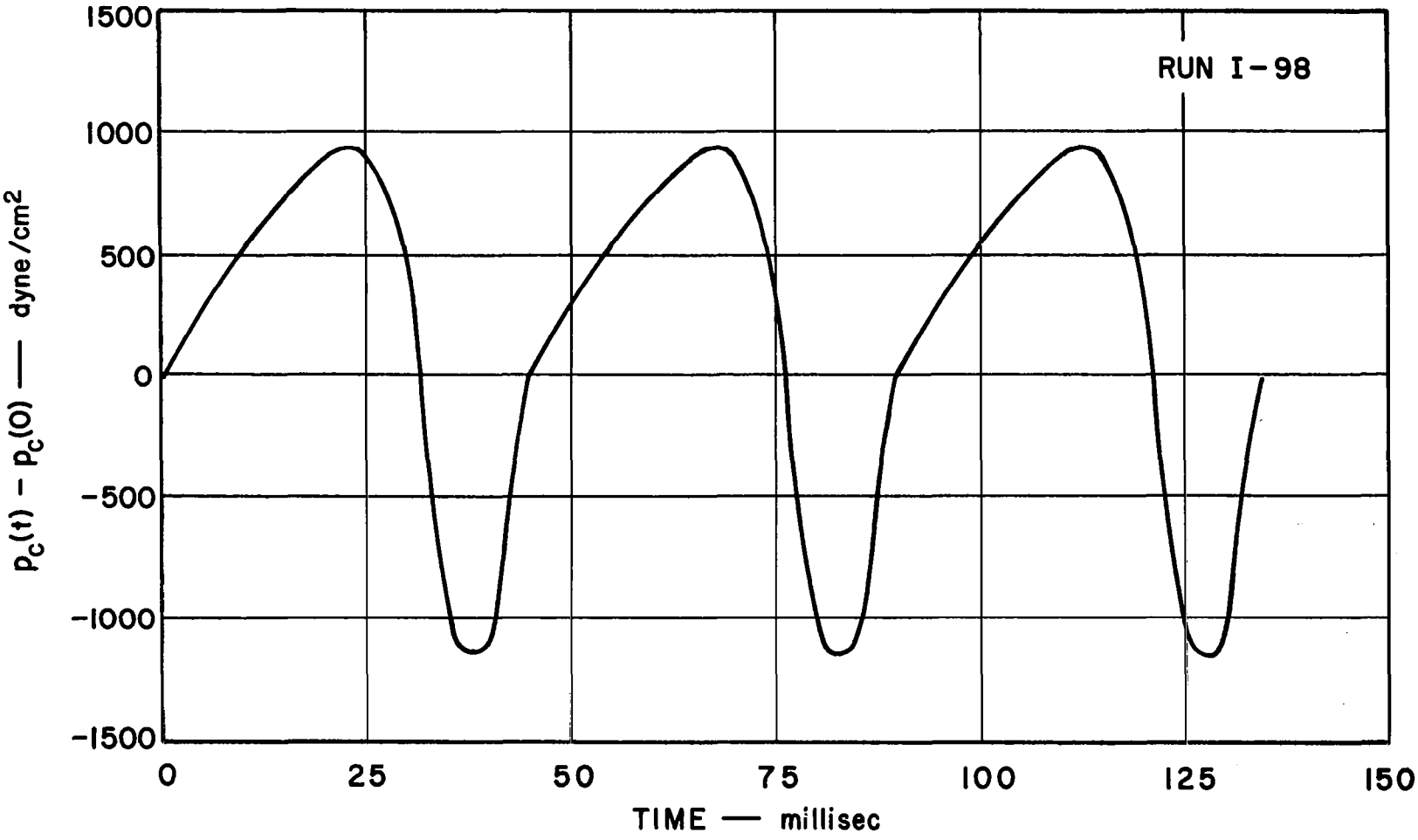

FIG. 30 VARIATION IN ANTE-CHAMBER PRESSURE DURING BUBBLE FORMATION

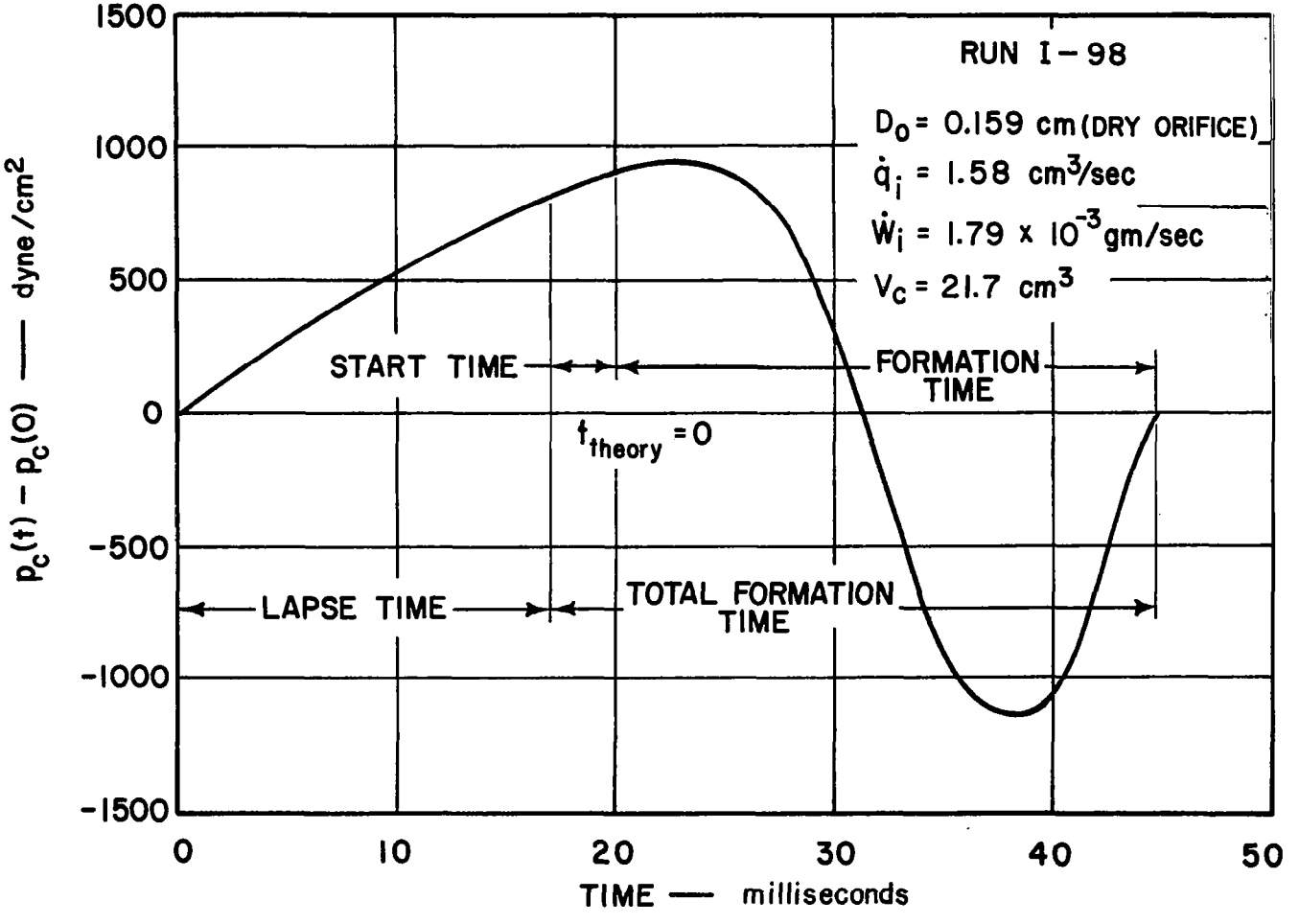

FIG. 31 VARIATION IN ANTE-CHAMBER PRESSURE DURING BUBBLE FORMATION (RUN I – 98)

when the bubble detaches from the orifice. That time interval is referred to in Section 3 as the "formation time". It is slightly less than the "total formation time."[1] The difference between the total formation time, t_f, and the formation time, t_f', referred to as the "start time," was readily determined from the high speed motion pictures of the growth of the bubble.

The instantaneous mass flow rate into a bubble for a given W_i, V_c, and $p_c(t)$ was calculated from equation 2.12 by means of a computer program described in Section 3.3.3. The computer program enabled the input of the varying values of p_c and the corresponding values of t for the bubble formation period. The slope of the pressure curve dp_c/dt at any t was determined by means of a spline fit interpolation subroutine in the computer program which, subsequently, enabled the calculation of dm/dt from equation 2.12. Figure 32 illustrates the instantaneous mass flow rate into the bubble normalized with respect to the steady mass flow rate into the system, W_i, for the conditions specified in Fig. 31. The variation of the rate of flow of mass into the bubble was quite significant. Figure 32 shows that initially ($t/t_f < 0.2$) the mass flow rate into the bubble was less than the mass flow rate into the ante-chamber which resulted in a further increase in the ante-chamber pressure even as the bubble was being formed. (See Fig. 31 at start of formation time.) Such an increase in p_c in the initial stages of formation was possibly required to overcome the inertia of the liquid which was being accelerated away from the orifice. As can be seen, the instantaneous rate of mass flow into the bubble increased to as much as 4.5 times the steady state value of the mass flow rate. During the latter portion of the formation period ($t/t_f > 0.8$), the mass flow rate into the bubble became apparently negative.

The transient ante-chamber pressures and the corresponding normalized mass flow rates for increasing values of mean gas flow rate (experimental runs 1-103, 112, 115) are presented in Figs. 33, 34 and 35, respectively. All such data, including those in Figs. 31 and 32, are for the same orifice size and ante-chamber volume. A comparison of the normalized mass flow rate plots in Figs. 33, 34, and 35 illustrates a remarkable similarity between the curves for the three different values of mean gas flow rate. The mass flow rate curve in Fig. 32, for the lowest mean flow rate, is considerably different from those in the aforementioned figures.

The transient ante-chamber pressure and the corresponding normalized mass flow rate, obtained with a larger ante-chamber (experimental run I-113), are presented in Fig. 36. By comparing Figs. 34 and 36, it can be seen that, for the same value of mean

[1] See Section 2.1.2 for an exact definition of the total formation time.

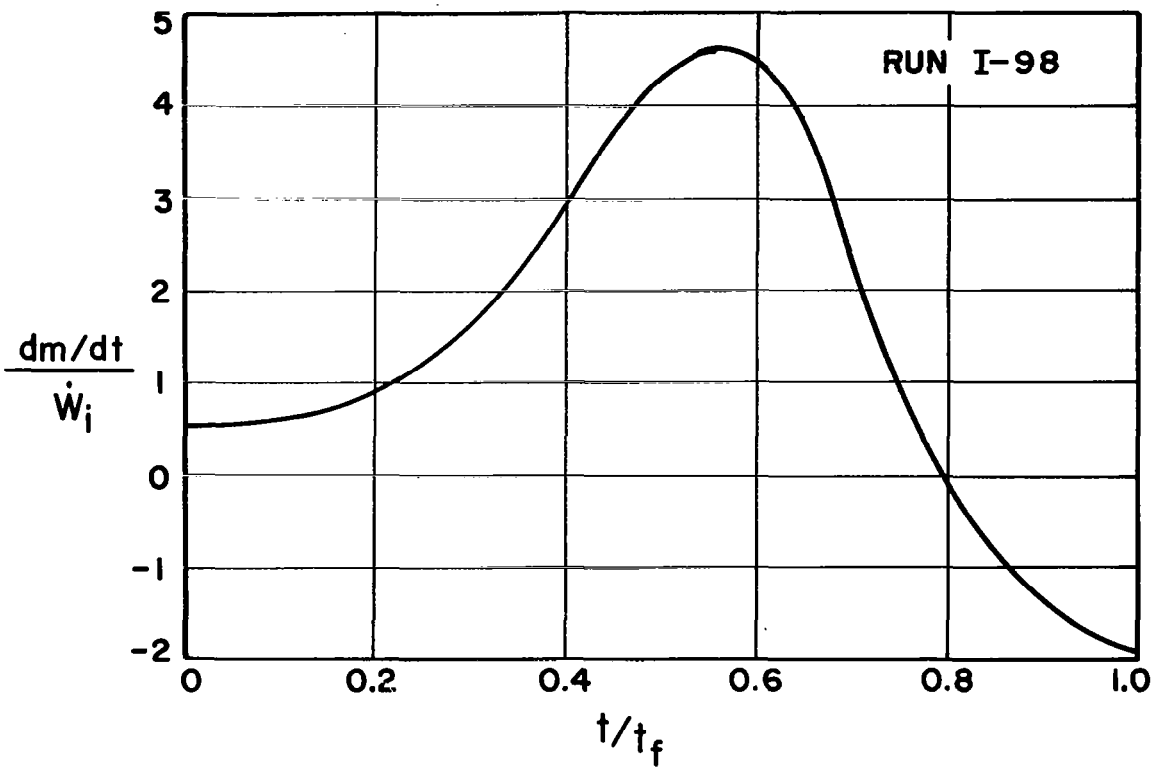

FIG. 32 RATE OF MASS FLOW INTO BUBBLE DURING ISOTHERMAL FORMATION (RUN I—98)

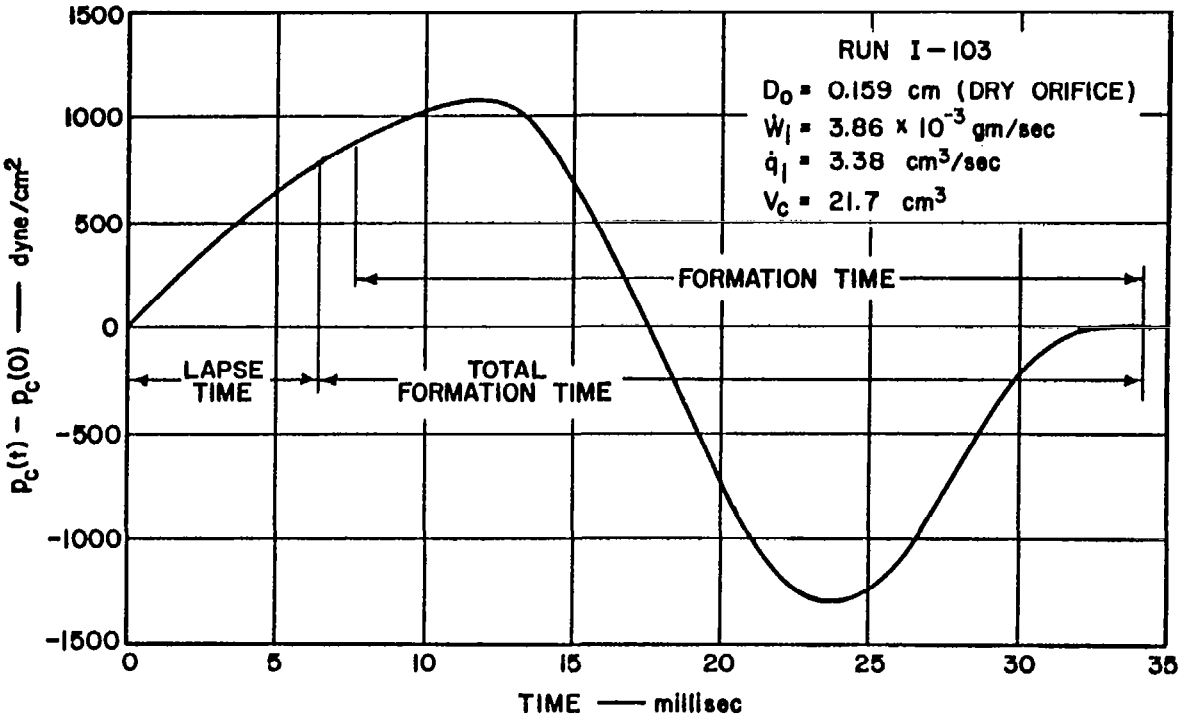

ANTE-CHAMBER PRESSURE

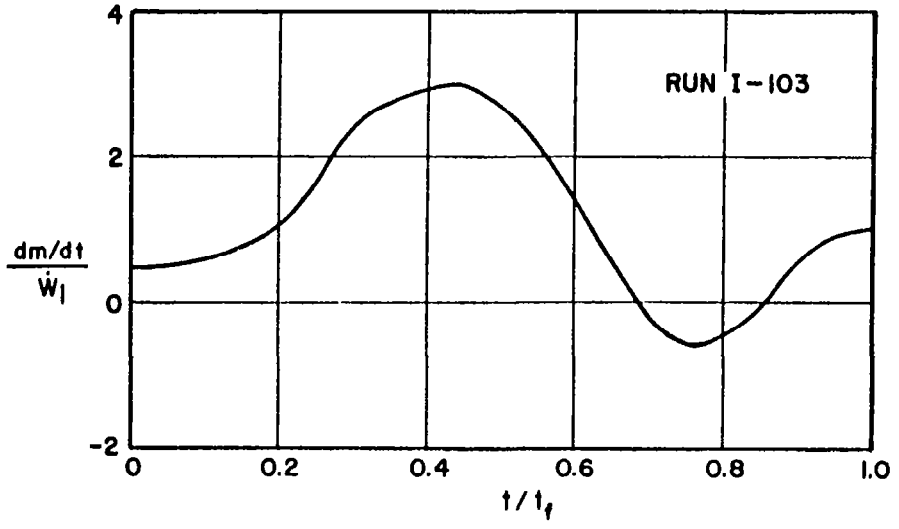

MASS FLOW INTO BUBBLE

FIG. 33 ISOTHERMAL FLOW CHARACTERISTICS (RUN I-103)

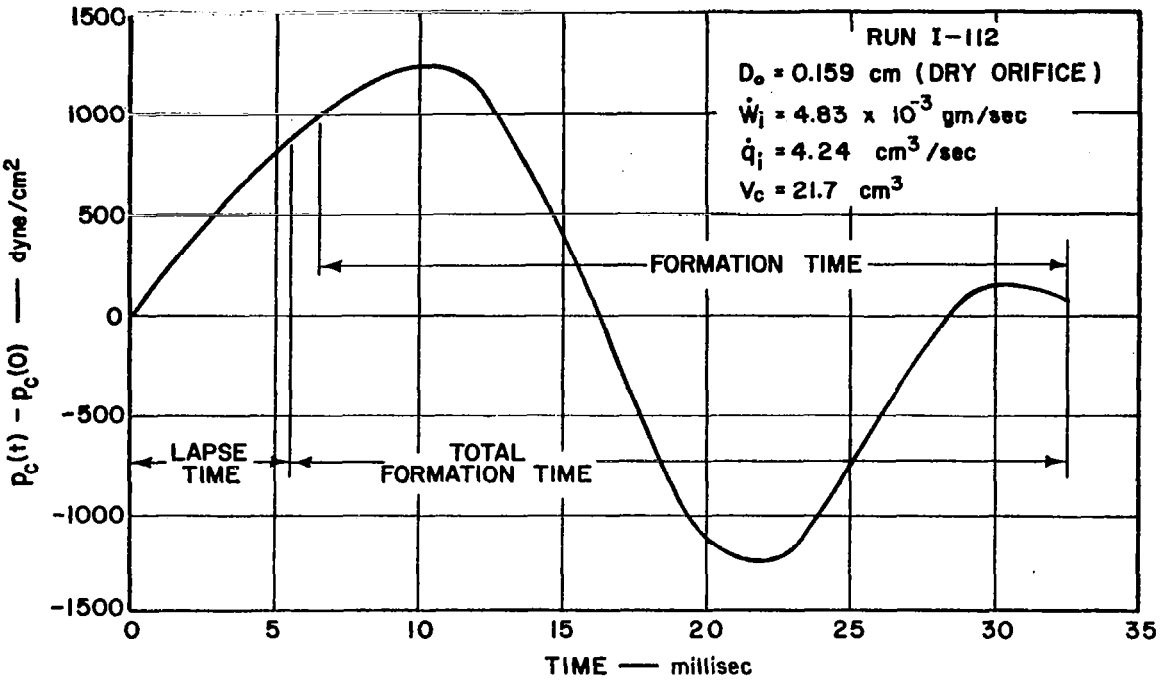

ANTE-CHAMBER PRESSURE

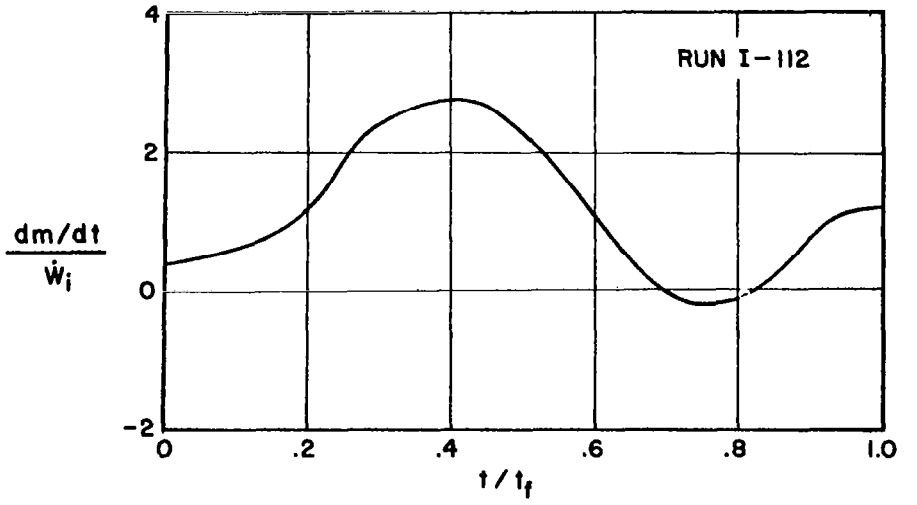

MASS FLOW INTO BUBBLES

FIG. 34 ISOTHERMAL FLOW CHARACTERISTICS (RUN I-112)

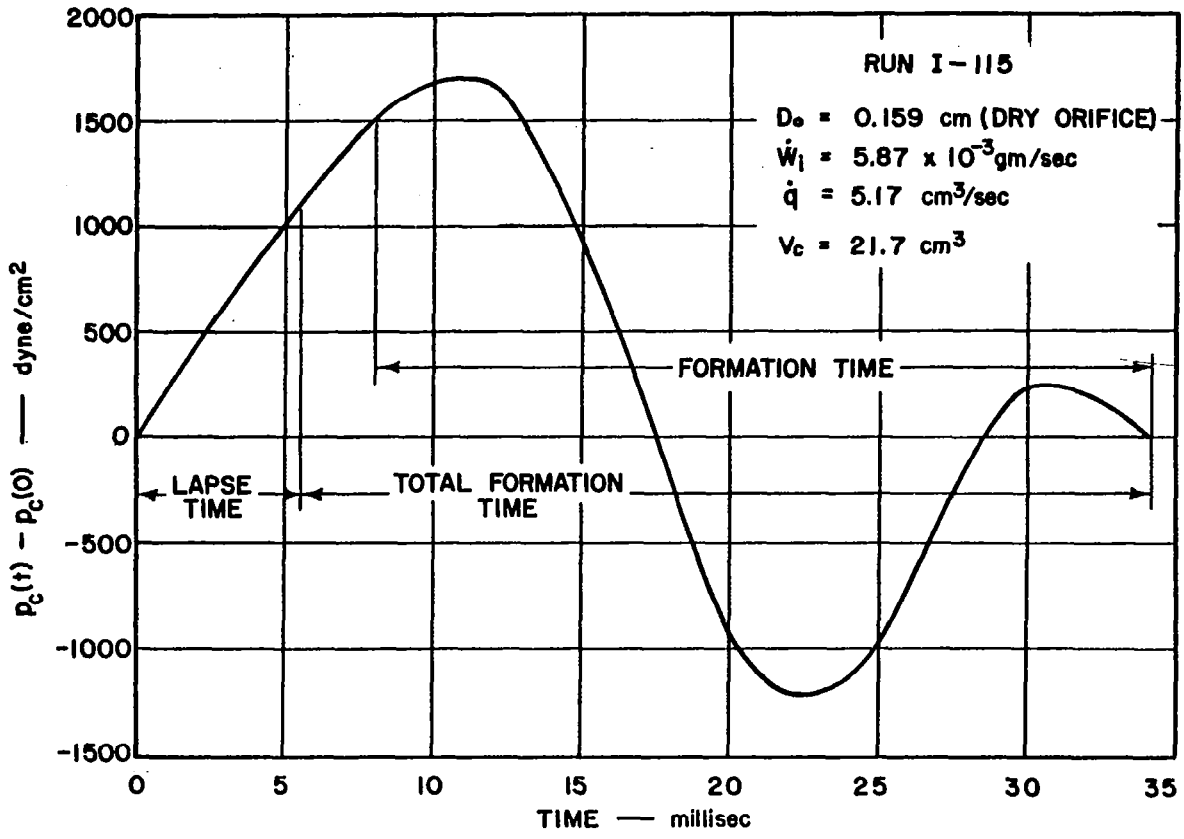

ANTE - CHAMBER PRESSURE

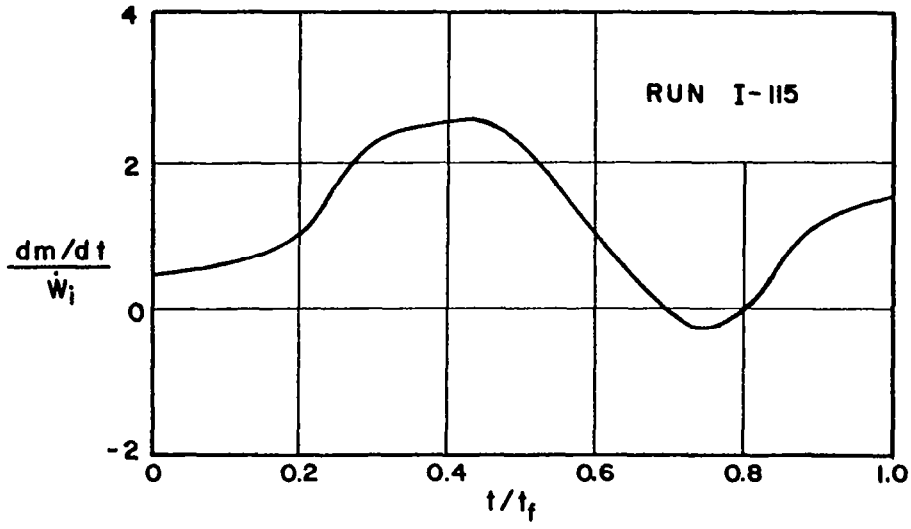

MASS FLOW INTO BUBBLE

FIG. 35 ISOTHERMAL FLOW CHARACTERISTICS (RUN I-115)

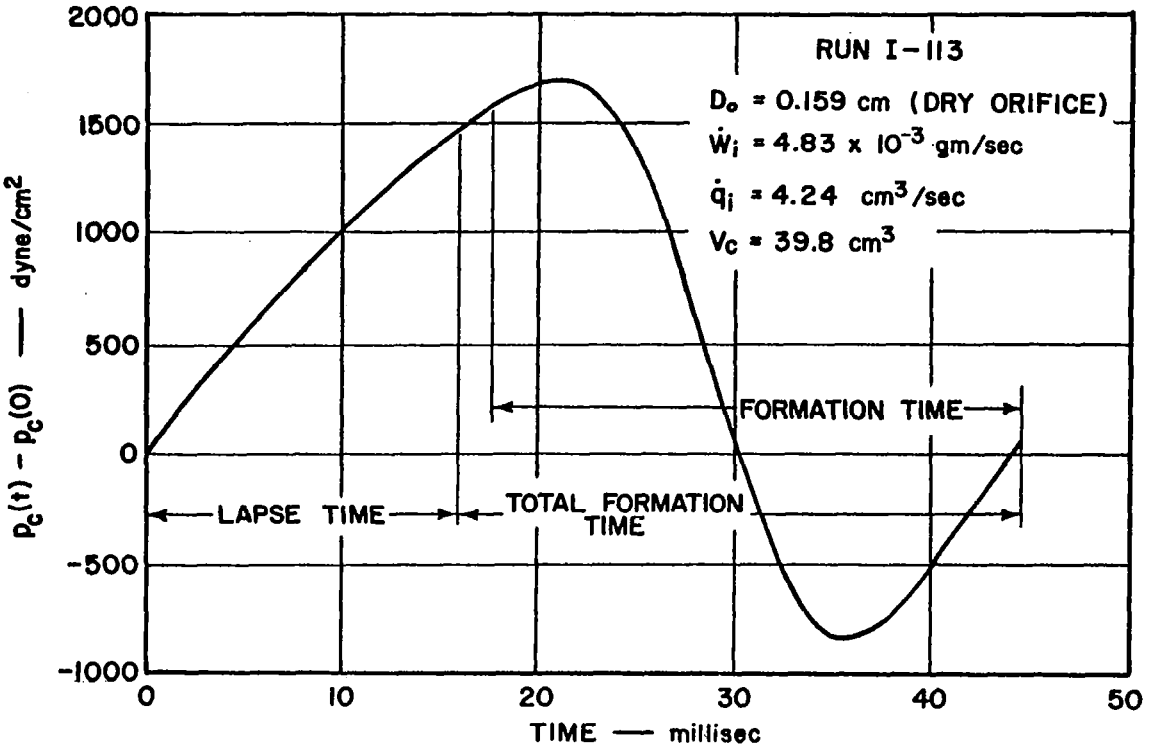

ANTE-CHAMBER PRESSURE

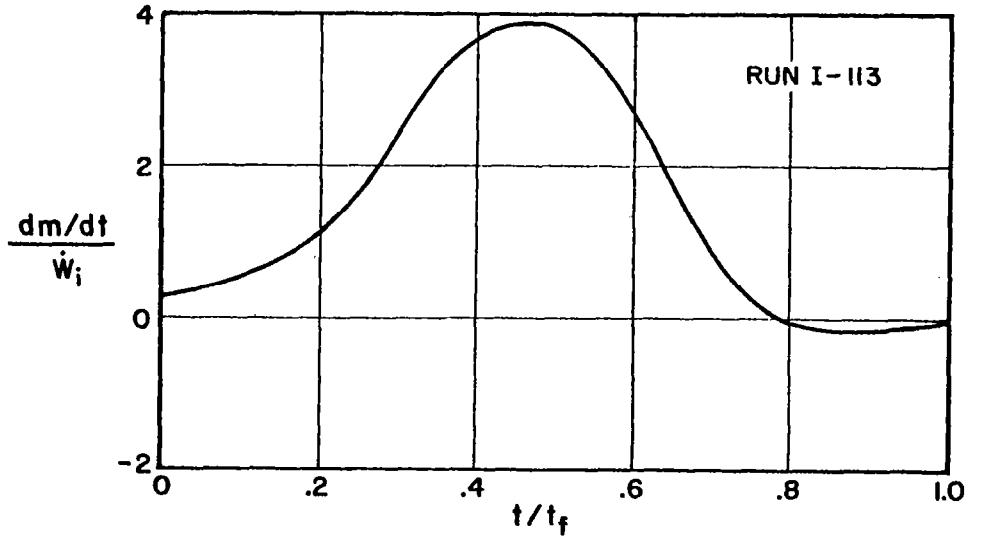

MASS FLOW INTO BUBBLE

FIG. 36 ISOTHERMAL FLOW CHARACTERISTICS (RUN I-113)

gas flow rate, the use of a larger ante-chamber significantly altered the normalized mass flow rate curve. Furthermore, it can also be seen (Figs. 34 and 36) that a change in the volume of the ante-chamber, while all other parameters remained constant, altered the transient ante-chamber pressure characteristics.

The preceding facts illustrate the effect of the coupling of the bubble formation mechanism with the fluid dynamic characteristics of the system supplying the gas to the orifice. The formation of a bubble is dependent upon the rate of flow of gas into the bubble which in turn depends upon the mean gas flow rate, the ante-chamber volume, and also the increase in ante-chamber pressure during the lapse time.

The high speed motion pictures of the bubble formation process obtained in conjunction with the transient pressure measurements enabled the calculation of the volume of the bubble as a function of time during the formation period according to the technique described in Appendix III. Figure 37 illustrates the experimentally determined values of bubble volume as functions of time during formation for the experimental runs I-98 and I-103. Those experimental curves are to be compared with analytically predicted values of V(t) in Section 4.

2.4.2 Orifice and Ante-Chamber Effects

Because of the coupling of the bubble formation process with the fluid dynamic characteristics of the system supplying the gas to the orifice, the flow processes occurring during the lapse time can have a significant influence upon bubble formation. In particular, the increase in the ante-chamber pressure during the lapse time and the ante-chamber volume were observed to have a significant influence upon the terminal volume of the bubbles formed. Such an influence can be explained on the basis of the mass of gas stored in the ante-chamber during the lapse time just prior to the formation of a bubble.

The increase in the ante-chamber pressure during the lapse time, referred to as the "excess pressure", p_f, was determined from the measurements of the transient ante-chamber pressure. For example, in Fig. 31 the excess pressure can be observed to be approximately 810 dyne/cm^2 (12 millipsi).

The variation of the terminal volume with the ante-chamber excess pressure is illustrated in Fig. 38 for four different mean gas flow rates and two values of ante-chamber volume. It can be observed that the slope of the lines, for V_c = 39.8 cm^3, is essentially independent of the mean gas flow rate and has a

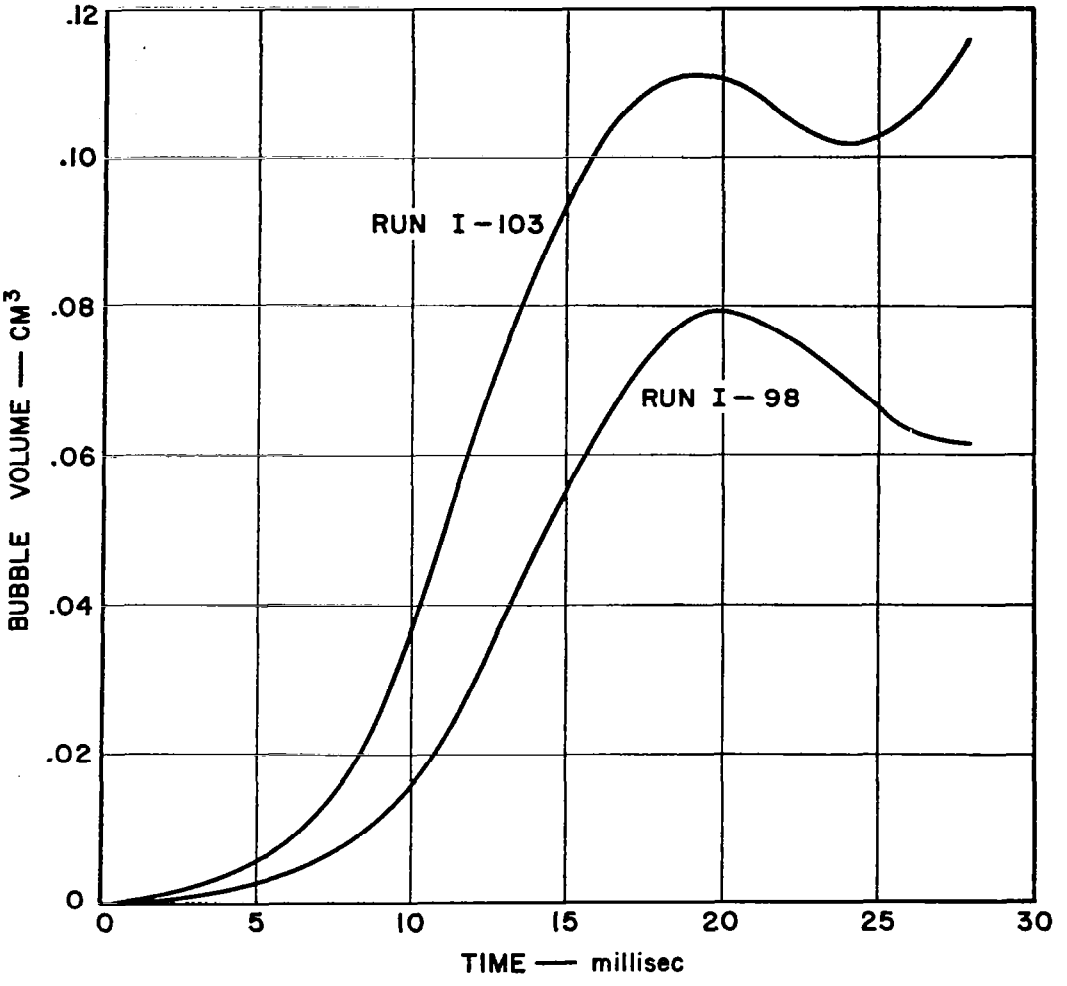

FIG. 37 EXPERIMENTAL ISOTHERMAL BUBBLE GROWTH
(RUNS I-98 AND I-103)

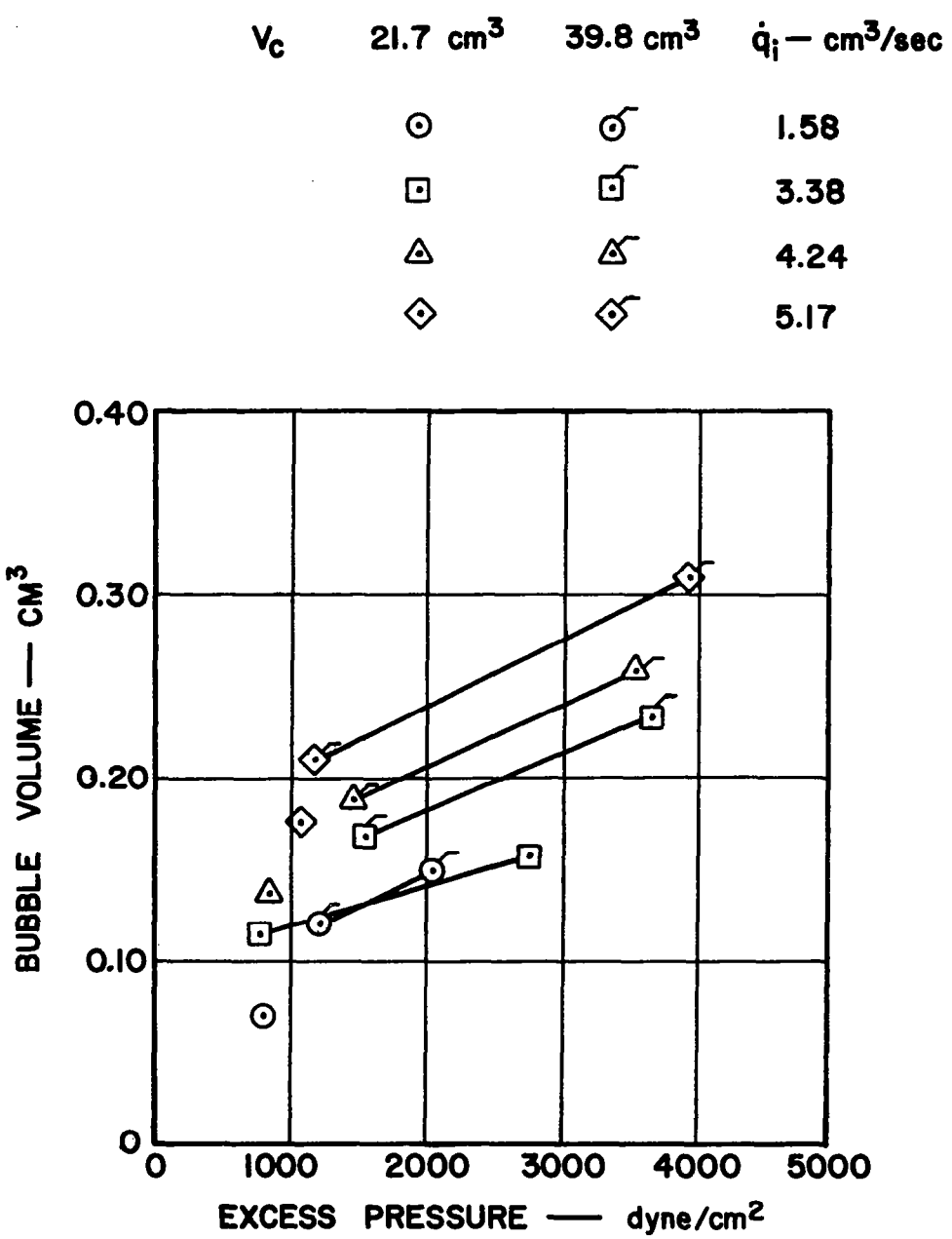

FIG. 38 TERMINAL BUBBLE VOLUME VERSUS ANTE-CHAMBER EXCESS PRESSURE

value of approximately 3.62×10^{-5} cm³/(dyne/cm²). That change in V_b with p_f can be explained by considering the mass of gas stored in the ante-chamber during the lapse time. Assuming isothermal flow, the stored mass is given as

$$m_{stored} = \frac{p_f V_c}{\bar{R} T_c} \tag{2.13}$$

If it is assumed that the density of the gas in the bubbles is approximately the same as that in the ante-chamber, m_{stored} will correspond to a portion of the volume of the bubble given by

$$V_{b_{stored\ mass}} = \frac{m_{stored}}{\rho_{gas}} = \frac{p_f V_c}{\bar{R} T_c} \frac{\bar{R} T_b}{p_b} = \frac{p_f V_c}{p_b} \tag{2.14}$$

Next, if it is assumed that the change in the terminal volume of the bubbles due to a change in the ante-chamber excess pressure arises entirely from the difference in the mass stored during the lapse time, then from equation 2.14 one obtains the following expression for the variation of the terminal bubble volume with the ante-chamber excess pressure.

$$\frac{d V_b}{d p_f} = \frac{V_c}{p_b}$$

For $V_c = 39.8$ cm³, equation 2.15 gives

$$\frac{d V_b}{d p_f} = \frac{39.8 \text{ cm}^3}{9.93 \times 10^5 \text{ dyne/cm}^2} = 4.01 \times 10^{-5} \text{ cm}^3/(\text{dyne/cm}^2)$$

Similarly, for the smaller ante-chamber, equation 2.15 gives

$$\frac{d V_b}{d p_f} = \frac{21.7 \text{ cm}^3}{9.93 \times 10^5 \text{ dyne/cm}^2} = 2.19 \times 10^{-5} \text{ cm}^3/(\text{dyne/cm}^2)$$

These values may be compared with the experimental data in Fig. 38.

The effect of V_c upon the terminal bubble volume is further illustrated by comparing, in Fig. 38, the difference between the terminal bubble volume for $V_c = 39.8$ cm³ and for $V_c = 21.7$ cm³,

D-2547

for the different mean gas flow rates considered. That difference was approximately the same for all values of the mean gas flow rate. These facts indicate that the change of the terminal bubble volume due to a change in the ante-chamber volume or the ante-chamber excess pressure is most probably due to a change in the mass of gas stored during the lapse time.

In the course of the investigation it was found that the value of the excess pressure in the ante-chamber was predominantly influenced by the degree to which the liquid wetted the orifice during the lapse time of the bubble formation cycle. As mentioned in Section 2.1.2, the orifice employed was made of plexiglass, 0.159 cm in diameter, with an L/D ratio of 4. The motion pictures of the process of bubble formation were also taken including the orifice, which enabled a determination of the degree of wetting of the transparent orifice by the liquid. The degree of wetting of the orifice was characterized by the depth to which the meniscus entered the orifice channel during the lapse times of successive bubbles. A "dry orifice" refers to the condition wherein the meniscus did not visibly enter the orifice channel, whereas a "wet orifice" refers to the condition wherein the liquid wetted the entire orifice channel in between successive bubble formation periods.

It was found that there was no unique value for the depth of wetting for a given system. In other words, with a fixed ante-chamber volume and mean gas flow rate, the depth of wetting was found to be consistent and stable for any given run but was found to vary somewhat arbitrarily from run to run. The particular depth of wetting which occurred for a given run was found to depend somewhat upon the state of the orifice channel when the liquid was introduced into the container and the bubble formation was started. If the orifice channel was carefully dried and the desired rate of gas flow was passing through the orifice before the liquid was introduced, the bubble formation proceeded indefinitely with a dry orifice. Similarly, if the orifice channel was purposely wetted before the liquid was introduced, the bubble formation proceeded with a wet orifice. As one would expect, it was found that there was a limit of the depth of wetting for high frequencies of bubble formation.

Figure 39 illustrates a plot of the ante-chamber excess pressure as a function of the depth (in terms of number of diameters) of wetting of the orifice channel. The plot includes data for four different values of mean gas flow rate and two values of ante-chamber volume. It is significant to note that all of the data are represented by the curve shown within ± 12 percent at the lower pressures and ± 5 percent at the upper.

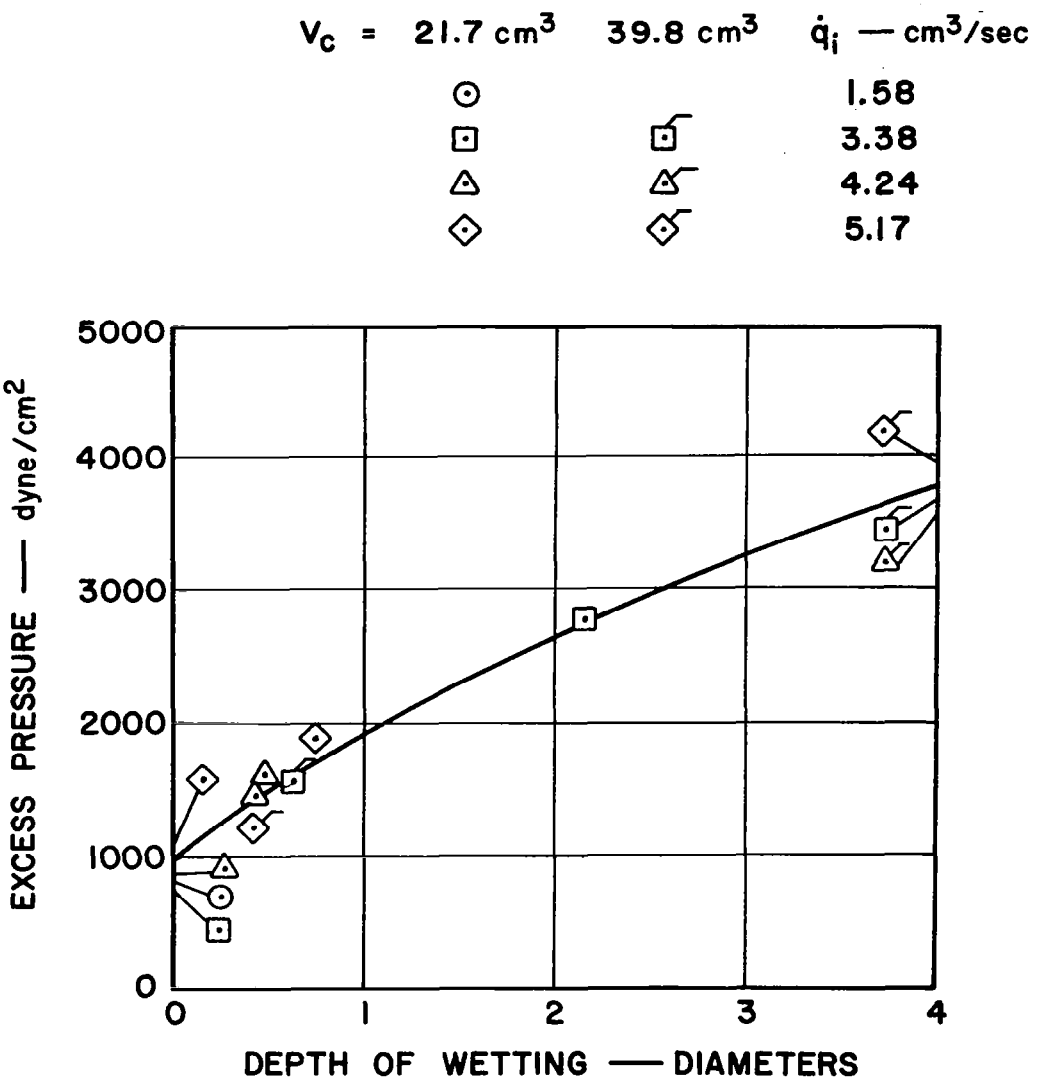

FIG. 39 ANTE-CHAMBER EXCESS PRESSURE VERSUS ORIFICE WETTING DEPTH

3. ANALYTICAL INVESTIGATION

The injection of a gas into a liquid through a submerged orifice results under certain conditions in the periodic formation of discrete gas bubbles of approximately equal volume. The study of the mechanism of the formation of such bubbles has been the subject of numerous investigations (see Section 1.1.1) particularly because of the importance of that phenomenon in connection with distillation, absorption, extraction, and other mass and energy transfer processes. Such investigations have, however, been concerned principally with the determination of the terminal volume of the bubbles produced under various liquid and gas flow conditions, because of the importance of knowing the size of the bubbles rising through the liquid in the evaluation of the overall mass or energy transfer rates for the bubbling process. There is general agreement in the literature that the size of the bubbles produced is primarily governed by (a) the mean rate of flow of gas through the system, (b) the physical properties of the liquid phase, (c) the size of the orifice and (d) the fluid dynamic characteristics of the system supplying the gas to the orifice. However, the nature of the flow into the bubbles has made it difficult to specify quantitatively the dynamic characteristics of the gas supply system. Except for two limiting cases (see Section 1.1.1), the type of bubbles formed by a given apparatus may be characteristic of the particular apparatus employed because of the complex interaction of the many variables which influence the process of bubble formation.

In studying the period of formation of the bubbles, one is also concerned with the details of the growth of the bubbles at the orifice. Thus, in order to analyze the process of energy transfer to gas bubbles during the period of bubble formation, it becomes necessary to consider the detailed interaction of the various variables which govern the dynamic growth of a bubble as well as those variables which influence the transfer of energy from the liquid to the gas in the bubble. It is the object of the analysis presented herein to take into account at least some of the intercoupling that exists among the various parameters.

The overall analytical problem may be stated as follows:

1. Given the necessary properties of the liquid and the gas, what are the variations with time in the radius of the bubble, the rate of growth of the bubble, and the temperature and pressure of the gas in the bubble for prescribed conditions of gas injection and other initial conditions?
2. When there is heat transfer to the gas in the bubble during formation, what is the overall increase in the

mean temperature of the gas during the formation period?

3. If an average heat transfer coefficient may be specified for the entire period of bubble formation, what is its value for the particular class of bubbles under consideration?

3.1 Physical Model

In general, the periodic formation of the bubbles may be divided, for convenience, into the following two stages, each characterized by a certain period of time (see Section 2.1.3):

1. the lapse time and
2. the total formation time.

The lapse time is dependent upon the rate of flow of gas into the chamber, the chamber volume and the increase in pressure required to initiate bubble formation. Each of those parameters will subsequently influence the rate of flow of gas into the bubble during the formation time, and hence, the coupling that has been referred to in Section 2.4.1 between the growth of a bubble and the flow characteristics of the supply system. Also, the increase in pressure that is required seems to depend in a complex fashion upon the depth to which the liquid wets the orifice channel during the lapse time as discussed in Section 2.4.2.

The current understanding of the mechanism, by which discrete gas bubbles are formed, suggests (5,7,8,25), furthermore, the importance of liquid inertia, viscous drag, surface tension, and hydrostatic pressure forces acting on the gas-liquid interface generated in the formation of a bubble. The motion of the interface during the growth of the bubble is governed by the interaction of those forces with the forces associated with the flow of gas through the orifice into the bubble.

In addition, there is the possibility of energy and mass transfer from the liquid phase to the gas in the bubble. There is no simple theory for the formation of bubbles of the type being considered here, which takes into account the energy and mass transfer processes as well as the simultaneous interaction of all the forces during the non-steady growth of the bubbles. The analysis presented here is concerned with the prediction of the growth rate of a bubble, under given operating conditions, in the presence of heat transfer to the gas in the bubble due to a difference between the temperature of the liquid and the temperature of the gas entering the bubble; it is then possible to determine the change in the temperature of the gas in the bubble during formation.

3.2 Analytical Model

In order to proceed with the mathematical formulation of the problem, a simplified model of the physical processes has been developed. The features considered most significant therein are (a) the effect of the inertia of the liquid on the dynamic pressure in the bubble, (b) the effect of energy transfer from the liquid to the gas in the bubble, and (c) the possibility of unsteady flow from the reservoir into the bubble. The liquids of particular interest in the present investigation are relatively inviscid, and the effect of the viscosity of the liquid phase is treated only in an approximate way. Similarly the effect of mass transfer from the liquid to the bubble and the nature of the flow within the bubble have not been included in the present analysis (some discussion is presented in the last part of the next section).

3.2.1 Assumptions Employed to Develop an Analytical Model

A simplified analytical model for the formation of a bubble has been obtained by making the following assumptions.

1. The gas-liquid interface is spherical at all times during growth.
2. The medium surrounding the interface is quiescent, incompressible, and of infinite extent.
3. The pressure and temperature of the gas in the bubble are uniform throughout at any instant.
4. There is no transfer of liquid vapor into the bubble.
5. The gas is ideal.

The assumption of a spherical shape for the bubble throughout the period of growth simplifies the geometrical specification of the bubble surface and enables the determination of the (inviscid) flow field in the liquid by means of potential theory. The photographic observations illustrated in Figs. 5 and 17 do show that the bubbles depart to some extent from a spherical shape during part of the formation time; however, it may also be observed that the spherical shape is a reasonable approximation for the major portion of the formation time in most cases for the class of bubbles obtained experimentally.

The assumption 2 is introduced to neglect all effects due to preceding bubbles. However, some circulation is induced in the liquid due to the upward motion of a bubble at the instant of detachment from the orifice. The effect of that circulation upon the formation of the succeeding bubble is difficult to take into account theoretically. However, it has been found (7) that the effect of liquid circulation on bubble formation is minimized when the liquid is prevented from circulating up along the base

of the bubble. That is ensured to an extent, for example, in the case of a bubble formed above a flat plate orifice.

The postulation of a uniform pressure and temperature throughout the bubble at any instant (assumption 3) entirely neglects the nature of the motion of the gas within the bubble and, furthermore, implies instantaneous and complete mixing of the gas in the bubble. The experimental heat transfer results discussed in Section 2.3.2, on the other hand, seem to exhibit a trend which can be attributed to the degree of mixing within a bubble. However, despite the apparent significance of such effects of mixing on the energy and mass transfer processes, it is assumed here that the motion of the gas within the bubble may be considered of secondary importance in examining the forces which govern the rate of formation of a bubble. In effect, therefore, it has been assumed that there is continuous equilibrium of pressure and temperature throughout the bubble during formation. The equilibrium values, of course, vary with time during the formation period of the bubble.

Lastly, the present analysis does not take into account the possibility of mass transfer from the liquid phase to the gas bubble. It has been demonstrated (38) that the transfer of liquid vapor into a bubble during the period of formation can be significant when operating with the liquid phase at a temperature such that the magnitude of the liquid vapor pressure is significant relative to the total static pressure on the bubble ($p_v/p_{bubble} \gtrsim 0.1$). However, for water at temperatures below 27C (80F), it has been shown that the change in the volume of a bubble due to vapor transfer is less than 2 percent; and such contributions have been considered negligible in this analysis. In order to isolate the effect of heat transfer upon bubble formation the experimental investigation discussed in Section 2 was confined to such regimes wherein vapor transfer effects could be considered negligible.

3.2.2 Idealized Analytical Model

Figure 40 illustrates a sequence of the growth of an ideal spherical gas-liquid interface. As can be seen therein, the bubble, which is defined by the spherical interface and the orifice plane, is at all times a portion of a sphere which can be completely specified in terms of the instantaneous values of the bubble radius, R(t), and the limiting angle $\theta^*(t)$ shown in Fig. 41. It is apparent that at any instant of time

$$\cos \theta^* = - \sqrt{1 - (R/R_o)^2} \qquad (\theta^* \geq \frac{\pi}{2})$$

$$\sin \theta^* = R_o/R$$

and, for a given orifice radius, R_o, $\theta^*(t)$ is a function only of $R(t)$.

The initiation of the formation of the bubble has been arbitrarily taken to occur at the instant when the bubble is a hemisphere of radius equal to that of the orifice. That is, $R = R_o$ when $t = 0$, the arbitrary beginning of the formation period. The growth of the bubble proceeds with the addition of mass through the orifice until the instant of detachment of the bubble, the termination (by definition) of the formation period. The period of time, hereinafter referred to simple as the "formation time" or the "formation period", is defined as the interval of time between the instant when the gas-liquid interface is a hemisphere of radius equal to that of the orifice and the instant when the bubble is detached from the orifice. The difference between the "total formation time," as defined in Section 2.1.3, and the "formation time" is defined as the "start time", which is the interval of time between the instant when the meniscus first becomes visible above the orifice and the instant when the meniscus is a hemisphere of radius equal to that of the orifice. Consequently, the "total formation time" is the sum of the "start time" and the "formation time." The analysis presented here applies only to the motion of the gas-liquid interface during the "formation time."[1]

The motion of the bubble surface can be analyzed by considering such motion as consisting of two simple superposable motions[2] (a) the motion of the surface due to pure radial growth and (b) the motion of the surface due to vertical translation. The radial growth of the bubble results from the addition of mass, while the vertical translation of the center of the bubble is required in order that the base of the bubble be maintained at the orifice plane up to the instant of actual detachment. Figure 42 illustrates those motions individually as though they are two successive stages of motion, with a radial growth at a velocity $\frac{dR}{dt}\bar{r}$ and a vertical translation at a velocity $V_y\bar{j}$. By considering the hypothetical downward displacement of the bubble rim in contact with the orifice due to the radial growth, it can be shown that the magnitude of the vertical velocity required to maintain the base of the bubble at the orifice plane (zero net velocity) is

$$V_y = - \frac{1}{\cos \theta^*} \frac{dR}{dt} \qquad (3.1)$$

[1] See Sections 2.1.3 and 2.4.1 for a complete definition and illustration of the time intervals cited.

[2] The geometrical growth of the model bubble is similar to that suggested by Hayes, et al (8).

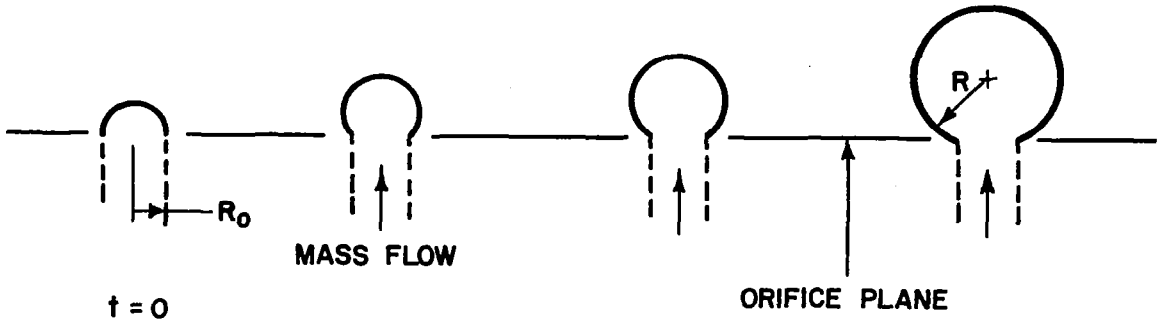

FIG. 40 SEQUENCE OF BUBBLE GROWTH

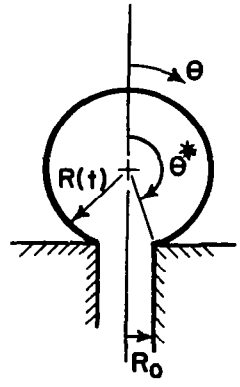

FIG. 41 INSTANTANEOUS SPECIFICATION OF BUBBLE

The resultant velocity of a point on the bubble surface, as shown in Fig. 43, is given by

$$\overline{V} = \left(\frac{dR}{dt}\right) \overline{r} + V_y \overline{j}$$

or when resolved into normal and tangential components with reference to the bubble surface, the resultant velocity becomes

$$\overline{V} = \left(\frac{dR}{dt} + V_y \cos \theta\right) \overline{r} - V_y \sin \theta \, \overline{r}_\theta \qquad (3.2)$$

The vertical velocity of translation given by equation 3.1 should be recognized as the minimum vertical velocity for the assumed spherical bubble shape. Photographic observation of the formation of a bubble (see Figs. 5 and 17) indicates that at some instant during the formation period the buoyant force acting on the bubble begins to exceed the liquid inertia, viscous drag, and surface tension forces which tend to restrain the bubble at the orifice. At such time, the net upward force acting on the bubble accelerates the bubble, increasing V_y above the value given by the equation 3.1. The situation is further aggravated as time proceeds, due to a continuous modification in the magnitude of the operating forces as well as changes in the orientation of the interface, resulting finally in the stretching and narrowing of the interface into a cylindrical neck at the point of attachment to the orifice. That neck rapidly collapses, leading to a detachment of the bubble from the orifice, while a new gas-liquid interface closes at the orifice. The development of a criterion for the detachment of a bubble from an orifice and the determination of the exact instant of time when the bubble breaks away from the orifice would require a detailed stability analysis of the gas-liquid interface taking account of the unsteady interaction of all the forces acting at the interface. However, in the present analysis no attempt is made to develop such a criterion. Instead, the instant of detachment has been determined from experimental measurements of the total time of formation. The vertical velocity of translation, as given by equation 3.1, is employed throughout the bubble formation period.

The coordinate system employed in the analysis is relative to the bubble and is shown in Fig. 44 with the origin situated at the center of the spherical bubble. Because of the axial symmetry of the flow, a point in space need only be specified in terms of the radial coordinate, r, and the angular coordinate, θ. In a moving coordinate system it is necessary to consider the changes in the coordinates r, θ with time. Thus, for a fixed point (45)

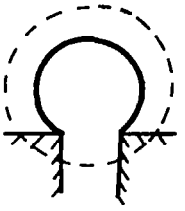

RADIAL GROWTH

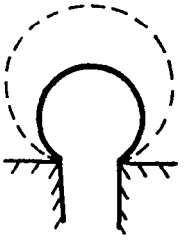

VERTICAL TRANSLATION

FIG. 42 STAGES OF BUBBLE MOTION

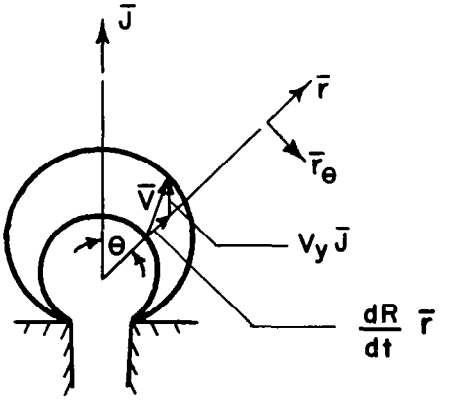

FIG. 43 RESULTANT BUBBLE MOTION

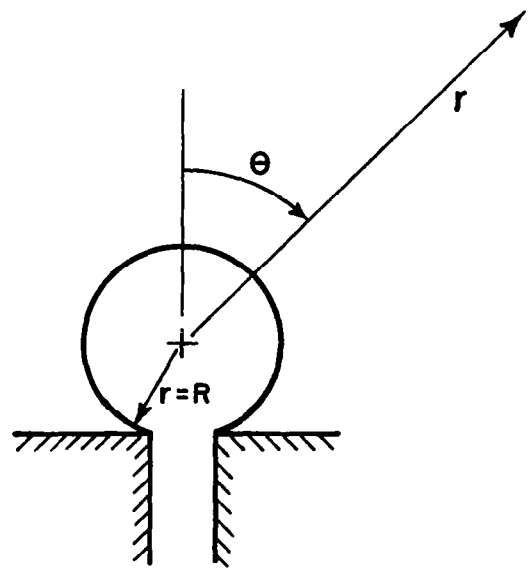

FIG. 44 COORDINATE SYSTEM

$$\frac{\partial r}{\partial t} = - V_y \cos \theta \qquad \frac{\partial \theta}{\partial t} = \frac{V_y \sin \theta}{r} \tag{3.3}$$

A point on the surface of the bubble is given by r = R. The normal velocity component at the bubble surface is given by (see equation 3.2)

$$(V_r)_{r=R} = (\frac{dR}{dt} + V_y \cos \theta) \tag{3.4}$$

This is a boundary condition to be satisfied by the solution for the motion of the liquid at every point on the bubble surface, r=R.

3.3 Analytical Solution

Employing the aforementioned idealized model, a mathematical description of the growth of a gas bubble is obtained by an application of the conservation equations. The mathematical formulation of the problem results in a system of five non-linear first order differential equations involving the time dependent pressure, temperature, mass, radius and rate of growth of the gas bubble. Each of those quantities is obtained as a function of time by a simultaneous solution of the system of equations.

3.3.1 Formulation of the Problem

The analysis of the growth of a gas bubble as a result of mass input through an orifice and of energy transfer across the gas-liquid interface is obtained by applying the principles of conservation of mass, momentum, and energy to the growing bubble.

The analysis of Davidson and Schuler (25) has indicated that for bubble formation in liquids of relatively low viscosity (e.g., water) the viscous drag force acting on the bubble during its formation is of secondary importance, and that the principal resistance offered by the liquid to the growth of the interface is in the form of an inertia force resulting from the acceleration of the liquid away from the orifice. In the research reported herein, the liquids of interest are relatively inviscid liquids, such as water and ethyl alcohol (also liquid metals). However, unlike in reference (25), the effects of viscosity are not entirely neglected in the present analysis. Initially, the motion of the interface is taken to be occurring in inviscid surroundings so that the motion of the liquid surrounding the bubble

surface is reduced to a solution of the potential motion of an infinite liquid medium surrounding a bubble which is simultaneously growing and translating. That solution yields the potential velocity distribution in the liquid which, at the bubble surface, coincides with the motion of the surface. One can then calculate the retardation that would be produced due to the presence of viscosity and linearly superpose the viscous forces on the other forces acting at the interface. Thus, in the present analysis the viscous forces are determined from a momentum balance equation in which the inertia forces are considered small and, in which the tangential velocity gradient for the calculation of the shear force at the interface is based on the gradients of velocity obtained from the inviscid potential solution. The viscous forces so calculated are added on by simple superposition to the other forces in the final momentum balance equation. The limitations of such a supposition of superposability of forces are well known. Thus, where the nonlinear interaction of such forces is fundamental, as in stability problems, superposability is generally inadmissible. However, this method of calculating the inviscid flow field and then superposing the viscous force is employed here entirely for the purpose of an approximate determination of the effect of viscosity on the rate of growth of the bubble. In fact the computed results (see Section 3.3.3) will show that these effects are negligible.

The Equation of Motion

The derivation of the equation of motion for an expanding and translating spherical bubble boundary in an infinite, incompressible, inviscid liquid with constant external pressure p_∞ at infinity is presented in Appendix IV. The equation of motion which relates the pressure $p_L(R,\theta,t)$ in the liquid at the bubble boundary to the bubble size and the radial and translational velocity and acceleration of the boundary is as follows.

$$\frac{p_L(R,\theta,t)-p_\infty}{\rho} = R\frac{d^2R}{dt^2} + \frac{3}{2}\left(\frac{dR}{dt}\right)^2 + \frac{3}{2}V_y\cos\theta\frac{dR}{dt}$$

$$+ V_y^2\left(\frac{\cos^2\theta}{2} - \frac{5}{8}\sin^2\theta\right) + \frac{1}{2}R\cos\theta\frac{\partial V_y}{\partial t} \qquad (3.5)$$

where R = instantaneous bubble radius

$\frac{dR}{dt}$ = instantaneous radial velocity

V_y = vertical translational velocity

ρ = liquid density

with the coordinate system as illustrated in Fig. 44.

As seen from equation 3.5, the pressure in the liquid at the bubble boundary is a function of θ, the angular position of the point under consideration. In order that the pressure of the gas inside the bubble be independent of θ, a mean pressure $\bar{p}_L(R,t)$ in the liquid at the bubble boundary is defined as

$$\bar{p}_L(R,t) = \frac{\iint p_L(R,\theta,t)\,dA}{\iint dA} \tag{3.6}$$

where dA is an element of area, with the integration performed over the bubble surface area $(0 \le \theta \le \theta^*)$.

From equations 3.5 and 3.6, the mean pressure in the liquid at the bubble boundary is given by

$$\frac{\bar{p}_L(R,t)-p_\infty}{\rho} = R\frac{d^2R}{dt^2} + \frac{3}{2}\left(\frac{dR}{dt}\right)^2 + V_y^2\left(-\frac{1}{4} + \cos\theta^* + \cos^2\theta^*\right)$$

$$+ \frac{3}{4}V_y\frac{dR}{dt}(1+\cos\theta^*) + \frac{1}{4}R\frac{\partial V_y}{\partial t}(1+\cos\theta^*) \tag{3.7}$$

The instantaneous pressure, p(t), of the gas in the bubble can be obtained from equation 3.7 by accounting for the increase in pressure across the gas-liquid interface due to the surface tension along the interface and the viscosity of the liquid. Thus,

$$p(t) - \bar{p}_L(R,t) = \Delta p_\sigma + \Delta p_\mu \tag{3.8}$$

where

$\Delta p_\sigma = \frac{2\sigma}{R}$ = increase in pressure across a spherical interface of curvature R and interfacial tension σ.

Δp_μ = increase in pressure in the bubble due to the viscosity of the liquid.

An approximate value of the effect of viscosity on the pressure in the bubble is obtained as demonstrated in Appendix V. The expression for the increase in pressure in the bubble due to the viscosity of the liquid is shown to be given by

$$\Delta p_{\mu} = 4 \frac{\mu}{R} \frac{dR}{dt} \tag{3.9}$$

Substituting the value of $\bar{p}_L$ (R,t) from equation 3.7, and equation 3.9 into equation 3.8, the pressure in the bubble is given by

$$\frac{p(t)-p_{\infty}}{\rho} = \frac{2\sigma}{R} + 4 \frac{\mu}{R} \frac{dR}{dt} + R \frac{d^2R}{dt^2} + \frac{3}{2} \left(\frac{dR}{dt}\right)^2$$

$$+ V_y^2 \left(-\frac{1}{4} + \cos\theta^* + \cos^2\theta^*\right) \tag{3.10}$$

$$+ \frac{3}{4} V_y \frac{dR}{dt} (1+\cos\theta^*) + \frac{1}{4} R \frac{\partial V_y}{\partial t} (1+\cos\theta^*)$$

Equation 3.10 specifies the dynamic pressure in the bubble required to produce the motion of the spherical bubble boundary surrounded by liquid. The equation is written in a general form in terms of V_y which, as discussed in Section 3.2.2, is given by

$$V_y = - \frac{1}{\cos\theta^*} \frac{dR}{dt} \tag{3.1}$$

The Energy Equation

The energy equation for the open system defined by the spherical bubble boundary is obtained by equating the sum of the heat transferred into the system and the energy carried in by the gas stream to the sum of the change in internal energy and the work done by the system on its surroundings. Written on an energy-per-unit-time basis, the energy equation is

$$h A (T_L - T) + c_p T_i \frac{dm}{dt} = \frac{d(m c_v T)}{dt} + p \frac{dV}{dt} + \sigma \frac{dA}{dt}$$

$$+ \pi\mu V_y^2 R \left[\frac{2}{3} - \cos\theta^* + \frac{1}{3}\cos^3\theta^*\right] \tag{3.11}$$

where

$hA(T_L-T)$ = rate of heat transfer to the bubble

$c_p T_i \frac{dm}{dt}$ = rate of energy carried into bubble by the gas stream

mc_vT = internal energy of the system

$p \frac{dV}{dt}$ = expansion work rate

$\sigma \frac{dA}{dt}$ = surface work rate

$\pi\mu V_y^2 R \left[\frac{2}{3} - \cos\theta^* + \frac{1}{3}\cos^3\theta^*\right]$ = viscous work rate

The rate of energy transfer across the bubble boundary is expressed in terms of a convective transfer coefficient characteristic of the gas-liquid interface and the mixing within the bubble. The energy carried in by the gas stream, written in the form of a total temperature, includes the enthalpy and kinetic energy associated with the gas stream, though the kinetic energy is negligible. The expression for the work done in increasing the surface area of the bubble arises from the fact that the superficial energy per unit area associated with the common surface of two immiscible fluids is equal to σ, the surface tension (force/unit length). The derivation of the expression for the viscous work rate, presented in Appendix V, has been obtained by a modification of Stokes' solution for viscous flow past a sphere to satisfy the boundary conditions of the present model.

The volume, V(t), and surface area, A(t), of the spherical bubble are related to R(t) and $\theta^*(t)$ by means of the following expressions which have been derived in Appendix VI.

$$V = \frac{2\pi}{3} R^3 \left(1 - \cos\theta^* - \frac{1}{2}\cos\theta^* \sin^2\theta^*\right) \qquad \text{(VI-1)}$$

$$A = 2\pi R^2 \left(1 - \cos\theta^*\right) \qquad \text{(VI-2)}$$

The Equation of State

The equation of state for the gas in the bubble relating the instantaneous values of bubble pressure, volume, mass, and temperature is assumed to be as follows.

$$pV = m \overline{R} T \qquad (3.12)$$

where

$\bar{R}$ = gas constant

The Equation of Continuity

The equation of continuity for the rate of flow of mass into the bubble is obtained by considering the flow of gas through the chamber which supplies the submerged orifice. In other words, the control volume for the purpose of obtaining the mass balance equation has been taken as the volume between the orifice plane and the point in the gas supply system where there exists a large pressure drop which, thereby, controls the mean rate of flow of the gas through the system. Since the flow of mass out of the ante-chamber equals the flow of mass into the bubble, a mass balance on the ante-chamber gives the rate of flow of mass into the bubble as

$$\frac{dm}{dt} = \dot{W}_i - \frac{V_c}{\bar{R}\, T_c} \frac{dp_c}{dt} \qquad (3.13)$$

where

m = instantaneous bubble mass

$\dot{W}_i$ = mass flow rate into the chamber

V_c = volume of the chamber

T_c = temperature of the gas in the chamber

p_c = pressure of the gas in the chamber

In the statement of equation 3.13, it has been assumed that the flow of gas through the ante-chamber is isothermal, and the chamber dimensions are such that the pressure, $p_c(t)$, is uniform throughout the chamber at any instant. In most cases, the mass flow rate into the system, W_i, is constant, being regulated externally, and therefore the second term on the right hand side of equation 3.13 reflects the effect of the coupling of the bubble formation mechanism with the gas supply system.[1]

[1] It is interesting to note that equation 3.13 seems to indicate the absence of any coupling between the bubble formation process and the supply system in the two limiting cases (discussed in Section 1.1.1), namely (i) when the bubble is formed at the tip of a long capillary, and (ii) when the gas is supplied from an infinite reservoir.

Equations 3.10, 3.11, 3.12, and 3.13 comprise a system of four equations in four unknowns, namely, the bubble radius R, the bubble mass m, the mean pressure p, and the mean temperature T. Since a spherical bubble geometry has been assumed in all stages of the growth, the volume and surface area of the bubble are related to the radius by equations VI-1 and VI-2.

It is apparent that a closed form integration of the system of equations is not feasible. However, it is possible to employ standard techniques for the numerical integration of the system of equations to yield a solution for R(t), m(t), and T(t) as functions of time for a given orifice size and liquid properties and for specified gas flow conditions. The initial conditions for the integration are

$$R(0) = R_o$$

$$p(0) = p_o$$

$$T(0) = T_1$$

$$\left(\frac{dR}{dt}\right)_{t=0} = 0^1 \qquad (3.14)$$

$$V(0) = V_o = \frac{2\pi}{3} R_o^3$$

$$m(0) = m_o = \frac{p_o V_o}{\bar{R} T_o}$$

The integration can be performed for any desired length of time up to a value of t_f, the formation time, which, by definition, specifies the termination of the formation period.

3.3.2 Solution of the Problem

In order to simplify the numerical solution, it is convenient to non-dimensionalize equations 3.10 through 3.13 by defining[2] the following dimensionless variables and parameters.

---

[1] This initial condition is apparent when one considers that the radius of curvature of the spherical gas-liquid interface passes through a minimum at $R = R_o$.

[2] The non-dimensionalizing procedure is similar to that of Chern and Enig (46).

$$P = \frac{p}{p_0} \qquad M = \frac{m}{m_0}$$

$$P_\infty = \frac{p_\infty}{p_0} \qquad \Theta_L = \frac{T_L}{T_1}$$

$$\Theta = \frac{T}{T_1} \qquad \Theta_1 = \gamma$$

$$S = \frac{R}{R_0} \qquad C = \frac{W_1 R_0 \sqrt{\rho/p_0}\ \bar{R} T_1}{p_0 \left(\frac{2\pi}{3} R_0^3\right)}$$

$$\tau = \frac{t}{R_0 \sqrt{\rho/p_0}} \qquad G_1 = \frac{V_c T_1}{\frac{2\pi}{3} R_0^3 T_c} \qquad (3.15)$$

$$P_c = \frac{p_c}{p_0}$$

The trigonometric functions of θ^* in terms of the dimensionless variable S are

$$\cos\theta^* = -\sqrt{1 - \left(\frac{R_0}{R}\right)^2} = -\sqrt{1 - \frac{1}{S^2}}$$

$$\sin\theta^* = \frac{R_0}{R} = \frac{1}{S} \qquad (3.16)$$

Using equations 3.1 for the translational velocity and substituting the dimensionless variables 3.15, equation 3.10 can be transformed to the dimensionless form

$$P - P_\infty = \frac{E_3}{S} + \frac{E_2}{S}\frac{dS}{d\tau} + (S+Y_7)\frac{d^2S}{d\tau^2} + \left(\frac{3}{2} + Y_5 + Y_6 - Y_{20}\right)\left(\frac{dS}{d\tau}\right)^2 \qquad (3.17)$$

where

$$Y_5 = \frac{S^2}{(S^2-1)}\left[-\frac{1}{4} - \frac{\sqrt{S^2-1}}{S} + \frac{(S^2-1)}{S^2}\right]$$

$$Y_6 = \frac{3}{4}\left[\frac{S}{\sqrt{S^2-1}} - 1\right]$$

$$Y_7 = \frac{S}{4}\left[\frac{S}{\sqrt{S^2-1}} - 1\right]$$

$$Y_{20} = \frac{1}{4} \frac{S}{(S^2-1)^{3/2}} \left[1 - \frac{\sqrt{S^2-1}}{S} \right]$$

$$E_2 = \frac{4\mu}{p_0 R_0 \sqrt{\rho/p_0}}$$

$$E_3 = \frac{2\sigma}{R_0 p_0}$$

The energy equation 3.8 is transformed to dimensionless form by substituting the dimensionless variables 3.15 and using equations 3.1, VI-3, and VI-4 to give

$$E_1 Y_4 (\Theta_L - \Theta) + \left(\frac{1}{\gamma-1}\right) \Theta_1 \frac{dM}{d\tau} = \left(\frac{1}{\gamma-1}\right) \frac{d(M\Theta)}{d\tau} + P Y_1 \frac{dS}{d\tau} + E_5 Y_3 \frac{dS}{d\tau} + E_4 Y_2 \left(\frac{dS}{d\tau}\right)^2 \quad (3.18)$$

where

$$Y_1 = 3S^2 + 3S\sqrt{S^2-1} + \frac{3}{2} \frac{\sqrt{S^2-1}}{S} + \frac{3}{2} \frac{1}{S\sqrt{S^2-1}}$$

$$Y_2 = \frac{S^3}{(S^2-1)} \left[\frac{2}{3} + \frac{\sqrt{S^2-1}}{S} - \frac{1}{3} \frac{(S^2-1)^{3/2}}{S^3} \right]$$

$$Y_3 = 2S + 2\sqrt{S^2-1} + \frac{1}{\sqrt{S^2-1}}$$

$$Y_4 = S^2 \left[1 + \frac{\sqrt{S^2-1}}{S} \right]$$

$$E_1 = \frac{3 h T_1 \sqrt{\rho/p_0}}{p_0}$$

$$E_4 = \frac{3}{2} \frac{\mu}{p_0 R_0 \sqrt{\rho/p_0}}$$

$$E_5 = \frac{3\sigma}{p_o R_o}$$

The energy transfer term in equation 3.18 can be written in a more illustrative form as follows:

$$E_1 Y_4 (\Theta_L - \Theta) = \frac{3\sqrt{\rho/p_o}}{p_o} Y_4 h T_i (\Theta_L - \Theta)$$

or

$$E_1 Y_4 (\Theta_L - \Theta) = \left(\frac{3\sqrt{\rho/p_o}}{p_o}\right) Y_4 h (T_L - T_i) \left(\frac{\Theta_L - \Theta}{\Theta_L - 1}\right)$$

The product $h(T_L - T_i)$ represents the maximum heat flux to the bubble (cal/sec-cm^2), occurring when Θ is a minimum of 1.0. The ratio $(\Theta_L - \Theta)/(\Theta_L - 1)$ represents the active fraction of the maximum driving force $(\Theta_L - 1)$.

The equation of state in dimensionless form simply becomes

$$P Y_8 S^3 = M \Theta \tag{3.19}$$

where

$$Y_8 = 1 + \frac{\sqrt{S^2 - 1}}{S} + \frac{\sqrt{S^2 - 1}}{2 S^3}$$

The continuity equation 3.13 is transformed to

$$\frac{dM}{d\tau} = C - G_1 \frac{dP_c}{d\tau} \tag{3.20}$$

It is interesting to note that in the expression for the dimensionless flow parameter C, namely

$$C = \frac{\dot{W}_i \bar{R} T_i}{p_o} \left[\frac{R_o \sqrt{\rho/p_o}}{\frac{2\pi}{3} R_o^3} \right]$$

the term in the brackets is constant for a given liquid and orifice size. Since the density of the gas entering the bubble, ρ_g, is equal to $p_o/\bar{R} T_i$ it is apparent that C is proportional to the mean volumetric rate of flow of gas through the system.

Finally, the initial conditions 3.14 become

$$S(0) = 1 \qquad \left(\frac{dS}{d\tau}\right)_{\tau=0} = 0$$

$$P(0) = 1$$

$$\Theta(0) = 1 \qquad M(0) = 1 \tag{3.21}$$

An expression for the dimensionless pressure derivative, $\frac{dP}{d\tau}$, is obtained by differentiating equation 3.18 with respect to τ and substituting from equations 3.18 and 3.20 for $\frac{d\Theta}{d\tau}$ and $\frac{dM}{d\tau}$ and is as follows.

$$\frac{dP}{d\tau} = (\gamma-1)E_1 \frac{Y_4}{Y_8 S^3}(\Theta_L-\Theta) + \frac{\Theta_1 C}{Y_8 S^3} - \frac{\Theta_1 G_1}{Y_8 S^3}\frac{dP_c}{d\tau} - (\gamma-1)\frac{Y_1}{Y_8 S^3} P \frac{dS}{d\tau}$$

$$- (\gamma-1)E_4 \frac{Y_2}{Y_8 S^3}\left(\frac{dS}{d\tau}\right)^2 - (\gamma-1)E_5 \frac{Y_3}{Y_8 S^3}\frac{dS}{d\tau} - \frac{Y_9}{Y_8} P \frac{dS}{d\tau} - 3\frac{P}{S}\frac{dS}{d\tau} \tag{3.22}$$

where

$$Y_9 = \frac{1}{\sqrt{S^2-1}} - \frac{\sqrt{S^2-1}}{S^2} + \frac{1}{2}\frac{1}{S^2\sqrt{S^2-1}} - \frac{3}{2}\frac{\sqrt{S^2-1}}{S^4}$$

The system of equations 3.17, 3.18, 3.20, and 3.22 can be reduced to a system of five first order ordinary differential equations by defining a new variable $U = ds/d\tau$. Making that substitution one obtains the following system of equations

$$\frac{dS}{d\tau} = U \tag{3.23}$$

$$\frac{dU}{d\tau} = \frac{1}{(S + Y_7)}\left[P - \frac{E_2 U}{S} - \frac{E_3}{S} - P_\infty - \left(\frac{3}{2} + Y_5 + Y_6 - Y_{20}\right) U^2\right] \tag{3.24}$$

$$\frac{d\Theta}{d\tau} = (\gamma-1)\, E_1\, Y_4 \frac{(\Theta_L-\Theta)}{M} + \frac{(\Theta_1-\Theta)}{M}\frac{dM}{d\tau} - (\gamma-1)\, Y_1 \frac{PU}{M}$$

$$- (\gamma-1)\, E_4\, Y_2 \frac{U^2}{M} - (\gamma-1)\, E_5\, Y_3 \frac{U}{M} \tag{3.25}$$

$$\frac{dP}{d\tau} = (\gamma-1)\, E_1 \frac{Y_4}{Y_8\, S^3} (\Theta_L - \Theta) + \frac{\Theta_i C}{Y_8\, S^3} - \frac{\Theta_i G_1}{Y_8\, S^3} \frac{dP_c}{d\tau}$$

$$- (\gamma-1) \frac{Y_1}{Y_8\, S^3} PU - (\gamma-1)\, E_4 \frac{Y_2}{Y_8\, S^3} U^2$$

$$- (\gamma-1)\, E_5 \frac{Y_3}{Y_8\, S^3} U - \frac{Y_9}{Y_8} PU - 3 \frac{PU}{S} \qquad (3.26)$$

$$\frac{dM}{d\tau} = C - G_1 \frac{dP_c}{d\tau} \qquad (3.27)$$

with the initial conditions

$$S(0) = P(0) = \Theta(0) = M(0) = 1 \qquad U(0) = 0 \qquad (3.28)$$

The system of five first order ordinary differential equations, 3.23 through 3.27, in five unknowns, U, S, P, Θ, and M, and the initial conditions 3.28 are sufficient for the determination of U, S, P, Θ, and M as functions of the independent variable τ for specified conditions on E_1, E_2, E_3, E_4, E_5, γ, Θ_L, Θ_i, C, G_1, P_c, P_∞. Standard techniques for the numerical integration of ordinary differential equations can be employed for the solution of equations 3.23 to 3.27 to give the computed values of U, S, P, Θ, and M for specified limits of τ.

3.3.3 Computation of the Solution

In Section 3 it has been stated that the overall analytical problem may be divided into three parts. The first part related to the prediction of the changes (with respect to time) of the several variables pertaining to the growth of the bubble and to the state of the gas within the bubble during the formation period. The determination of the overall increase in the temperature of the gas in the bubble during formation was stated as the second part of the analytical problem. In order to solve that problem one needs to postulate a mechanism of energy transfer to the bubble. No such mechanism may be postulated until one could state with reasonable certainty the nature of the gas motion within the bubble. In order to circumvent that difficulty, an average heat transfer coefficient, obtained from experimental results (see equation 2.4), is introduced into the energy balance equation to enable the prediction of the overall increase in the temperature of the gas in the bubble during the formation period. However, the validity of postulating an average heat transfer coefficient

applicable over the entire formation period must be checked, the third part of the problem stated in Section 3. This is accomplished by calculating, on the basis of the theoretical analysis, another significant parameter pertaining to the bubble which is a strong function of the energy transfer and which may also be checked with independent experimental results. The most significant parameter which is easily compared with experimental results (obtained by high speed photography) is the rate of growth of the bubble volume during the formation period. The approach taken is, therefore, to predict analytically the mean temperature of the gas in the bubble at the end of the formation period by means of an experimental average heat transfer coefficient applicable throughout the formation period and in turn to check the value of the average heat transfer coefficient employed by comparing the predicted bubble volume as a function of time with the experimental bubble volume growth rate.[1]

The numerical integration of equations 3.23 to 3.27 has been accomplished as follows.

1. The values of the parameters, E_1, E_2, E_3, E_4, E_5, γ, Θ_L, Θ_1, G_1, $P_c(\tau)$, P_∞ for which the solution is desired are specified.[2]
2. The initial conditions 3.28 are substituted into equations 3.23-3.27 to determine the derivatives of the variables at $\tau=0$. Reference should be made to Appendix VII for a description of the determination of the limits of certain terms which are indeterminant upon the substitution of the initial conditions for S and U.
3. Equations 3.23-3.27 are then used in conjunction with the classical fourth-order Runga-Kutta technique (47, 48) for determining the variables S, U, P, Θ, and M for increasing values of the independent variable τ. The Runga-Kutta technique is used for the numerical integration for the first four incremental changes in τ.
4. For the fifth and all succeeding incremental changes in τ, the numerical integration is accomplished by using equation 3.23-3.27 in conjunction with the fourth-order Adams-Moulton predictor-corrector method (47,48).

The method used in step 4 can be applied to cover any desired range of the independent variable yielding the computed values of S, U, P, Θ, and M for each successively increasing value of τ.

---

[1] Obtained from high speed photographs (see Figs. 17 and 18).

[2] Unless otherwise specified, the following values have been used: $p_\infty = p_0$, therefore $P_\infty = 1$, and $T(0) = T_1 = T_c$.

The procedure for the numerical integration of equations 3.23-3.25 was programmed for an IBM 7090 digital computer. The computer program incorporated a subroutine developed by Welsh (49) for the simultaneous integration of ordinary differential equations using the Runga-Kutta and Adams-Moulton methods as described. The program enables the calculation of the dimensionless variables S, U, P, Θ, and M as functions of τ for the specified parameters: (a) liquid properties, ρ, μ, σ,[1] (b) gas properties, γ, $\bar{R}$, (c) orifice radius, R_o, (d) heat transfer conditions, h, T_L, T_i, and (e) gas flow conditions, W_i, T_c, V_c, $p_c(t)$. The solutions for the dimensionless variables S, U, P, Θ, and M can of course be transformed to dimensional form to determine R(t), dR/dt, p(t), T(t), and m(t). The volume of the bubble, V(t), can be computed from R(t) and equation VI-1 and is of particular interest, since that is one variable that can be measured experimentally by means of high speed photography.

Computed solutions have been obtained for three distinct types of bubble formation hereinafter referred to as (a) adiabatic bubble formation, (b) isothermal bubble formation, and (c) non-isothermal bubble formation. Adiabatic bubble formation is defined as the type of bubble formation obtained theoretically in which the energy transfer between the liquid and the gas is entirely neglected, whatever be the actual difference in temperature between the liquid and the gas. The calculation is performed by assuming that the heat transfer term in the energy equation 3.25 is zero, or in the computations, by setting the heat transfer coefficient, h, equal to zero.

Isothermal bubble formation refers to the case where it is assumed that whatever be the mechanism or the rate of energy transfer between the liquid and the gas in the bubble, the gas is at some arbitrarily constant temperature. Those conditions could be approximated in an experimental set-up either (a) when there is initially no temperature difference between the gas and the liquid (comparable to the conditions mentioned in Section 2.2), or (b) when the bubble volume is sufficiently large, the rate of growth of the bubble is sufficiently small, and further the gas is "well mixed" during the entire formation time. Thus, in the former case, if $T = T_i = T_L$ = constant, there is energy transfer to or from the gas in the bubble sufficient to maintain T = constant. The mechanism by which the energy transfer occurs is unspecified. In order to perform the computations for that case, the following changes in the differential equations

---

[1] In the computations it has been assumed that the dynamic value of the surface tension is the same as the static value in view of the absence of appropriate information regarding the dynamic surface tension (see Roll (50)).

are required. Equation 3.25, of course, becomes

$$\frac{d\Theta}{d\tau} = 0 \tag{3.25a}$$

and equation 3.26 is changed to read

$$\frac{dP}{d\tau} = \frac{\Theta_i C}{Y_s S^3} - \frac{\Theta_i G_1}{Y_s S^3} \frac{dP_c}{d\tau} - \frac{Y_g}{Y_s} PU - 3 \frac{PU}{S} \tag{3.26a}$$

By setting equation 3.25 equal to zero it is also possible to obtain an expression for the dimensionless energy transfer, Q', required to maintain the isothermal condition. Thus, noting that $\Theta_i = \Theta$ = constant, equation 3.25 gives

$$0 = (\gamma-1) \frac{Q'}{M} - (\gamma-1) Y_1 \frac{PU}{M} - (\gamma-1) E_4 Y_2 \frac{U^2}{M} - (\gamma-1) E_5 Y_3 \frac{U}{M}$$

where the convective energy transfer term, $E_1 Y_4 (\Theta_L - \Theta)$, has been replaced by the gross energy transfer term, Q'. From the preceding expression, the dimensionless gross energy transfer rate is given by

$$Q' = Y_1 PU + E_4 Y_2 U^2 + E_5 Y_3 U \tag{3.25b}$$

The computations for the isothermal case are performed as described in steps 1 through 4 (see page 107) while noting that equations 3.25a and 3.26a are used in place of equations 3.25 and 3.26, respectively.

It may be pertinent to point out that the conditions of isothermal bubble formation defined herein is similar to the condition of "isothermal" bubble formation defined in the presentation of the experimental data in Section 2.2. Both conditions refer to the case where the liquid and the incoming gas are at least initially at the same temperature, $T_i = T_L$.

Lastly, non-isothermal bubble formation refers to the case of bubble formation under the most general conditions considered in the present analysis. Heat transfer from the liquid to the gas in the bubble is assumed to occur on account of the temperature difference between the liquid and the gas, and the temperature of the gas in the bubble is allowed to vary during the formation time, depending upon the extent of the energy transfer to the bubble. However, at any instant of time during the growth of the bubble, the gas is supposed to be at a mean temperature

over the entire bubble volume, a consequence of the assumption of perfect mixing. The condition of non-isothermal bubble formation defined herein is comparable to the experimental conditions referred to in Section 2.3.

Determination of the flow into a bubble from an ante-chamber of finite volume requires a knowledge of $p_c(t)$[1], which is obtained only from experimental measurements. A number of solutions are computed for the case of a variable rate of mass flow into the bubble based on the flow data obtained during the experimental investigation described in Section 2.4. However, in order to illustrate the procedure in obtaining the solutions, a constant flow rate into the bubble is employed in some of the following examples.

Constant Flow Rate Computations

Figures 45 and 46 illustrate the computed solutions for the dimensionless bubble pressure and temperature for the case of adiabatic bubble formation with constant flow into the bubble, $C = 0.791$. The effects of surface tension and liquid viscosity have been omitted by setting $\sigma = \mu = 0$. The plots illustrate the oscillatory nature of the solution with a significant first maximum of bubble pressure and temperature occurring very early in the formation period followed by minima and maxima of successively decreasing amplitude. The value of the flow parameter $C = 0.791$ corresponds to the typical flow conditions given in Table 2. For those conditions, the oscillatory behavior was predominant only up to a value of $\tau = 100$, corresponding to a time interval of $t = 8 \times 10^{-3}$ seconds. Davidson and Schuler (25) have shown that a bubble formed under the above conditions has a total formation period of approximately 40×10^{-3} seconds ($\tau = 500$). It may therefore be observed that the predicted oscillations in bubble pressure and temperature have a relatively small amplitude over most of the formation period.

The effect of surface tension and liquid viscosity was determined by computing the solutions for the cases (a) $\sigma = 72$ dyne/cm, $\mu = 0$ and (b) $\sigma = 72$ dyne/cm, $\mu = 0.9$ cp; the latter corresponding to the values for water at 27C. It was found for case (a) that the surface tension had only a very small effect on the solution, with the amplitude of all pressure

[1] Or some auxiliary information which enables the determination of the rate of flow into the bubbles. See the last of this section.

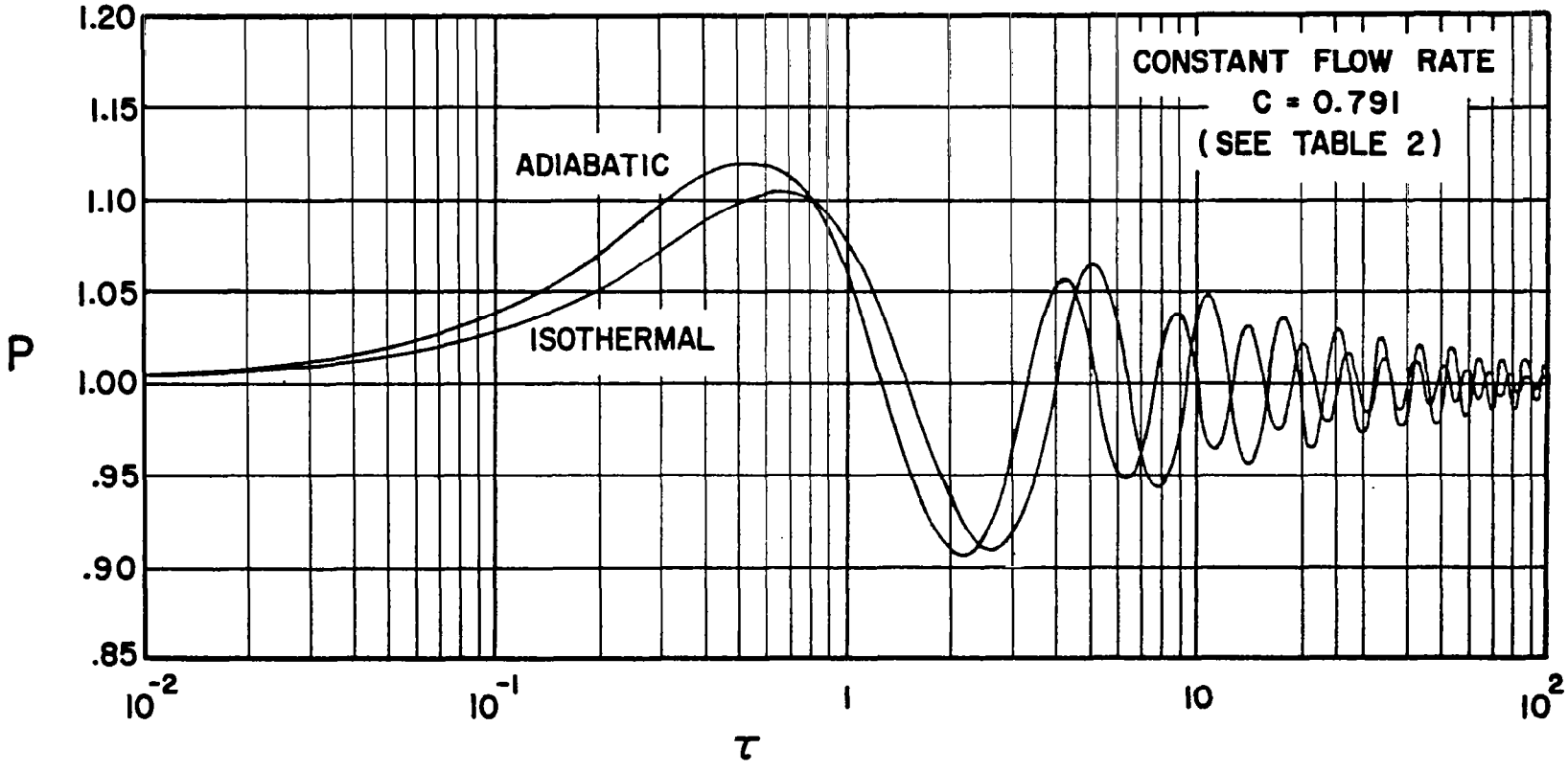

FIG. 45 DIMENSIONLESS PRESSURE FOR ADIABATIC AND ISOTHERMAL FORMATION (CONSTANT FLOW RATE)

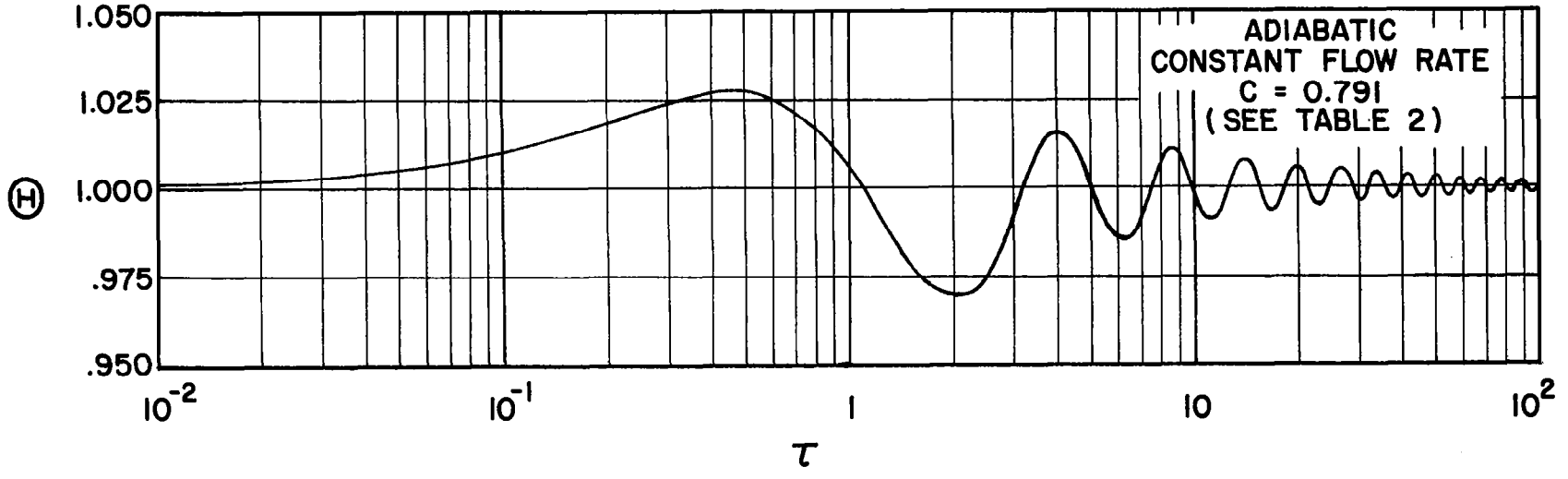

FIG. 46 DIMENSIONLESS TEMPERATURE FOR ADIABATIC FORMATION (CONSTANT FLOW RATE)

maxima and minima being slightly larger (< 0.02%) and the amplitude of all temperature maxima and minima being slightly smaller (< 0.05%) in comparison with the solution for the case of $\sigma = \mu = 0$. The effect of the viscosity of the liquid as determined in case (b) was also detectable but was yet another order of magnitude smaller than the effect of surface tension, thus justifying, largely, the approximate manner in which that effect has been included in the basic formulation of the problem in Section 3.3.1. In fact, in all subsequent computations both the effect of the viscosity of the liquid and the effect of surface tension are neglected.

Table 2

Typical Flow Conditions for C = 0.791
Adiabatic or Isothermal

R_o	0.0795 cm
$\dot{W}_i$	1.19×10^{-2} gm/sec
$T(0) = T_c = T_i = T_L$	300 K (540 R)
$\dot{q}_i$	10 cm^3/sec
ρ	1 gm/cm^3
$\sigma = \mu$	0
$\bar{R}$	0.0709 cal/K-gm
γ	1.4
p_o	1 atm
h	0 (for adiabatic case)

Referring again to Fig. 45, the computed solution of the dimensionless bubble pressure is presented for the case of isothermal bubble formation with constant flow into the bubble, C = 0.791.[1] It may be observed that the isothermal solution still possesses an oscillatory character with the amplitudes of the first maximum and minimum somewhat less than that for the adiabatic case. The amplitudes of all succeeding maxima and

[1] The typical flow conditions presented in Table 2 are applicable for the isothermal case also.

minima appear, however, to be larger for the isothermal case than for the adiabatic case. That may be due to a reduced rate of damping for the isothermal case as a result of the oscillatory energy transfer required to maintain, even approximately, the isothermal condition. Equation 3.25b was employed to compute the energy transfer rate which oscillated from positive (energy in) to negative (energy out) values during the formation period with an order of magnitude of 10^{-2} cal/sec. However, it was found that over the total bubble formation period the net energy transfer during isothermal bubble formation was essentially zero.

The solutions for the dimensionless bubble pressure and temperature for the case of non-isothermal bubble formation with a constant flow into the bubble, C = 0.791, were computed for an overall temperature difference, T_L-T_i, of 16.7C (30.0F). A mean value for the average convective heat transfer coefficient was obtained from the experimental data presented in Section 2.3.2. The mean value for h from experimental data is employed at this stage primarily for comparison of the theoretical solutions for different types of bubble formation. A check on the validity of employing such an average value for the heat transfer coefficient for the entire formation period is discussed at the end of this section.

Table 3 gives the values of the parameters pertinent to the computation of the solution for non-isothermal formation and illustrates typical flow conditions for C = 0.791.

The computed solution for the dimensionless bubble pressure (not illustrated) was found to be practically the same as that obtained for the adiabatic case (see Fig. 45). The amplitude of the dimensionless bubble pressure appeared to be slightly less for the non-isothermal case than for the adiabatic case.

Figure 47 illustrates the oscillatory nature of the solution for the dimensionless temperature, Θ, for the non-isothermal case (T_L-T_i = 16.7C). The solution computed for the non-isothermal case indicates clearly that Θ could reach a value of approximately 1.435 during bubble formation if the length of the bubble formation period is not significantly altered by the heat transfer effects and if the average value of the heat transfer coefficient employed is representative of the rate of energy transfer to the bubble. That result implies that the heat transfer during the bubble formation period could reduce the difference between the temperature of the liquid and the mean temperature of the gas within the bubble from 16.7C (i.e., T_L-T_i = 16.7C) to 3.7C (i.e., T_L-T = 3.7C).

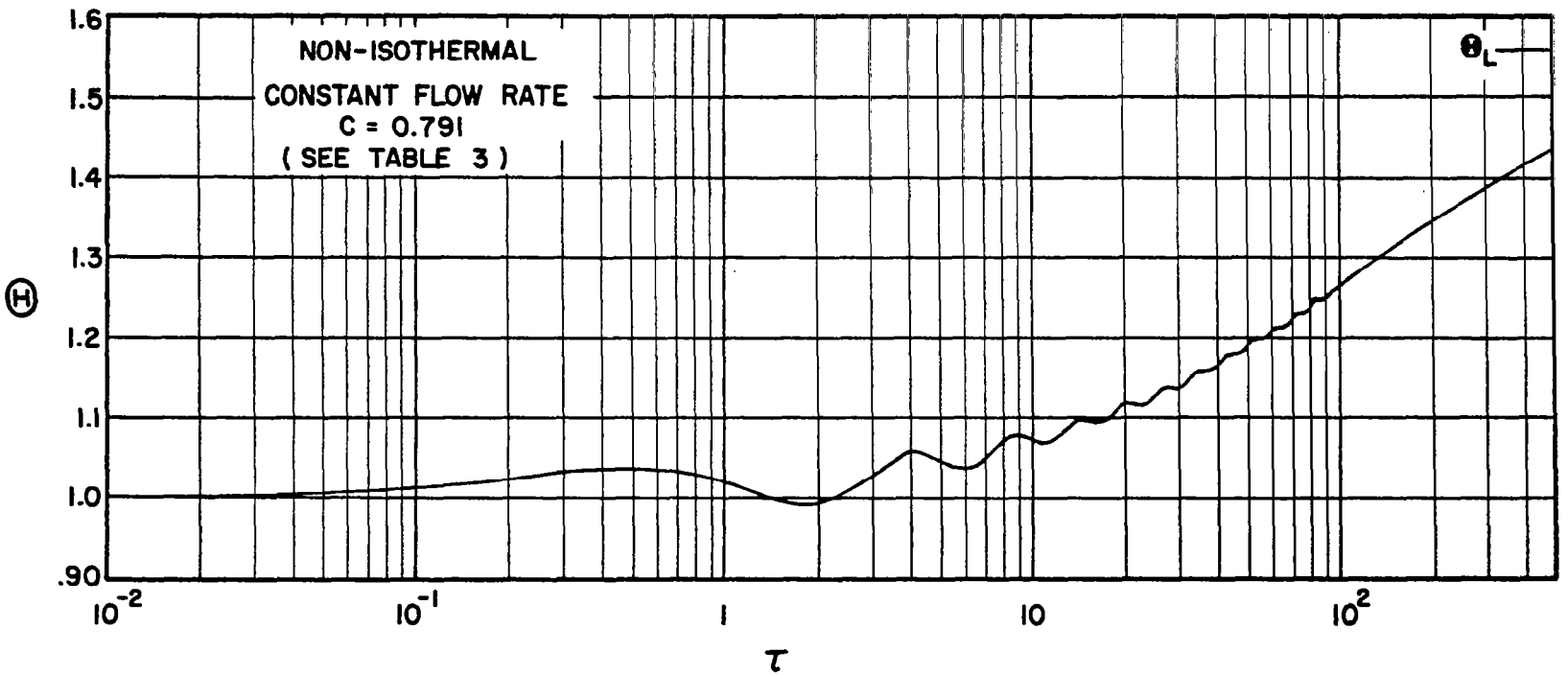

FIG. 47 DIMENSIONLESS TEMPERATURE FOR NON-ISOTHERMAL FORMATION (CONSTANT FLOW RATE)

Non-Constant Flow Rate Computations

Computed solutions for the case of a non-constant flow rate into the bubble can be obtained in an identical manner for adiabatic, isothermal, and non-isothermal bubble formation. However, in order to specify,

Table 3

Typical Flow Conditions for C = 0.791
Non-Isothermal

R_o	0.0795 cm
$\dot{W}_i$	1.19×10^{-2} gm/sec
$T(0) = T_c = T_i$	300 K (540 R)
$\dot{q}_i$	10 cm^3/sec
$T_L - T_i$	167 C (300F)
$\bar{h}$	3.66×10^{-3} cal/sec-cm^2-C (27B/hr-ft^2-F)
ρ	1 gm/cm^3
$\sigma = \mu$	0
$\bar{R}$	0.0709 cal/K-gm
γ	1.4
p_o	1 atm

completely, the condition for the flow into the bubble, the pressure, $p_c(t)$, in the ante-chamber during the bubble formation period must be known. The computed solutions for the cases of non-constant flow into the bubble were obtained using the experimentally measured functions of $p_c(t)$ discussed in Section 2.4. The technique for determining the transient pressure function for the formation period is described in Section 2.4.1. Figure 31 presented one such record of one complete cycle of $p_c(t)$ relative to the value of p_c at the start of the cycle over a period including the lapse time, start time, and formation time. The instant at which the bubble formation period commences, determined as described in Section 2.4.1, is indicated on that curve. The computer program employed for computing the analytical solution of equations 3.23-3.27 permitted the input of $p_c(t)$

in the form of a finite number of values of p_c and the corresponding values of t. (The computer program incorporated a spline fit interpolation subroutine (51) which was employed for determining $dp_c/dt = f(t)$ thus enabling the complete specification of the flow into the bubble.) The numerical integration of equations 3.23-3.27 is accomplished in the manner previously described using the instantaneous values of dp_c/dt to complete the evaluation of equation 3.27.

The dimensionless bubble pressure was computed, for the isothermal case with a non-constant flow rate, for the gas flow conditions prescribed in Fig. 31 and was found to possess the same oscillatory character as that previously illustrated in Fig. 45. However, the amplitude of the oscillatory pressure was considerably less ($P_{max} < 1.006$) for the present case (from Fig. 31) because of the smaller mean gas flow rate. A plot of the computed bubble volume as a function of time, V(t), is presented in Fig. 48, which, as previously mentioned, is utilized in the comparison of the analytically predicted and the experimentally determined values of V(t), (see Section 4).

In order to compute the analytical solution for the non-isothermal case with a non-constant flow rate, one again needs information concerning the variation of the pressure, $p_c(t)$, in the ante-chamber. However, in the experimental study of bubble formation under non-isothermal conditions discussed in Section 2.3 for a variable rate of mass flow into the bubbles, the experimental apparatus did not permit the measurement of $p_c(t)$. Therefore, in the case of non-isothermal bubble formation computed for a non-constant flow rate into the bubble, it has been assumed that the instantaneous volumetric rate of flow into the bubble under the non-isothermal conditions is the same as that obtained under the isothermal conditions provided that the mean volumetric rate of flow is the same and all other parameters related to the apparatus and the liquid are also held identical in the two cases. One such case refers to the non-isothermal formation obtained with System I (see Table 1) for a flow rate of approximately 3.1 cm^3/sec[1] (see Fig. 18) and the isothermal bubble formation obtained with the same system (I) for a flow rate of approximately 3.2 cm^3/sec (see Fig. 6). Therefore, on the basis of the equivalence of all parameters known to govern the flow into a bubble for those two cases (at $\dot{q}_i \sim 3.2$ cm^3/sec) (except the difference in temperatures in the non-isothermal case) it has been assumed that the instantaneous

[1] It also happens (see Fig. 19) that at that flow rate, the volume of "unheated" gas passed into the bubble in the non-isothermal case is equal to that passed in the isothermal case.

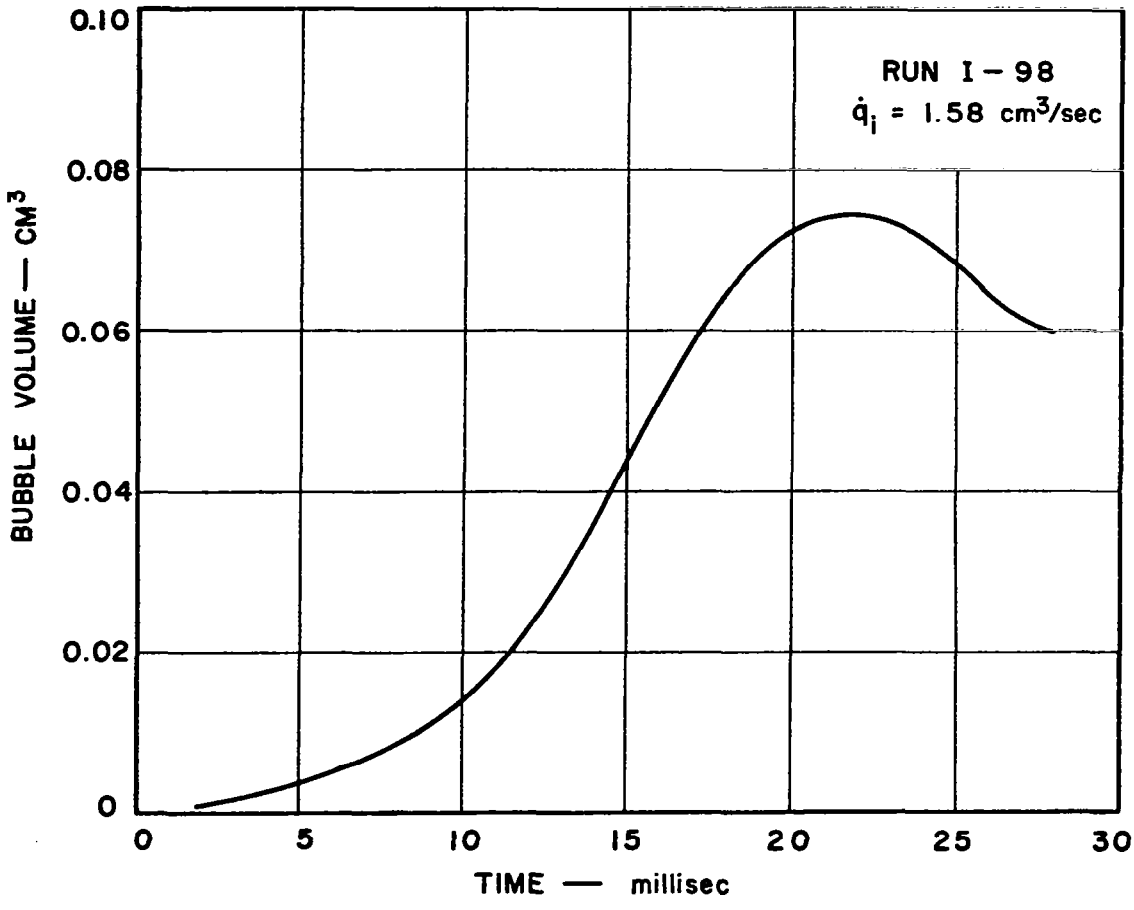

FIG. 48 PREDICTED ISOTHERMAL BUBBLE GROWTH (RUN I – 98)

volumetric rate of gas flow into the bubble is the same for both the non-isothermal and isothermal cases. The validity of that assumption, of course, depends upon whether the difference between the experimentally determined instantaneous values of bubble volume for the two cases (as illustrated in Fig. 20) may be adduced wholly to the volume expansion of the gas in the bubble as a result of heat transfer to the gas in the non-isothermal case. However, it will be assumed that the data in Fig. 6 for the isothermal growth rate is applicable to the non-isothermal case, that is,

$$\left(\frac{dV}{dt}\right)_{\text{Isothermal}} = \left(\frac{dV_{\text{unheated}}}{dt}\right)_{\text{Non-Isothermal}} \tag{3.29}$$

Therefore, the mass rate of flow in the non-isothermal case is given by

$$\left(\frac{dm}{dt}\right)_{\text{Non-Isothermal}} = \rho_i \left(\frac{dV_{\text{unheated}}}{dt}\right)_{\text{Non-Isothermal}} \tag{3.30}$$

where

ρ_i = density of the gas entering the bubble in the non-isothermal case.

By employing the perfect gas law, equations 3.29 and 3.30 give

$$\left(\frac{dm}{dt}\right)_{\text{Non-Isothermal}} = \frac{p_o}{\overline{R}\, T_i} \left(\frac{dV}{dt}\right)_{\text{Isothermal}} \tag{3.31}$$

According to the notation in Section 3.3.2, the non-dimensional form of equation 3.31 is

$$\frac{dM}{d\tau} = E_6 \left(\frac{dV}{dt}\right)_{\text{Isothermal}} \tag{3.32}$$

where

$$E_6 = \frac{R_o \sqrt{\rho / p_o}}{\frac{2\pi}{3} R_o^3}$$

Equation 3.32 is used in place of equation 3.27 to compute the solutions for the case of non-constant flow under non-isothermal

conditions. The computer program enables the input of the varying values of $V_{Isothermal}$ and the corresponding values of t (from Fig. 6) from which $(dV/dt)_{Isothermal} = f(t)$, at any time during formation, is determined by means of a spline fit interpolation subroutine. The numerical integration of equations 3.23-3.26 and 3.32 is accomplished in the manner described earlier in this section.

Figure 49 illustrates the computed solution for the dimensionless bubble gas temperature as a function of dimensionless time during formation for the case of non-isothermal bubble formation with the non-constant gas flow conditions prescribed in Fig. 6 by means of equation 3.32. Table 4 gives the values of the parameters pertinent to the analytical calculations. The average value of the heat transfer coefficient used throughout the formation period was that determined experimentally (run H-18) for the specific condition of non-isothermal formation considered. As can be seen from Fig. 49, the predicted dimensionless bubble gas temperature at the end of the formation period ($\tau = 334$) is 1.44, giving a predicted value for T_b of 221K (397R). The experimentally determined value for T_b (run H-18) was 232K (418R), showing that the bubble temperature at the end of the formation period has been approximated within 5 percent of the experimental value. The predicted overall increase in the bubble gas temperature during formation was then $(T_b - T_i)_{Predicted} = 221 - 152 = 69C$, whereas the experimental value was (run H-18) $(T_b - T_i)_{Experimental} = 80C$.

Figure 50 illustrates the predicted bubble volume as a function of time for the same case. Also included in Fig. 50 is the experimentally determined bubble volume previously illustrated in Fig. 18 (for run H-18). The predicted values of bubble volume are within 30 percent of the experimental values during approximately the first 1/3 of the formation time and within approximately 15 percent or less throughout the remainder of the formation period. It can be seen that the slope of the experimental curve is somewhat larger than that of the predicted curve up to approximately $t/t_f = 0.25$, indicating a greater volumetric rate of growth of the bubble in the experimental case. Such a trend is probably the result of the actual heat transfer coefficient in the experimental case being somewhat greater than the average value used for the predicted curve. The slopes of the two curves are approximately the same throughout the remaining time of formation indicating that the use of an average value for the heat transfer coefficient was a reasonable approximation to the experimental case.

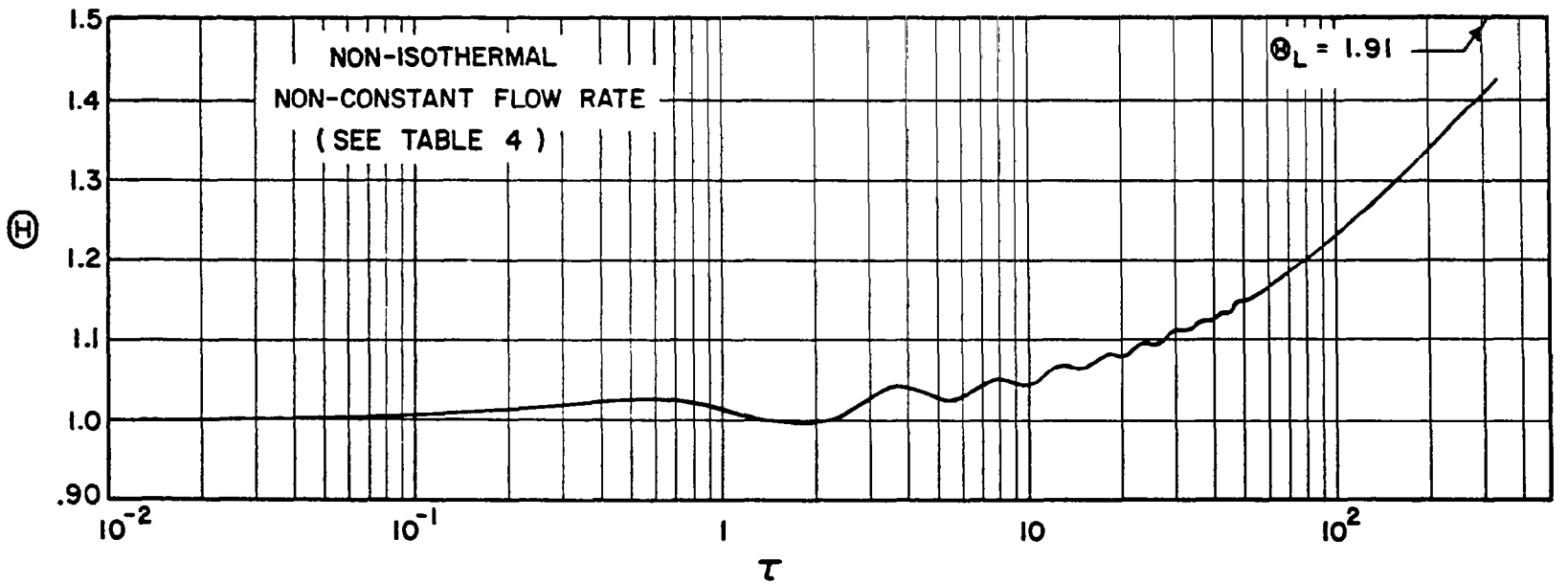

FIG. 49 DIMENSIONLESS TEMPERATURE FOR NON-ISOTHERMAL FORMATION
(NON-CONSTANT FLOW RATE)

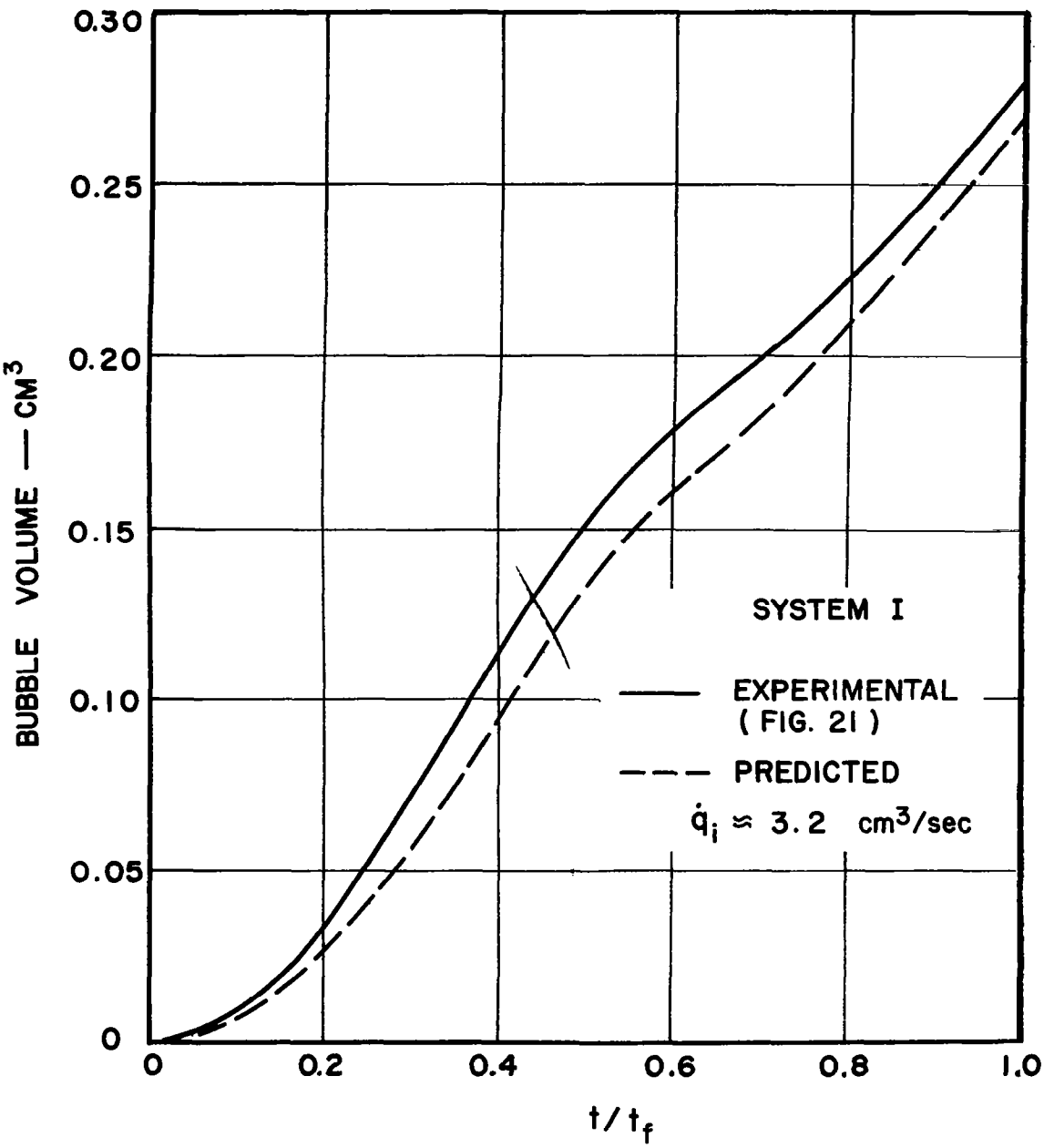

FIG. 50 COMPARISON OF PREDICTED AND EXPERIMENTAL NON-ISOTHERMAL BUBBLE GROWTH (SYSTEM I)

Table 4

Parameters for Non-Isothermal Bubble Formation
Non-Constant Flow (from Fig. 6)

R_o	0.0795 cm
$\dot{W}_i$	6.6×10^{-3} gm/sec
$T(o) = T_c = T_i$	152 K (274 R)
$\dot{q}_i$	3.1 cm^3/sec
$T_L - T_i$	138 C (248F)
$\bar{h}$	2.57×10^{-3} cal/sec-cm^2-C (19B/hr-ft^2-F)
ρ	1 gm/cm^3
$\sigma = \mu$	0
$\bar{R}$	0.0709 cal/K-gm
γ	1.4
p_o	0.974 atm
t_f	0.0277 sec

The analytical solutions for the case of non-constant flow under non-isothermal conditions have been computed in the identical manner for mean gas flow rates of 1.3 and 4.8 cm^3/sec (see Fig. 19). The predicted temperature of the gas in the bubble at the end of the formation period was within 7 percent of that determined experimentally for the lower flow rate and within 3 percent for the higher flow rate. Figures 50 A and 50 B respectively, illustrate the predicted and experimentally determined values of the bubble volume as functions of time for those two cases. As may be observed, the experimental volumetric growth rate in both cases was greater than the predicted growth rate during the initial stage of formation similar to that mentioned in connection with Fig. 50. It can be seen, by comparing Figs. 50A, 50, and 50B, that the agreement between the predicted and experimental bubble growth curves was best for the largest size of bubble considered.

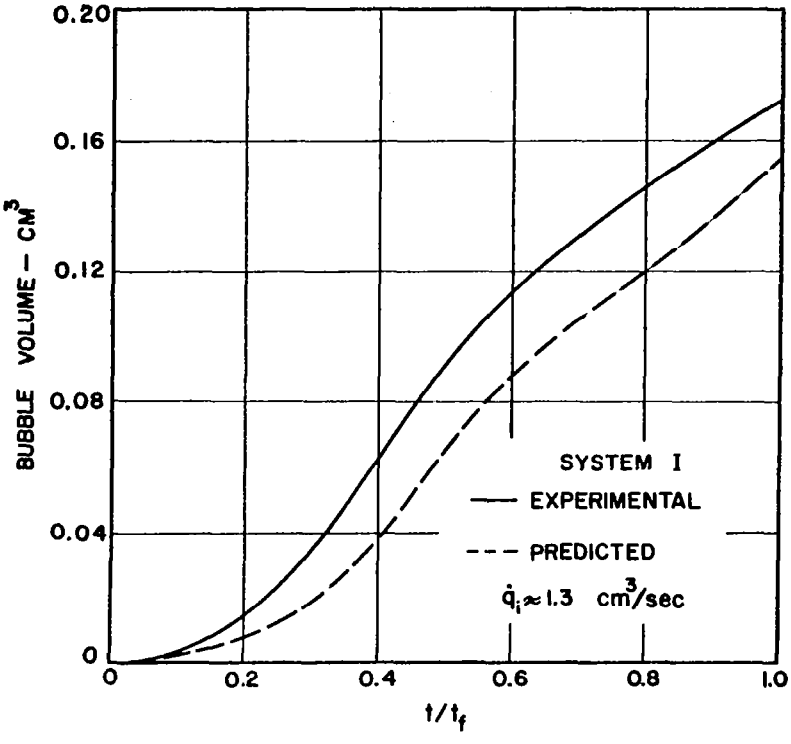

FIG. 50A COMPARISON OF PREDICTED AND EXPERIMENTAL NON-ISOTHERMAL BUBBLE GROWTH (1.3 cm³/sec)

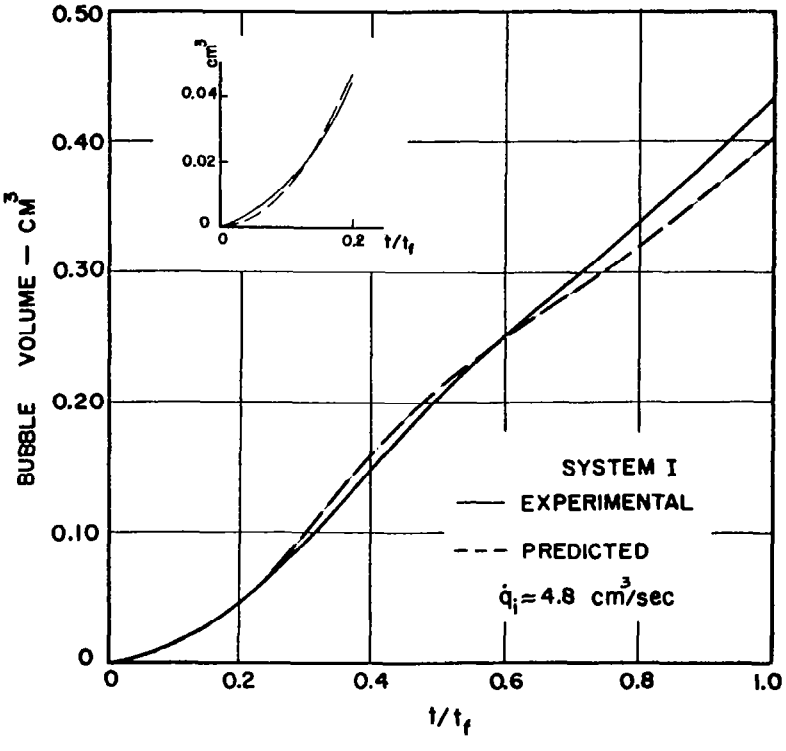

FIG. 50B COMPARISON OF PREDICTED AND EXPERIMENTAL NON-ISOTHERMAL BUBBLE GROWTH (4.8 cm³/sec)

3.4 Analytical Results

The method of computing the solutions for the dimensionless bubble pressure, temperature, radius and mass for the case of adiabatic, isothermal, and non-isothermal bubble formation are given in Section 3.3.3. The adiabatic case is primarily of academic interest. However, the isothermal and the non-isothermal cases (see definitions in Section 3.3.3) compare closely to the physical conditions for two types of bubble formation of considerable practical interest.

3.4.1 Isothermal Bubble Formation

Analytical computations for the case of isothermal bubble formation are useful for assessing the validity of the analytical description of the formation of a gas bubble under the simplest conditions. The gas flow conditions for the isothermal computations have been specified by the experimentally measured conditions presented in Section 2.4 in order that the solution for the predicted bubble volume may be compared with experimental values. Figure 31 presented the experimentally determined gas flow conditions ($p_c(t)$, W_i, V_c, T_i, R_o) for the experimental run I-98. The computed solution for the instantaneous bubble volume, for those flow conditions, is illustrated in Fig. 48. Similarly, the gas flow conditions for the experimental run I-103, presented previously in Fig. 33, have been employed for computing the solution for the instantaneous bubble volume, which is illustrated in Fig. 51.

3.4.2 Non-Isothermal Bubble Formation

Analytical computations for the case of non-isothermal bubble formation are of primary interest in predicting the overall change in the bubble gas temperature during the period of formation and for determining the validity of utilizing, in such computations, an average value for the heat transfer coefficient for the entire formation period.[1] A number of computations pertaining to non-isothermal bubble formation for several hypothetical cases have been made utilizing an average heat transfer coefficient. Thus, computations of the dimensionless bubble pressure and temperature have been made for constant flow into the bubble, $C = 0.791$, with overall temperature differences ($T_L - T_i$) of 167, 556, 1670C. (The solution for $T_L - T_i$ = 167C is

[1] See Section 3.0 and 3.3.3 for statements of the analytical problem.

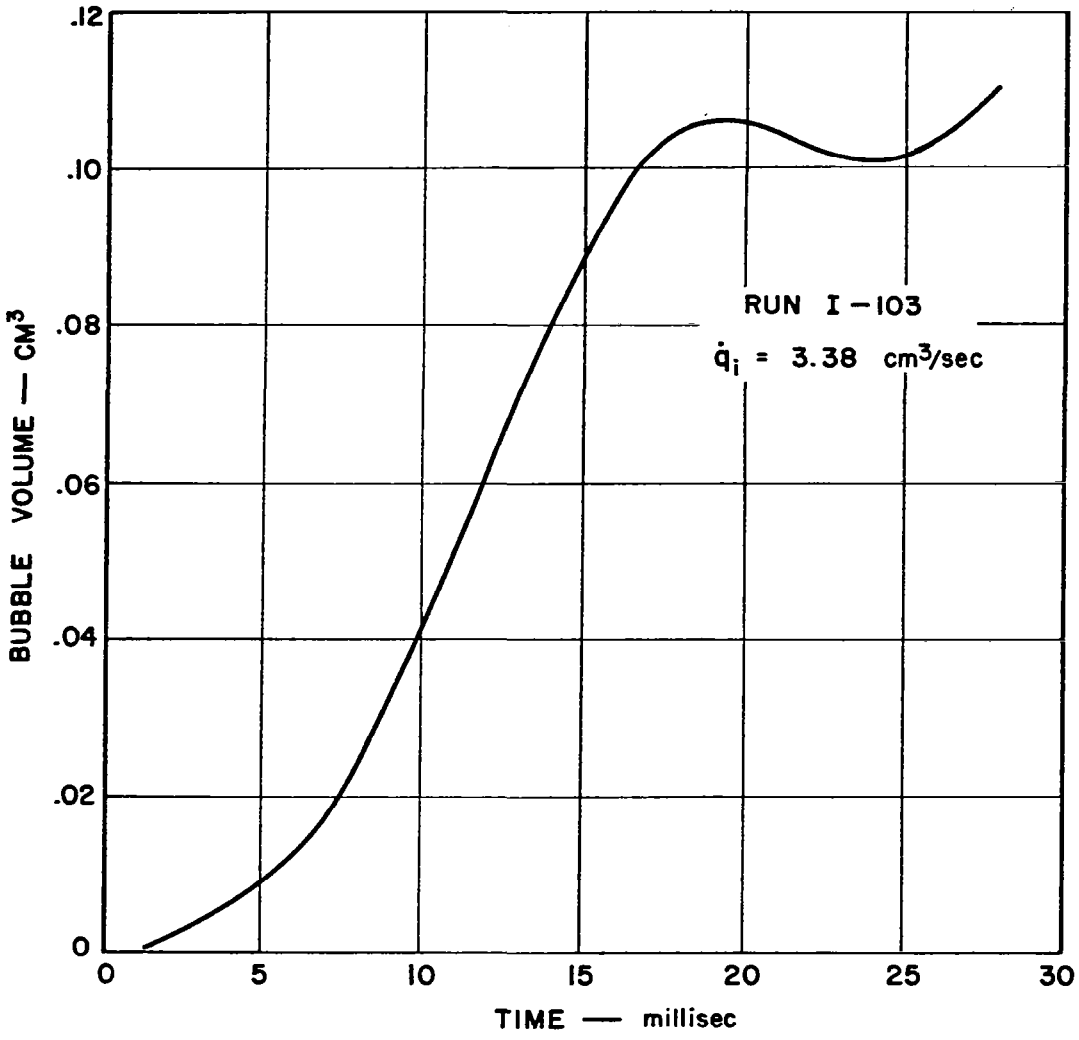

FIG. 51 PREDICTED ISOTHERMAL BUBBLE GROWTH (RUN I-103)

the same as that previously discussed in Section 3.3.3, see Fig. 47). The values of the parameters pertinent to the computations are given in Table 5. The solutions for the dimensionless bubble pressure and temperature for the aforementioned cases are presented in Figs. 52 and 53, respectively. The plots in Fig. 52 indicate that the increased heat flux to the bubbles when $T_L - T_i$ = 167C (300F) causes a noticeable increase in the rate of damping of the predicted pressure oscillations.

As expected, Fig. 53 shows that Θ increases steadily during the formation period approaching the maximum value, Θ_L, as illustrated. While it may have been expected that the heat transfer during bubble formation may alter the length of the formation period, such alterations have been found to be small (~ 10 percent; Section 2.3.1) for overall temperature differences of approximately 167C. The length of the bubble formation period for the flow conditions given in Table 5 has been determined (25)

Table 5

Parameters for Non-Isothermal Bubble Formation
C = 0.791

R_o	0.0795 cm
$\dot{W}_i$	1.19×10^{-2} gm/sec
$T(0) = T_c = T_i$	300 K (540R)
$\dot{q}_i$	10 cm^3/sec
$T_L - T_i$	B: 556 C (1000F) C: 1670C (3000F)
$\bar{h}$	B and C: 3.66×10^{-3} cal/sec-cm^2-C(27B/hr-ft^2-F)
ρ	1 gm/cm^3
$\sigma = \mu$	0
$\bar{R}$	0.0709 cal/K-gm
γ	1.4
p_o	1 atm
t_f' (for isothermal formation (25))	0.040 sec (τ = 500)

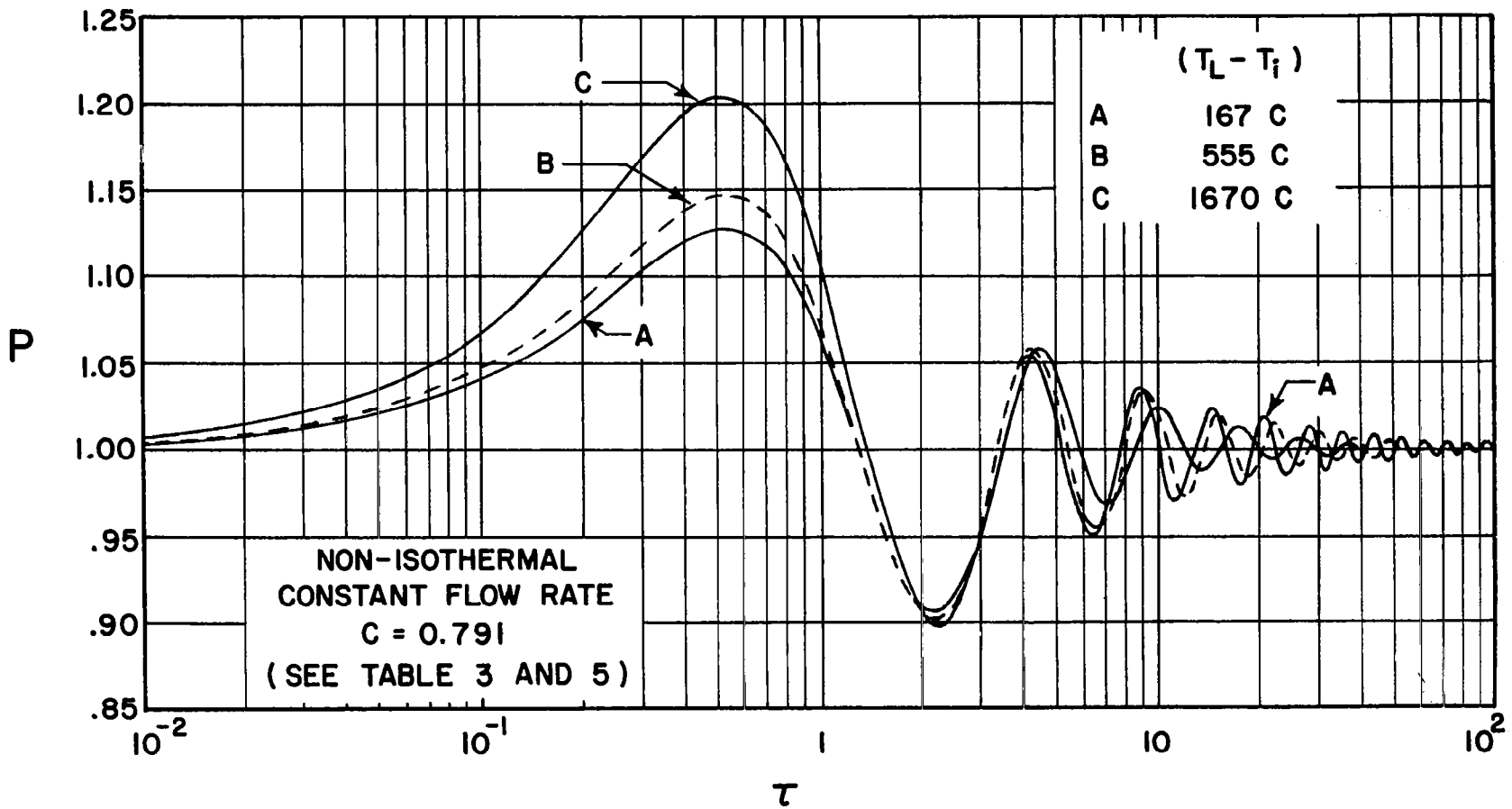

FIG. 52 DIMENSIONLESS PRESSURE FOR NON-ISOTHERMAL FORMATION (CONSTANT FLOW RATE)

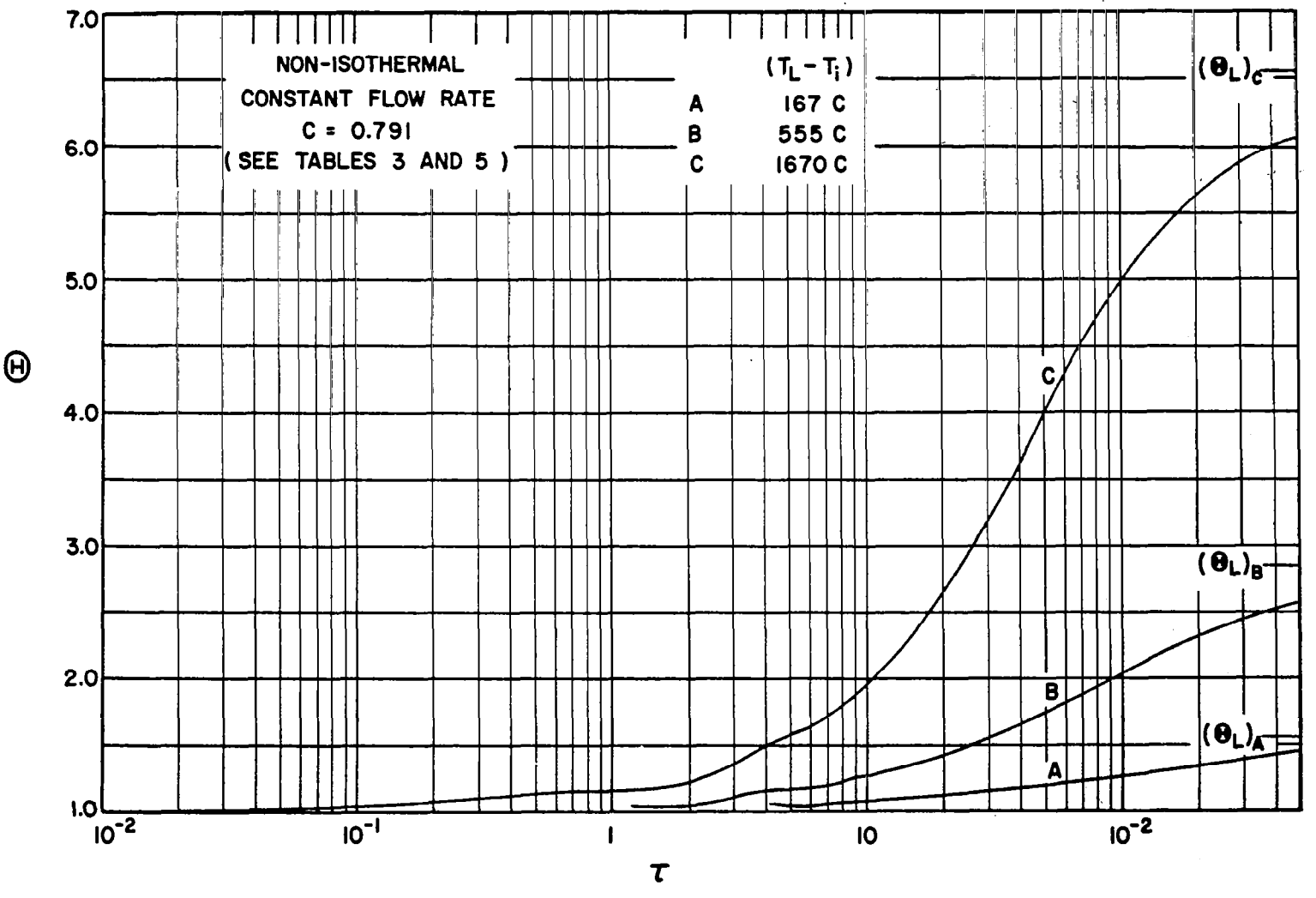

FIG. 53 DIMENSIONLESS TEMPERATURE FOR NON-ISOTHERMAL FORMATION (CONSTANT FLOW RATE)

to be approximately 40×10^{-3} sec, which corresponds to $\tau = 500$. Considering the length of the bubble formation period to be the same ($\tau = 500$) for all of the cases illustrated in Fig. 53, the fraction of the overall temperature difference, Y_t, which is unaccomplished during the period of formation is given in Table 6.

Table 6

Unaccomplished Temperature Change for Constant Flow
C = 0.791

$(T_L - T_i)$	$Y_t = \frac{(T_L - T)}{(T_L - T_i)}$ [1]
167C (300F)	0.219
556C (1000F)	0.178
1670C (3000F)	0.087

Finally, it is of interest to consider what change in the temperature of the gas in the bubble would be predicted for the conditions of non-constant flow into the bubble, discussed in Section 3.4.1, when there exists a difference between the temperature of the liquid and the temperature of the gas entering the bubble. A hypothetical case of non-isothermal bubble formation with an overall temperature difference, $(T_L - T_i)$, of 167C (300F) was investigated. The average heat transfer coefficient for the formation period was obtained from the empirical correlation given in Section 2.3, equation 2.11. Table 7, in conjunction with Fig. 31, gives one set of the values of the parameters pertinent to the computations. The solution for the predicted dimensionless bubble temperature as a function of τ for the aforementioned conditions is illustrated in Fig. 54. It can be seen that the dimensionless bubble temperature is approximately 1.535 at the end of the formation period. Thus, of the hypothetical initial overall temperature difference, $(T_L - T_i) = 167C$, the analysis predicts that only 4 percent remains unaccomplished at the completion of the bubble formation period.

[1] at $\tau = 500$

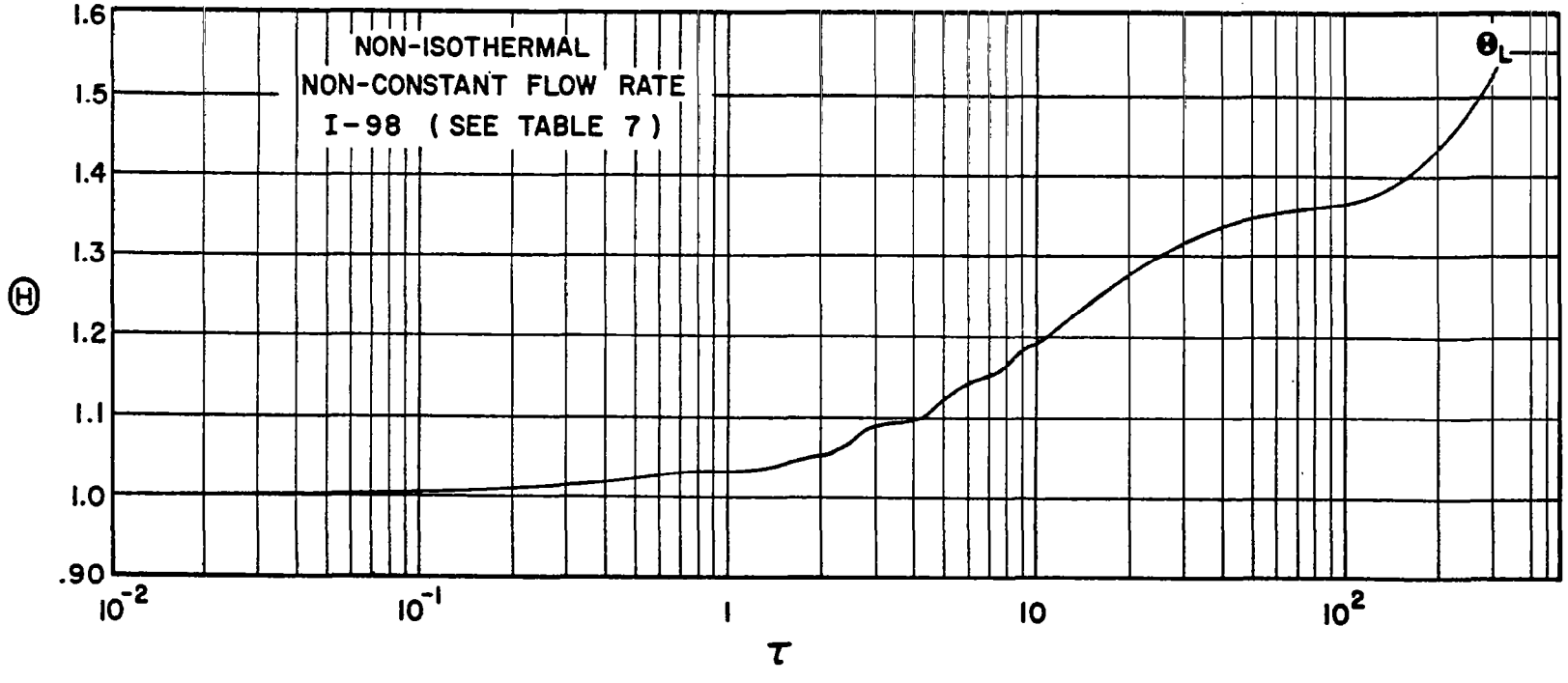

FIG. 54 DIMENSIONLESS TEMPERATURE FOR NON-ISOTHERMAL FORMATION
(NON-CONSTANT FLOW RATE, RUN I-98)

Table 7

Parameters for Non-Isothermal Bubble Formation
Non-Constant Flow (from Fig. 34, I-98)

R_o	0.0795 cm
$\dot{W}_i$	1.79×10^{-3} gm/sec
$T(0) = T_c = T_i$	300 K (540R)
$\dot{q}_i$	1.58 cm^3/sec
$T_L - T_i$	167C (300F)
$\bar{h}$	5.75×10^{-3} cal/sec-cm^2-C (40B/hr-ft^2-F)
ρ	1 gm/cm^3
$\sigma = \mu$	0
$\bar{R}$	0.0709 cal/K-gm
γ	1.4
p_o	1 atm
V_c	21.7 cm^3

Figures 33, 34 and 35 for the experimental runs I-103, 112, and 115 have also been employed to specify the gas flow conditions for the computation of the solutions to equations 3-23-3.27 for hypothetical cases of non-isothermal bubble formation with T_L-T_i = 167C (300F). The unaccomplished temperature ratio Y_t, along with the Fourier modulus, $\alpha\, t_f/R_m^2$, which characterizes the transient heating of the bubble, are presented in Table 8 for all of the cases investigated.

Table 8

Unaccomplished Temperature Ratio for Non-Constant Flow

Run No.	$Y_t = \frac{T_L-T}{T_L-T_i}$ [1]	$\frac{\alpha\, t_f}{R_m^2}$
I-98	0.0395	0.157
I-103	0.0845	0.101
I-112	0.1168	0.0895
I-115	0.1530	0.0819

[1] For a hypothetical T_L-T_i = 167C (300F)

4. DISCUSSION AND CONCLUSIONS

4.1 Discussion

The results of the present investigation are discussed in relation to the following:

1. Isothermal bubble formation mechanism as observed during the experimental investigation.
2. Theoretically predicted isothermal bubble volume growth rate.
3. Validity of the experimentally determined average heat transfer coefficient.
4. Dimensionless correlation of the average heat transfer coefficient.
5. Non-isothermal bubble formation process.
6. Theoretical prediction of the change in gas temperature due to energy transfer during bubble formation.

4.1.1 Isothermal Bubble Formation Mechanism

In the theoretical analysis presented in Section 3, it was shown that a knowledge of the rate of mass flow into a bubble during formation was essential for computing the terminal bubble volume. It is well known (5) that the terminal volume of the bubbles formed by gas injection can be significantly influenced by the volume of the ante-chamber supplying the orifice and the L/D ratio of the orifice channel. Because of the complex interaction of the mechanism of bubble formation with the flow through the system injecting gas into the liquid, the characteristics of the flow of gas into a bubble are not well known except for the case of a constant rate of flow into the bubble. Even in the case of flow into a bubble from a reservoir of constant pressure, there would remain considerable uncertainty in assessing the discharge coefficient for the orifice and the effective pressure drop across such an orifice. Consequently, the mass flow into a bubble for the specific system under consideration was obtained from the experiments described in Section 2.4.1, and those data were employed in a quantitative evaluation of the rate of growth of a bubble.

The pertinent experimental data concerning the rate of mass flow into a bubble, for increasing values of the mean gas flow rate into the ante-chamber (from Figs. 32, 33, 34, 35, and 36), are summarized in curves A, B, C, D, and E in Fig. 55, which presents the normalized mass flow rate into a bubble as a function of the normalized total formation time. The variation of the flow rate into the bubble from the mean flow rate into the ante-chamber was considerable, as can be observed. During

CURVE	$\dot{W}_i \times 10^3$ gm/sec	$\dot{q}_i$ cm^3/sec	V_c	RUN
A	1.79	1.58	21.7	I-98
B	3.86	3.38	"	I-103
C	4.83	4.24	"	I-112
D	5.87	5.17	"	I-115
E	4.83	4.24	39.8	I-113

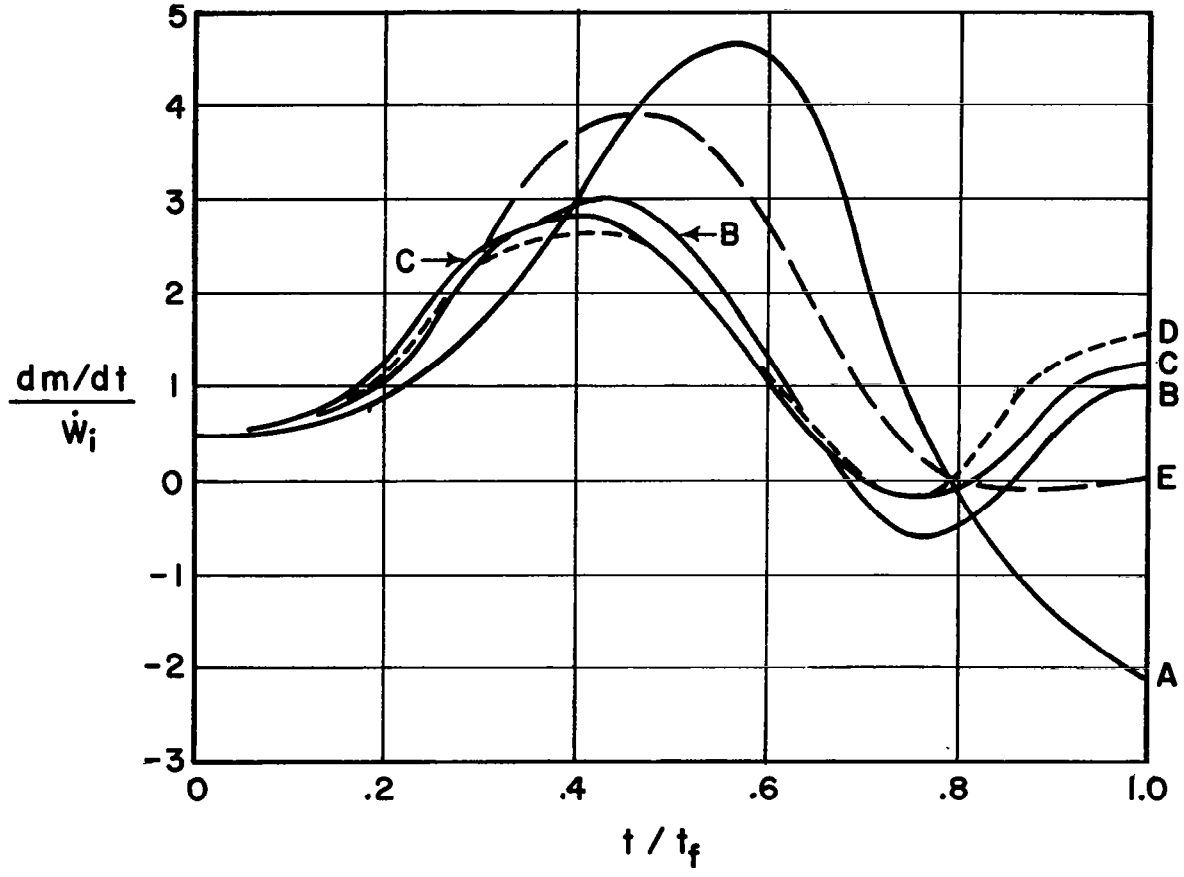

FIG. 55 RATE OF MASS FLOW INTO BUBBLE DURING ISOTHERMAL FORMATION

the initial 20 percent of the formation time, the mass flow rate into the bubble gradually increased to a value equivalent to the mean mass flow rate, probably as a result of accelerating the surrounding liquid away from the orifice. Thereafter, however, as a result of the excess pressure in the ante-chamber, there was a surge of gas into the bubble at rates of up to 2.5 to 4.5 times that of the mean flow rate. As the chamber was depleted of the mass stored during the lapse time, the chamber pressure dropped; and, simultaneously, the rate of flow into the bubble decreased. For relatively small ante-chamber volumes, the inertia of the flow associated with the maximum rates was apparently sufficient to reduce the chamber pressure below the equilibrium value, resulting in, what appears to be, a flow back to the chamber from the bubble prior to the end of bubble formation.

The characteristics of the flow into a bubble have been found to be strongly influenced by the volume of the ante-chamber. A comparison of the curves C and E in Fig. 55, which were obtained for the same mean gas flow rate but for different values of ante-chamber volume, illustrates the influence of the ante-chamber volume upon the rate of flow into the bubble. The rate of flow of gas into the bubble from the larger ante-chamber, curve E (from Fig. 36), was as much as 40 percent greater than the maximum flow rate from the smaller ante-chamber, which was, no doubt, the result of the need to expel a larger amount of stored mass in the former case. It is significant to observe that the flow characteristics presented in curves C and E are noticeably different, which indicates that the ante-chamber volume influenced not only the magnitude of the flow rate into the bubble but also its variation with time during formation.[1] On the other hand, the similarity of curves B, C, and D, which were obtained for the same ante-chamber volume, suggests that, for a given ante-chamber volume and for a limited range of mean mass flow rates, the normalized rate of mass flow into a bubble was approximately independent of the mean flow rate.

In the experimental study of the rate of mass flow into a bubble, it was also found that the magnitude of the ante-chamber excess pressure (during the lapse time) had a pronounced influence upon the rate of flow of gas into a bubble and the terminal bubble volume. As has been shown in Fig. 38, the change in the terminal bubble volume due to a change in the ante-chamber excess pressure or ante-chamber volume can be accounted for in terms of the difference in the mass stored in the ante-chamber during the lapse time.

---

[1] The curve for the larger ante-chamber volume, E, indicates that flow from the bubble to the chamber was negligible, which would be expected for a sufficiently large ante-chamber.

A more complicated feature is the magnitude of the ante-chamber excess pressure, which has been found to be primarily governed by the wettability of the liquid--orifice material combination. As was shown previously in Fig. 39, it was possible to correlate the ante-chamber excess pressure in terms of the depth to which the meniscus wetted the orifice channel during the lapse time. It was observed that the ante-chamber excess pressure was essentially independent of the ante-chamber volume and the mean gas mass flow rate into the ante-chamber, and was primarily a function of the depth of wetting of the orifice channel. However, such limited information can only serve to emphasize the importance of the interfacial phenomena during the lapse time as well as the formation time.

The preceding discussion illustrates the nature of the coupling of the bubble formation mechanism with the flow through the system injecting the gas into the liquid.

4.1.2 Predicted Isothermal Bubble Growth

The formation of the bubble has been studied by assuming the bubble to be of spherical shape throughout its formation and by entirely neglecting the motion of the gas within the bubble, considering only the mean properties associated with the state of the gas in the bubble at any instant. For the particular class of bubbles obtained in the experimental investigation, the assumption of a spherical bubble geometry was a reasonable approximation, as has been illustrated in Figs. 5 and 17. However, it should be recognized that bubble geometries which deviate considerably from that of a sphere have been observed (7,25,38), particularly for systems with a relatively large ante-chamber volume. Consequently, the assumed geometry may be reasonable only for certain classes of bubbles.

Perhaps the most serious limitation of the idealized analytical model was the neglect of the motion of the gas within the bubble. As such, it was considered that there was instantaneous and complete mixing of the gas in the bubble so that the state of the gas could be prescribed just in terms of mean properties. The consequences of such a simplification are expected to be of importance both in connection with the evaluation of the fluid dynamic forces governing the rate of growth of the bubble and also with the process of energy transfer to the gas in the bubble.

A quantitative evaluation of the accuracy of the theoretical analysis describing the bubble formation process, of course, requires a comparison of the predicted and experimental values of at least one parameter that is significantly descriptive of

the process. The parameter which can be experimentally measured for all conditions of the bubble formation process is the variation in the bubble volume with respect to time during the formation period. The predicted and experimental values of the bubble volume may, then, be compared throughout the formation period, thus obtaining one method of assessing the adequacy of the analysis of the bubble formation process.

Figure 56 illustrates the predicted bubble growth for two values of mean gas flow rate (from Figs. 48 and 51). The experimentally determined bubble growth curves (from Fig. 37) are included in Fig. 56 for comparison with the predicted values. It may be observed that a fairly good agreement was obtained between the predicted and experimental values of bubble volume. The terminal volume for both cases was predicted within 8 percent (or less) or that observed experimentally. The predicted rate of growth during the initial portion (approximately 1/3) of the formation period was greater than that determined experimentally. In the case of the smaller mean flow rate, the predicted values were within 20 percent of the experimental values during the initial stage of formation. However, the predicted values for the larger mean flow rate were as much as 50 percent greater than the experimental values during the initial stage (1/3 of the period). During the remaining 2/3 of the formation period, the predicted values were within 15 percent, or less, of the experimental values for both the cases. Similar agreement between predicted and experimental values have also been obtained for higher mean gas flow rates of 4.25 and 5.17 cm^3/sec (not illustrated). Agreement within 20 percent or less was obtained for the final 2/3 of the formation period, but again, during the initial 1/3 of the formation period, the predicted values were as much as 50 percent greater than the experimental values.

Except for the initial stage of bubble formation, it appears that the analysis presented in Section 3 does enable a reasonable prediction of the volume of a bubble when the mass flow into the bubble can be adequately specified. The cause for the larger value of bubble volume predicted during the initial stage of formation can perhaps be attributed to (a) an inadequate representation of the interfacial phenomenon involved at the beginning of the formation of a bubble; perhaps, as has been indicated in other instances (50), the interfacial resistance of a dynamic interface may be much larger than what would be predicted for a static interface; (b) the neglect of the mixing process occurring within the bubble; and (c) the limitations in the accuracy of the experimental measurements during the initial period.

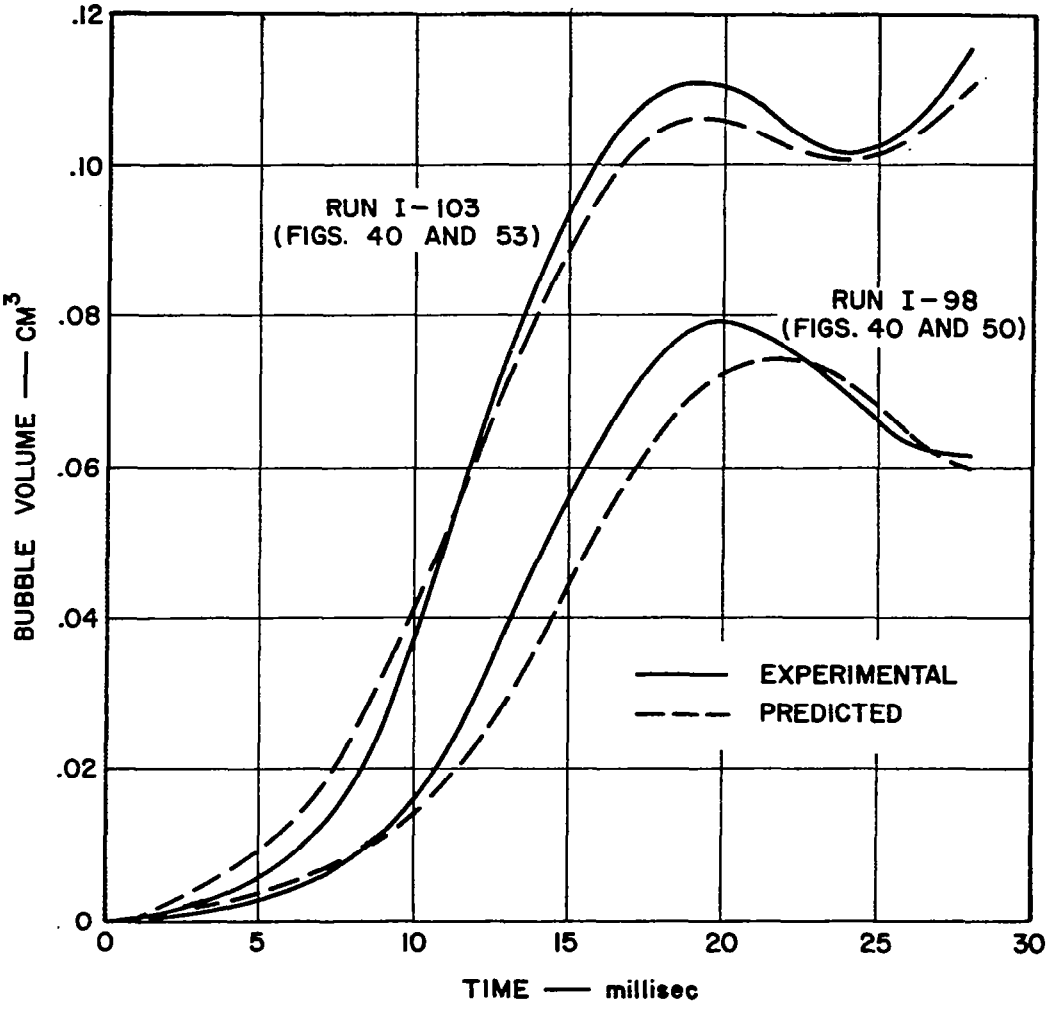

FIG. 56 COMPARISON OF PREDICTED AND EXPERIMENTAL ISOTHERMAL BUBBLE GROWTH

Unfortunately, it was not experimentally feasible to obtain quantitative information regarding the validity of the analytical solutions for the mean pressure and mean temperature of the gas in the bubble, previously illustrated (e.g., Figs. 45 and 46). It can only be inferred that, in view of the reasonable prediction of the growth of a bubble, the solutions for the mean temperature and mean pressure should be representative of the mean state of the gas in the bubble within the limitations of the assumptions regarding the uniformity of the pressure and temperature throughout the bubble and the existence of a continuous equilibrium state of the gas. The variation of the mean pressure and the mean temperature (see Figs. 45 and 46 for the case of constant flow) indicates the possibility of sizeable fluctuations in gas pressure and temperature very early in the bubble formation period, though little can be said regarding the significance of such oscillatory behavior.

4.1.3 Validity of an Average Heat Transfer Coefficient

Next, it was of interest to assess the validity of experimentally determining the quantity of energy transferred to a bubble during formation as the difference in the enthalpy levels of the gas at the beginning and end of the bubble formation period (see equation 2.3). It has been shown in Section 3.3.3, in connection with isothermal bubble formation, that, theoretically, there is energy transfer to or from a bubble to compensate for the moving boundary work done by or on the gas under a varying dynamic pressure, but the net energy transfer for the total formation period was found to be essentially zero. In other words, for all practical purposes, an isothermal state of the gas in a bubble during formation implies essentially zero net energy transfer to the gas for the overall formation period. In particular, it is concluded that the increase in the enthalpy of the gas during the formation under non-isothermal conditions is due essentially to energy input from the liquid to the gas in the bubble. That largely justifies the assumptions introduced in obtaining equation 2.3.

In order to postulate a mechanism for energy transfer between the liquid and the gas in the bubble, one would have to know with reasonable certainty the nature of the gas motion within the bubble. In view of the limited understanding of the interfacial phenomena involved, an alternative approach to the problem was selected to determine a value of the heat transfer coefficient. The experimental determination of an average heat transfer coefficient, based on equation 2.4, was supposedly representative of the energy transfer during the entire formation period and did not require knowledge of the details of any mechanism for the energy transfer process. The verification of the validity of

that value was accomplished by two independent checks: (a) the comparison of predicted and experimental values of the change in bubble gas temperature during the formation period, and (b) the comparison of the predicted and experimental bubble growth curves during formation. The mass flow into the bubble was prescribed by means of measurements made under isothermal conditions assuming that, on the basis of the equivalence of all parameters known to govern the flow into the bubble, the transient volumetric flow rate into the bubble was the same for both non-isothermal and isothermal bubble formation (see Section 3.3.3). The analytical solution for the dimensionless bubble gas mean temperature as a function of time during the formation period has been illustrated in Fig. 49. The predicted value of the mean temperature of the gas in the bubble at the end of the formation period was found to agree with the experimental value within 5 percent, and the predicted change in bubble gas temperature during formation was within 15 percent of that determined experimentally.

Regarding the bubble volume, comparisons of the predicted and experimental bubble growth curves for non-isothermal formation were given in Figs. 50, 50A and 50B showing reasonable agreement. The experimental data exhibited a somewhat larger volumetric growth rate during the initial 10 to 40 percent of the formation period which indicated that the actual rate of heat transfer to the bubble was probably greater than that predicted on the basis of the average heat transfer coefficient. The close comparison of the predicted and experimental volumetric growth rates throughout the remainder of the formation period indicated that, for that portion of the formation period, the use of an average heat transfer coefficient provided a reasonable approximation of the growth of a bubble under the combined effects of mass flow from the orifice and energy transfer from the liquid.

The difference between the experimental and the predicted growth curves during the initial stage of formation is not too surprising in view of a similar discrepancy discussed (see Fig. 56) in connection with isothermal bubble formation. However, the fact that the analysis in the non-isothermal case predicts a volumetric growth rate smaller than the experimental rate emphasizes all the more the fact that the heat transfer coefficient in the physical case was probably considerably higher during the initial stage of formation than the average value for the entire formation period. One would, of course, expect a variation in the heat transfer coefficient during the formation period due to changes in the motion of the gas in the bubble as the bubble size increases and as there occur variations of flow into the bubble. Even though no detailed mechanism has been postulated for the energy transfer process it seems legitimate to consider the influence of the mixing of the gas in the

bubble. The importance of the mixing of the gas within a bubble in determining the rate of energy transfer to the bubble has been illustrated in Fig. 28, where it has been shown that the fraction of the overall temperature difference that was not accomplished during the formation period was as much as 50 to 100 percent less than that predicted for an equivalent stagnant sphere.

4.1.4 Correlation of Average Heat Transfer Coefficient

It is significant to note in connection with the dimensionless correlation of the average heat transfer coefficient (Fig. 29; equation 2.11), that the experimental data for the four different systems considered (see Table 1) are correlated reasonably well by a single empirical relation consisting of variables descriptive of the bubble geometry and the gas physical and flow properties. Of course, only a very limited number of conditions for bubble formation have been considered in this investigation, but the reasonable correlation of the data indicates the feasibility of employing such a correlation procedure.

The effect of the thermal resistance of the liquid upon the energy transfer to the gas bubbles cannot be fully assessed from the results for bubble formation in the two liquids (distilled water and ethyl alcohol) considered in this investigation. There was, however, no significant effect of the threefold variation of the thermal conductivity of the liquid upon the energy transfer characteristics. As has been stated by Nelson and Grey (52), the thermal resistance of the liquid phase can be expected to be small, at least for isolated bubbles.

4.1.5 Non-Isothermal Bubble Formation

In addition to obtaining quantitative data regarding the change in the bubble gas temperature and the rate of energy transfer during bubble formation, it was of interest to consider what effect the energy transfer may have on the mechanism of bubble formation. As has been shown in Figs. 16, 23, and 25, there was a significant increase in the terminal bubble volume for non-isothermal formation over that observed for isothermal formation, which was apparently the result of thermal expansion of the gas in the former case. It has also been shown in Figs. 19, 23, and 25 that the unheated volume of gas passed into the bubble under non-isothermal conditions was less than that passed in under isothermal conditions for small volumetric gas flow rates and was approximately the same for the two conditions for large gas flow rates. Thus, it appears that for small volumetric gas flow rates, the increase in the bubble growth rate in the non-isothermal case due to thermal expansion of the gas can have a significant

influence upon the flow of gas into the bubble. However, as one would expect, for sufficiently large volumetric gas flow rates the effect of thermal expansion upon the bubble formation process is apparently of secondary importance.

The increase in the effective volumetric growth rate of a bubble under non-isothermal conditions, due to thermal expansion of the gas, has been further illustrated by the fact that irregularities in the bubble formation process (doubling) were observed at considerably smaller mean volumetric gas flow rates under non-isothermal conditions than were observed under isothermal conditions.

The total formation time of a bubble under non-isothermal conditions was found to be somewhat different from that for isothermal conditions as has been illustrated in Figs. 21, 24, and 26. The energy transfer during bubble formation apparently was the cause of a 10 percent (approximately) increase in the total formation time under non-isothermal conditions for Systems I and III (see Table 1). A 10 percent decrease in the total formation time under non-isothermal conditions was observed for System II. An explanation of those opposing trends would require, first, a detailed understanding of the interfacial phenomenon which governs the length of the formation period. Unfortunately, the analysis presented in Section 3 did not enable a prediction of the aforementioned influence of energy transfer on the rate of flow into a bubble or the total formation time, since, for all analytical computations, the rate of mass flow into a bubble and the length of the formation period had to be specified.

4.1.6 Gas Temperature Change During Formation

Lastly, it was of interest (see Section 3.4.2) to predict the change in bubble gas temperature for hypothetical conditions of non-isothermal bubble formation. The rate of mass flow, experimentally determined for runs I-98, 103, 112, and 115 (see Figs. 31, 32, 33, 34, and 35), was employed to specify the mass flow for the analytical computations for hypothetical cases of non-isothermal bubble formation with an overall temperature difference of 167C (300F). The average value of the heat transfer coefficient for the computations was determined from the empirical correlation, equation 2.11, assuming that the hypothetical case of non-isothermal bubble formation produced bubbles of approximately the same class as those investigated experimentally. The theoretically predicted values of the unaccomplished temperature ratio for the four cases (I-98, 103, 112, 115) considered have been presented in Table 8 and are illustrated in Fig. 57 along with the experimental values for systems I, II, III, and IV previously illustrated in Fig. 28.

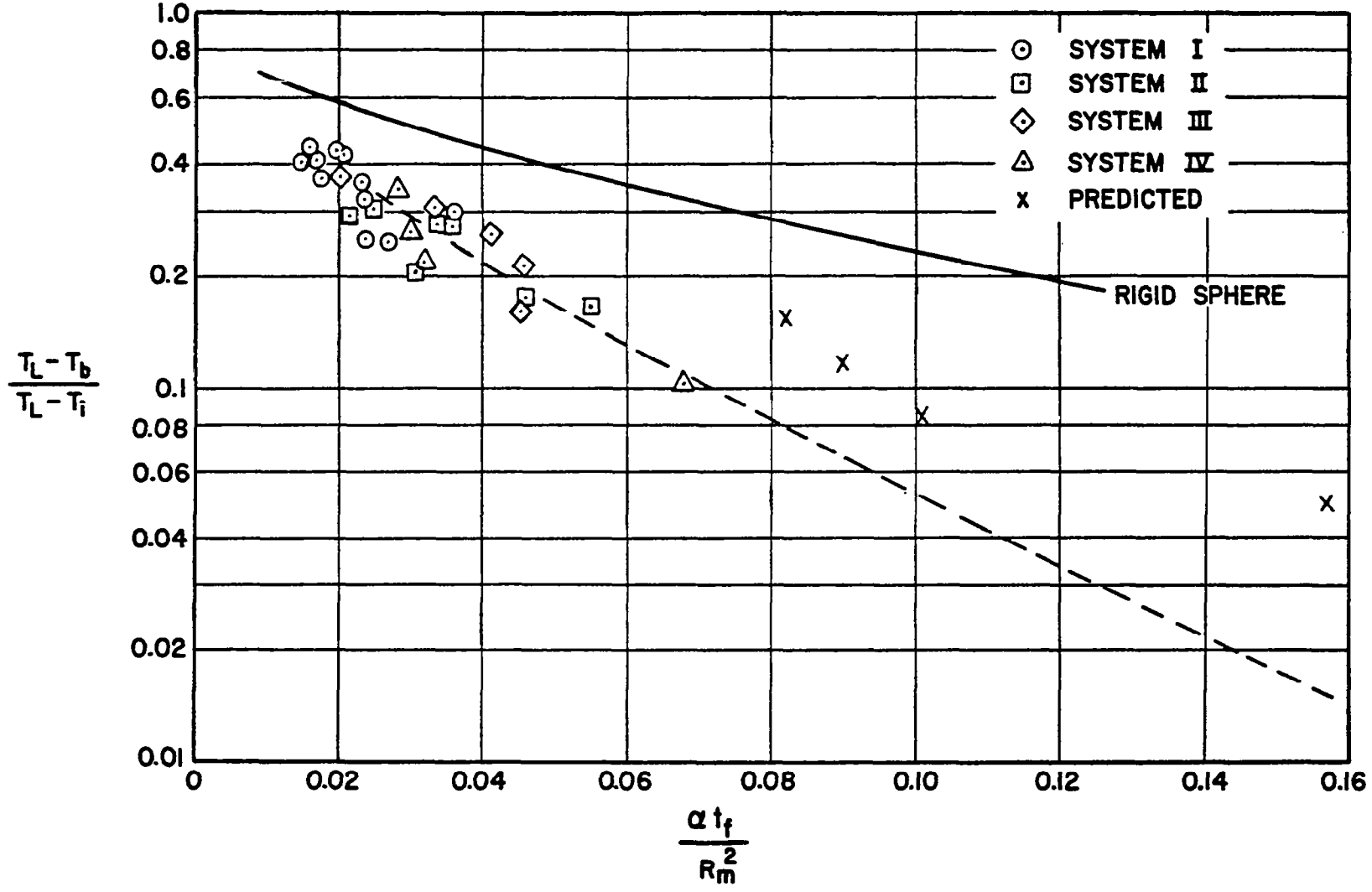

FIG. 57 UNACCOMPLISHED TEMPERATURE RATIO VERSUS FOURIER MODULUS

As can be seen, the predicted values exhibited the same trend as the experimental values. The predicted values were somewhat larger than those indicated by an extrapolation of the experimental data. They do, however, illustrate the possibility of approximately predicting the change in the bubble gas temperature during non-isothermal formation and emphasize, once again, what a large change in temperature may occur during that time.

Analytical computations pertaining to hypothetical cases of non-isothermal bubble formation have also been made for overall temperature differences of 556C (1000F) and 1670C (3000F) as discussed in Section 3.4.2. Of course, the analysis provides no means for determining the length of the bubble formation period under such extreme temperature differences. It may be expected that the volumetric growth rate of a bubble due to thermal expansion in such instances would significantly influence the gas flow into the bubble and the time of bubble formation. The unaccomplished temperature ratio for those cases has been presented in Table 6 merely to illustrate what sizeable changes in the bubble gas temperature could occur for a bubble formation period of specified length.

4.2 Conclusions

1. In line with the results of the diagnostic investigation related to the energy transfer to a gas injected into small depths of a liquid bath, it has been established from experimental data that the energy transfer during the formation period of a bubble could produce, at least for the particular class of bubbles under consideration, an increase in the gas temperature of 55 to 90 percent of the total difference in temperature between the cold gas and the warmer liquid.

2. The value of the average heat transfer coefficient computed for the entire formation period of the bubble varied from 2.4×10^{-3} to 5.3×10^{-3} cal/sec-cm^2-C (18 to 39 B/hr-ft^2-F).

3. The variation of the heat transfer coefficient appears, from experimental evidence, to depend upon (a) the mean mass velocity of the gas flow into the bubble, and (b) the mean bubble diameter.

4. The validity of a postulated average heat transfer coefficient has been examined by predicting, analytically, the rate of volume growth of the bubble and comparing that with the experimentally observed rate of growth. While the results show agreement in general, it appears that the predicted rate of volume growth of the bubble in the presence of energy transfer is considerably less in the initial stage of formation of the

bubble. That is adduced to the effect of mixing of the gas in the bubble and the effect of the size of the bubble during the initial stage.

5. The theoretical model which accounts in an elementary fashion for the viscous and interfacial forces present at the interface seems to show that the influence of such forces is, indeed, small.

6. The overall period of bubble formation between the instants of detachment of successive bubbles may be divided into (a) a lapse time, and (b) a total formation time. The fluid dynamic and interfacial phenomena during each of those periods seem to be equally significant in the understanding of the dynamics of formation of a bubble. The magnitude of those periods and the growth rate of the bubble are as important in identifying a class of bubbles as the final volume of the bubble.

5. BIBLIOGRAPHY

1. Fair, J. R.; Mayers, J. W.; Lane, W. H., "Commercial Ethylene Production by Propane Pyrolysis in a Molten Lead Bath," Chem. Eng. Prog. 53, 9, 433 (1957).

2. Rom, F. E., "Advanced Reactor Concepts for Nuclear Propulsion," Astronautics 4, 10, 20 (1959).

3. Chao, B. T., "Motion of Spherical Gas Bubbles in a Viscous Liquid at Large Reynolds Numbers," Physics of Fluids 5, 69 (1962).

4. Taylor, G., "The Instability of Liquid Surfaces When Accelerated in a Direction Perpendicular to their Planes. I," Proc. Roy. Soc. A, p. 192 (1950).

5. Hughes, R. R.; Handlos, A. E.; Evans, H. D.; Maycock, R. L., "The Formation of Bubbles at Simple Orifices," Chem. Eng. Prog. 51, 12, 557 (1955).

6. Davidson, L., "A Study of the Formation of Gas Bubbles from Horizontal Circular Submerged Orifices," Ph.D. Thesis, 1951, Columbia University.

7. Davidson, J. F.; Schuler, B. O. G., "Bubble Formation at an Orifice in a Viscous Liquid," Trans. Inst. Chem. Engr. 38, 144 (1960).

8. Hayes, W. B.; Hardy, B. W.; Holland, C. D., "Formation of Gas Bubbles at Submerged Orifices," A. I. Ch. E. Journal 5, 319 (1959).

9. Benzing, R. J.; Myers, J. E., "Low Frequency Bubble Formation at Horizontal Orifices," Ind. Eng. Chem. 47, 2087 (1955).

10. Turner, G. M., "Formation of Bubbles at Simple Orifices," Presented at San Francisco A. I. Ch. E. Meeting, Sept. 14, 1953.

11. Datta, R. L.; Napier, D. H.; Newitt, D. M., "The Properties and Behavior of Gas Bubbles Formed at a Circular Orifice," Trans. Inst. Chem. Engr. 28, 14 (1950).

12. Jackson, R., "Formation of Gas Bubbles from Orifices, "Ind. Chemist 28, 346, 391 (1952); 29, 16, 109 (1953).

13. Eversole, W. G.; Wagner, G. H.; Stackhouse, E., "Rapid Formation of Gas Bubbles in Liquids," Ind. Eng. Chem. 33, 1459 (1941).

14. van Krevelen, D. W.; Hoftijzer, P. J., "Studies of Gas Bubble Formation," Chem. Eng. Prog. 46, 29 (1950).

15. Davidson, L.; Amick, E. H., "Formation of Gas Bubbles at Horizontal Orifices," A. I. Ch. E. Journal 2, 337 (1956).

16. Walters, J. K.; Davidson, J. F., "The Initial Motion of a Gas Bubble Formed in an Inviscid Liquid," Jour. Fl. Mech. 12, 408 (1962).

17. Leibson, I.; Holcomb, E. G.; Cacoso, A. G.; Jacmic, J. J., "Rate of Flow and Mechanics of Bubble Formation From Single Submerged Orifices," A. I. Ch. E. Journal 2, 296, 300 (1956).

18. Silberman, E., "Production of Bubbles by the Disintegration of Gas Jets in Liquid," University of Minnesota; sponsored by David Taylor Model Basin, U. S. Dept. of Navy.

19. Rayleigh, Lord, "On the Stability of Cylindrical Fluid Surfaces," Phil. Mag. 34, 177 (1892).

20. Bryan, J. C.; Garber, H. J., "Formation of Bubbles at Submerged Orifices," A. I. Ch. E. Symposium on Mechanics of Bubbles and Drops, Detroit, Nov. 27-30, 1955, preprint 43.

21. Quigley, C. J.; Johnson, A. I.; Harris, B. L., "Size and Mass Transfer Studies of Gas Bubbles," Chem. Eng. Prog. Symp. Series 16, 31 (1955).

22. Halberstadt, S.; Prausnitz, P. H., "Concerning the Size of Bubbles and Liquid Droplets in Liquids," Z. Angew. Chem. 43, 970 (1930).

23. Schnurmann, R., Z. f. Phys. Chem. 143, 5, 456 (1929).

24. Johnson, A. I.; Robinson, D. G.; Michellepis, C. P., "Bubble Studies for Single-holed Perforated Plates," A. I. Ch. E. Symposium on Mechanics of Bubbles and Drops, Detroit, Nov. 27-30, 1955, preprint 48.

25. Davidson, J. F.; Schuler, B. O. G., "Bubble Formation at an Orifice in an Inviscid Liquid," Trans. Inst. Chem. Engr. 38, 335 (1960).

26. Handlos, A. E.; Baron, T., "Mass and Heat Transfer from Drops in Liquid-Liquid Extraction," A. I. Ch. E. Journal 3, 1, 127 (1957).

27. Garwin, L.; Smith, B. D., "Liquid-liquid Spray-Tower Operation in Heat Transfer," Chem. Eng. Prog. 49, 11, 591 (1953).

28. Calderbank, P. H., "Gas-Liquid Contacting on Plates," Trans. Inst. Chem. Engr. 34, 79 (1956).

29. Garner, F. H.; Skelland, A. H. P., "Mechanism of Solute Transfer from Droplets," Ind. Eng. Chem. 46, 6, 1255 (1954).

30. Johnson, A. I.; Bowman, C. W., "Mass Transfer in a Bubble Column," Canad. Jour. Chem. Eng. Dec. 1958, 253.

31. West, F. B.; Gilbert, W. D.; Shimizu, T., "Mechanism of Mass Transfer on Bubble Plates," Ind. Eng. Chem. 44, 10, 2470 (1952).

32. Deindoerfer, F. H.; Humphrey, A. E., "Mass Transfer from Individual Gas Bubbles," Ferm. Res. and Eng. 53, 9, 755 (1961).

33. Licht, W.; Pansing, W. F., "Solute Transfer from Single Drops in Liquid-Liquid Extraction," Ind. Eng. Chem. 45, 9, 1885 (1953).

34. McDowell, R. V.; Myers, J. E., "Mechanism of Heat Transfer to Liquid Drops," A. I. Ch. E. Symposium on Mechanics of Bubbles and Drops, Detroit, Nov. 27-30, 1955, preprint 49.

35. Sherwood, T. K.; Evans, J. E.; Longcor, J. V. A., Ind. Eng. Chem. 31, 1146 (1939).

36. West, F. B.; Robinson, P. A.; Morgenthaler, A. L.; Beck, T. R.; McGregor, D. K., Ind. Eng. Chem. 43, 234 (1951).

37. Licht, W.; Conway, J. B., Ind. Eng. Chem. 42, 1151 (1950).

38. Linquist, R. D., "Investigation into the Transfer of Mass from a Liquid to a Growing Gas Bubble During Formation," M. S. Thesis, August 1963, Purdue University.

39. Coulson, J. M.; Skinner, S. J., Chem. Eng. Sci. 1, 5 (1952).

40. Garner, F. H.; Skelland, A. H. P., "Liquid-Liquid Mixing as Affected by the Internal Circulation within Droplets," Trans. Instn. Chem. Engr. 29, 315 (1951).

41. Harriott, P., "A Review of Mass Transfer to Interfaces," Canad. Jour. Chem. Eng. April 1962, 60.

42. Bankoff, S. G.; Mason, J. P., "Heat Transfer from the Surface of a Steam Bubble in Turbulent Subcooled Liquid Stream" A. I. Ch. E. Jour. 8, 1, 30 (1962).

43. Grassman, P., Wyss, E., "Determination of Heat and Mass Transfer Coefficients Between Vapor Bubbles and Liquid. Water versus water vapor, and water versus water vapor and inert gas," Chem-Ingr-Tech 34, 755 (1962).

44. Eckert, E. R. G. and Drake, R. M., "Heat and Mass Transfer" McGraw-Hill, New York, 1959, p. 199.

45. Lamb, Sir Horace, "Hydrodynamics," Dover, New York, 1932, p. 124.

46. Chern, B.; Enig, J. W., "On the Numerical Solution of the Adiabatically Expanding Gas Bubble of Variable Mass in Infinite Medium," Chem. Res. Dept., U. S. Naval Ord. Lab., NAVORD Report 5735, Jan. 1958.

47. Hildebrand, "Introduction to Numerical Analysis," McGraw-Hill, New York, 1956, p. 199, 237, 247.

48. Scarborough, "Numerical Mathematical Analysis," The Johns Hopkins Press, 1962, p. 325, 356.

49. Welsh, F. F., "Floating-Point Adams-Moulton Runga-Kutta Integration Subroutine," Computer Sciences Center, Purdue University, Library Routine No. D2.01.1.

50. Roll, J. B., "The Effect of Surface Tension on Boiling Heat Transfer," Ph.D. Thesis, August 1961, Purdue University.

51. "Continuous Derivative Interpolation Subroutines" SHARE Dist. Agency, IBM Corp., SHARE No. 760.

52. Nelson, S. T.; Grey, J., "Conceptual Design Study of a Liquid-Core Nuclear Rocket" Aero. Eng. Lab., Princeton University, Report No. 665, September 1963.

53. Zwick, S. A., "The Growth and Collapse of Vapor Bubbles," Hydrodynamics Lab., Cal. Inst. Tech., Report No. 21-19, Dec. 1954.

54. Poritsky, H., "The Collapse or Growth of a Spherical Bubble or Cavity in a Viscous Fluid," Proc. of First Nat. Cong. of Appl. Mech., 1952 (New York: ASME).

APPENDIX I

NOTATION

A = surface area of the bubble

$\bar{A}$ = integrated average bubble surface area

A_o = orifice cross-sectional area

C = dimensionless flow parameter (see 3.15)

c = acoustic speed in the gas

c_p, c_{p_g} = constant pressure specific heat of the gas

c_v = constant volume specific heat of the gas

D_g = molecular diffusivity

D_o = orifice diameter

d_m = mean bubble diameter, $(\frac{6}{\pi} V_i)^{1/3}$

E = net energy transfer during bubble formation

$E_1, E_2, E_3, E_4, E_5, E_6$ = dimensionless parameters; see equations 3.17, 3.18, 3.32.

Fo = Fourier modulus, $\alpha t_f / R_m^2$

f = bubble frequency

f_{max} = maximum bubble frequency

G_1 = dimensionless ante-chamber parameter (see 3.15)

g = acceleration of gravity

h = convective heat transfer coefficient

$\bar{h}$ = average convective heat transfer coefficient for bubble formation period

$\bar{j}$ = unit vector in vertical direction

k_g = thermal conductivity of the gas

L = length of orifice channel; characteristic dimension of bubble.

M = dimensionless bubble mass

m = bubble mass

$\bar{m}$ = mean mass velocity into bubble, $m_b/t_f A_o$

m_b = terminal bubble mass

m_o = bubble mass at $t = 0$

Nu = Nusselt number, $\bar{h} d_m/k_g$

N_c = ante-chamber parameter (see equation 1.1)

N_R = orifice parameter (see equation 1.1)

P = dimensionless mean bubble pressure, p/p_o

Pr = Prandtl number, $\mu_g c_{p_g}/k_g$

P_c = dimensionless ante-chamber pressure, p_c/p_o

P_∞ = dimensionless pressure at infinity, p_∞/p_o

p = mean bubble pressure

p_b = mean bubble pressure at end of formation

p_c = ante-chamber pressure

p_f = ante-chamber excess pressure

p_∞ = pressure in the liquid at infinity

p_L = pressure in the liquid

p_o = mean pressure in the bubble at $t = 0$

Q' = dimensionless energy transfer

$\dot{q}_i$ = mean volumetric gas flow rate based on T_i

R = radius of the bubble

Re = Reynolds number, $\bar{m} d_m/\mu_g$

$\bar{R}$ = gas constant

R_m = mean bubble radius = $(\frac{4}{3\pi} V_i)^{1/3}$

R_o = orifice radius

r = radial coordinate

$\bar{r}$ = unit vector in radial direction

$\bar{r}_\theta$ = unit vector in θ direction

S = dimensionless bubble radius, R/R_o

St = Stanton number, Nu/(Re · Pr)

T = mean bubble temperature

T_b = mean temperature of the bubble at end of formation

T_c = temperature of the gas in the ante-chamber

T_i = temperature of the gas entering the orifice

T_L = temperature of the liquid

T_m = mean gas temperature during formation, for property evaluation

t = time

t_f = total formation time

t'_f = formation time

t_l = lapse time

t_t = $t_l + t_f$

U = dimensionless radial velocity

V = bubble volume

$\bar{V}$ = velocity

V_b = terminal bubble volume

$V_{b_{iso}}$ = isothermal terminal bubble volume

V_c = ante-chamber volume

= unheated bubble volume

= mean velocity of the gas through the orifice

= radial velocity component

= angular velocity component

= vertical translational velocity

= mean mass flow rate

= accomplished temperature ratio, $(T_b-T_i)/(T_L-T_i)$

Y_e = experimental unaccomplished temperature ratio, $(T_L-T_b)/(T_L-T_i)$

= theroretical unaccomplished temperature ratio, $(T_L-T)/T_L-T_i)$

, Y_2, Y_3, Y_4, Y_5, Y_6, Y_7, Y_8, Y_9, Y_{20} = functions of S, see equations 3.17, 3.18, 3.19, 3.22

= limit of $U/\sqrt{S^2-1}$ at $\tau = 0$

= limit (see App. VII)

= thermal diffusivity of the gas

= specific heat ratio of gas, c_p/c_v

= dimensionless mean bubble temperature, T/T_i

= see 3.15

= see 3.15

= angular coordinate (clockwise +)

= limiting angle

μ_L = dynamic viscosity of the liquid

= dynamic viscosity of the gas

$'_L$ = density of the liquid

= density of the gas

= surface tension

τ = dimensionless time (3.15)

$\tau_{r\theta}$ = tangential shear stress in the liquid

φ = velocity potential

ψ = stream function

APPENDIX II

ANTE-CHAMBER PRESSURE INSTRUMENTATION

The transient ante-chamber pressure was measured by means of a pressure microphone[1] mounted within a chamber integral with the ante-chamber as has been previously illustrated in Fig. 3. The microphone output was fed to a cathode follower[2] prior to being displayed on a dual-beam oscilloscope[3] as shown schematically in Fig. A.1. The cathode follower was employed for isolating the microphone to eliminate significant loading of the microphone by the oscilloscope. A 60 cycle reference voltage was simultaneously displayed on the oscilloscope to enable an accurate calibration of the time base of the microphone output. A permanent record of the displayed microphone output was obtained by means of a scope-mounted Polaroid camera; a sample of such a record is illustrated in Fig. A.2.

An accurate determination of the true microphone output voltage as a function of time was obtained in the following manner:

1. The Polaroid record of the displayed voltage was enlarged ($\sim$ 6X) to enable an accurate measurement and tabulation of the displayed voltage as a function of time during a given cycle.
2. The true microphone output voltage was obtained from the displayed voltage by the application of a scale factor accounting for the attenuation of the cathode follower.

scale factor = 0.956 volt out/volt in

The determination of the microphone output voltage per unit of pressure change was obtained from the standard microphone

[1] Model 98-108, Shure Brothers, Inc.

[2] Model F-408-M-1, Gulton Ind. Inc.

[3] Type 502, Tektronix.

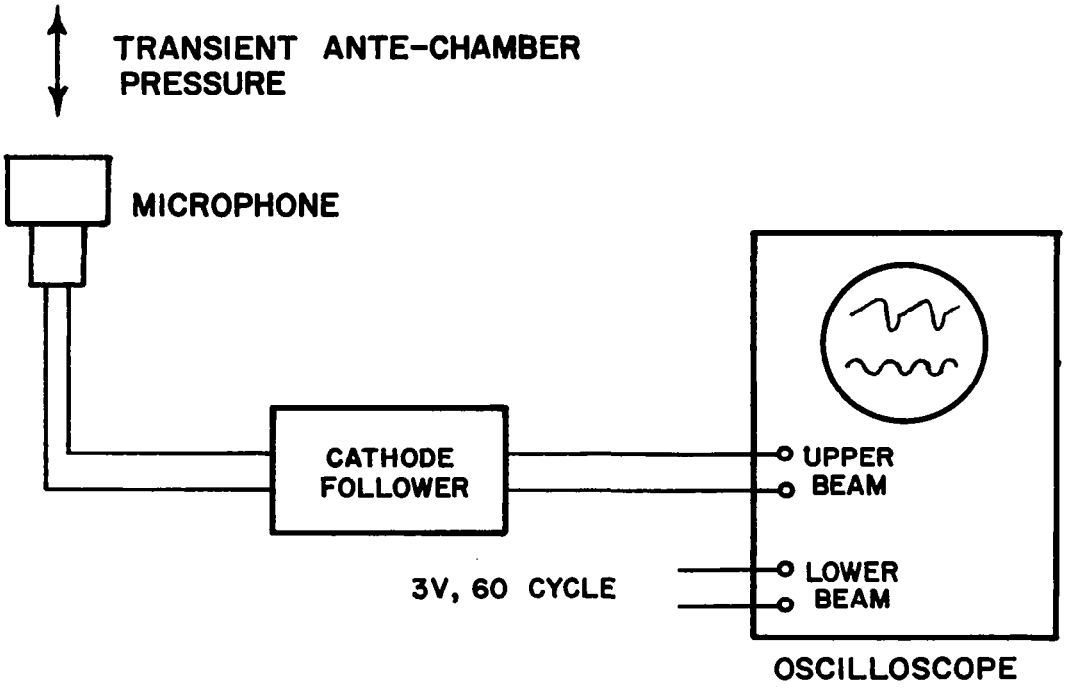

FIG. A.I SCHEMATIC OF MICROPHONE CIRCUIT

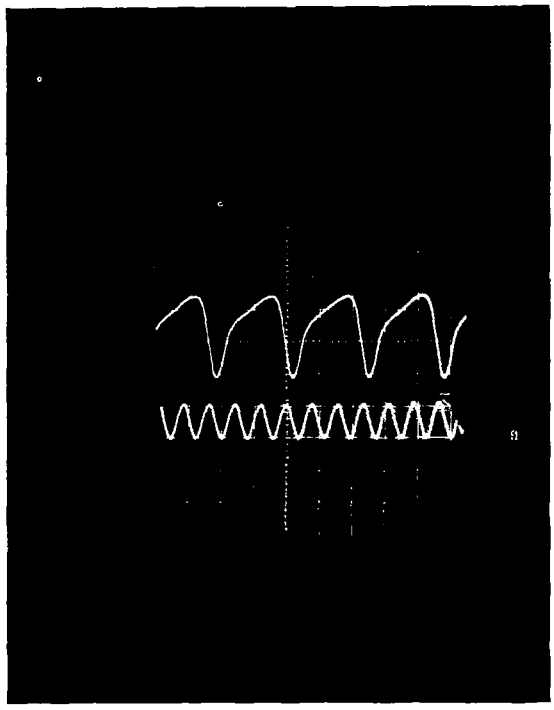

FIG. A.2 RECORD OF TRANSIENT ANTE-CHAMBER PRESSURE

calibration curve supplied by the manufacturer,[1] illustrated in Fig. A.3. The frequency of the periodic microphone voltage, or in other words the frequency of bubble formation, was in the range of 20 to 40 cycles/second, indicating, from Fig. A.3, an output of +1 Db with reference to 0 Db = 60 Db below 1 volt per microbar.[2] The microphone output was computed from

$$Db = 20 \log_{10} \frac{E}{E_{ref.}} \qquad \text{(II-1)}$$

where

$$E_{ref.} = 1 \text{ volt/microbar.}$$

Therefore, for the frequency range of 20 to 40 cycles per second,

$$Db = (-60) + 1 = -59 = 20 \log_{10} \frac{E}{E_{ref.}}$$

from which one obtains the microphone calibration factor

$$E = 1.122 \text{ millivolt/microbar}$$

The transient ante-chamber pressure as a function of time during the lapse and total formation times (see Section 2.4.1) was determined from the true microphone output voltage and the microphone calibration factor, E.

It should be noted that the microphone calibration was obtained in a free field (see Fig. A.3). Normally, one would not expect such a calibration to be applicable for the case of a microphone confined in a chamber of small volume as in the present application. However, for the very low frequencies of interest (< 40 cycles/second) and for ante-chamber volumes of the order of 20 cm^3, it can be assumed that the acoustical loading of the microphone was negligible and the calibration was considered to be accurate within 10 percent.[3]

---

[1] Shure Brothers, Inc., Evanston, Illinois.

[2] microbar = $dyne/cm^2$

[3] Brouns, A., Microphone Laboratory, Shure Brothers, Inc., Evanston, Illinois; private communication.

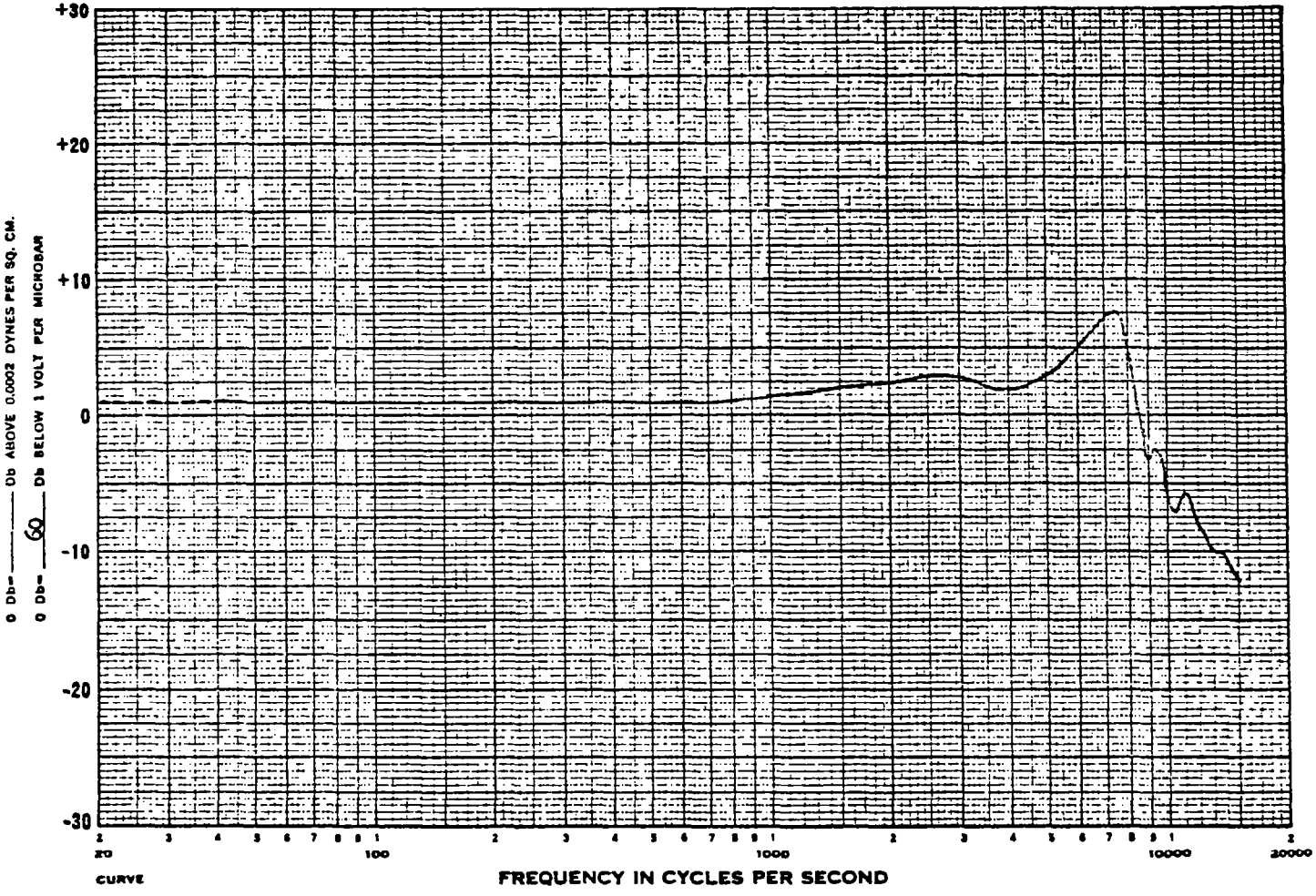

CURVE 1355

Subject: Non-Directional Ceramic Cartridge Mfr.: Shure Brothers, Inc.

E. No.: ~~99-103~~ 99-103 Temperature: 80 °F. Distance: 12" Coupler: Free-Field

Nº 94130 Date: 11-1-63 Impedance: ~~440 mfd~~ Azimuth: 0° Source: Sound Room "G"

By: AB Calibration: Termination: 160 megohms Input: 10 mbars

Form No. 753

FIG. A.3 MICROPHONE CALIBRATION CURVE

APPENDIX III

METHOD OF DATA REDUCTION AND SAMPLE CALCULATIONS

(a) Calculation of Bubble Volume and Surface Area

The volume and surface area of a bubble (at any instant during formation) were determined from the frames of high speed motion pictures as follows.

1. The picture frame from which the bubble volume and surface area was to be calculated was projected on the screen of an optical comparator (~ X 10).
2. An enlarged tracing was obtained from the projected image.
3. The enlarged outline of the bubble was divided into a series of truncated cones by means of horizontal lines. Fig. A.4 illustrates one such outline.
4. Assuming the bubble to be symmetrical with respect to the orifice axis, the "enlarged bubble volume" and "enlarged bubble surface area" was computed from the following.

$$V_E = \frac{\pi}{3} H_1^2 (3 R_1 - H_1) + \sum_{i=1}^{n-1} \frac{\pi}{12} H_3 (d_i^2 + d_{i+1}^2 + d_i d_{i+1}) + \frac{\pi}{12} H_3 (d_n^2 + d_{n+1}^2 + d_n d_{n+1}) \quad \text{(III-1)}$$

$$A_E = 2\pi R_1 H_1 + \sum_{i=1}^{n-1} \frac{\pi}{2} (d_i + d_{i+1}) \sqrt{H_3^2 + \frac{1}{4} (d_{i+1} - d_i)^2} + \frac{\pi}{2} (d_n + d_{n+1}) \sqrt{H_3^2 + \frac{1}{4} (d_{n+1} - d_n)^2} \quad \text{(III-2)}$$

5. The true bubble volume and surface area were computed from the enlarged values by the application of an appropriate scale factor.[1]

[1] The scale factor was obtained from a picture of a scale in the plane of the orifice axis.

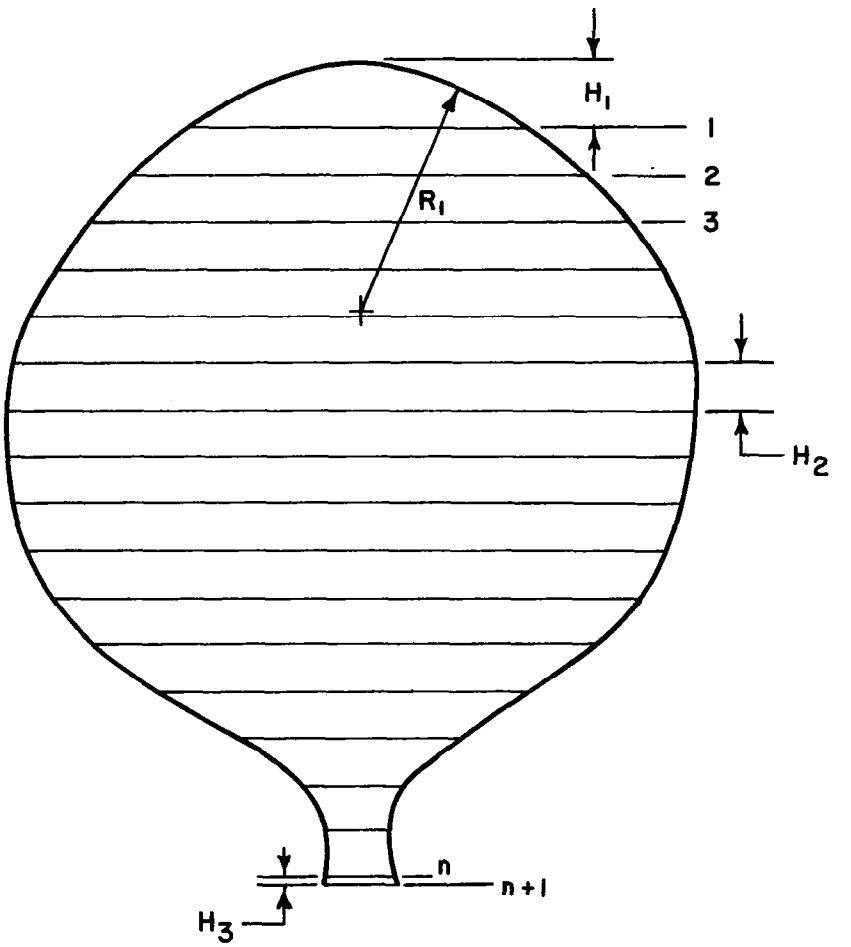

FIG. A.4 ENLARGED BUBBLE OUTLINE FOR VOLUME AND SURFACE AREA CALCULATIONS

(b) Net Energy Transfer During Bubble Formation

The energy balance equation for a perfect gas in an open system defined by the gas-liquid interface of a bubble during formation can be written as follows:

$$\frac{\delta Q}{dt} + c_p T_i \frac{dm}{dt} = \frac{d(mc_vT)}{dt} + p \frac{dV}{dt} + \sigma \frac{dA}{dt} \qquad \text{(III-3)}$$

where

δQ = energy transfer to the gas

$c_p T_i \, dm$ = energy carried in by the gas stream

mc_vT = internal energy of the gas

pdV = pressure boundary work

$\sigma \, dA$ = surface work

Work against viscous forces is neglected.

In order to determine the net energy transfer to the gas in the bubble during formation, equation III-3 is integrated over the time of the formation period. Thus,

$$\int_o^Q \delta Q + \int_o^{m_b} c_p T_i \, dm = \int_o^{m_b c_v T_b} d(mc_vT) + \int_o^{V_b} pdV + \int_o^{A_b} \sigma \, dA \qquad \text{(III-4)}$$

Assuming that c_p, T_i, and σ are constant throughout the bubble formation period, equation III-4 gives

$$Q + c_p T_i m_b = c_v m_b T_b + \int_o^{V_b} p \, dV + \sigma A_b \qquad \text{(III-5)}$$

The variation of the pressure of the gas in the bubble during formation is unknown. The analysis presented in Section 3 attempts to account for such variations. It is assumed here, however, that the pressure of the gas in the bubble during formation is approximately constant and equal to the mean hydrostatic pressure.

$$p \approx \bar{p} = p_{atm} + p_{hydrostatic}$$

On the basis of that assumption, equation III-5 reduces to

$$Q = c_v m_b T_b - c_p m_b T_i + \bar{p} V_b + \sigma A_b \qquad \text{(III-6)}$$

For a perfect gas, equation III-6 becomes

$$Q = m_b c_p (T_b - T_i) + \sigma A_b \qquad \text{(III-7)}$$

It is known that the interfacial tension, σ, of a dynamic interface can be greater than that of a static interface, although there is no basis for a quantitative determination of the dynamic interfacial tension. Consequently, a static value of σ is employed in considering the order of magnitude of the two terms in equation II-7. For bubble formation in water and for a final bubble surface area of 1.2 cm^2, which is representative of the class of bubbles studied experimentally, (Section 2.3.1),

$$\sigma A_b \approx 2 \times 10^{-6} \text{ cal}$$

The change in the enthalpy of the gas in the bubbles during formation, for the class of bubbles considered, was of the order of

$$m_b c_p (T_b - T_i) \approx 8 \times 10^{-3} \text{ cal}$$

Thus, for the class of bubbles considered,

$$m_b c_p (T_b - T_i) >> \sigma A_b$$

and the net energy transfer to the gas in the bubbles during the formation period can, on the basis of the assumption regarding the pressure of the gas in the bubble, be closely approximated by

$$Q = m_b c_p (T_b - T_i) \qquad \text{(III-8)}$$

(c) Sample Calculations for Isothermal Bubble Formation

The following is a sample of the calculation of quantities pertinent to isothermal bubble formation:

Run I-14 (System I)

Measured quantities

$\dot{W}_i = 3.71 \times 10^{-3}$ gm/sec

$p_b = p_{atm} + h + \Delta p_\sigma = 1023 + 8.25 + 0.5 = 1031.8$ cm H_2O[1]

$T_L = 299$ K (538R)

$T_i = 298$ K (537 R)

$t_l = 0.0325$ sec

$t_f = 0.0254$ sec

$t = 0.0579$ sec

Derived quantities

terminal bubble mass

$$m_b = W_i \times t = 2.15 \times 10^{-4} \text{ gm}$$

terminal bubble volume

$$V_b = \frac{m_b \overline{R} T_L}{p_b} = 0.189 \text{ cm}^3$$

mean volumetric flow rate

$$\dot{q}_i = \frac{\dot{W}_i}{\rho_i} = \frac{\dot{W}_i}{(p_b/\overline{R} T_i)} = 3.2 \text{ cm}^3/\text{sec}$$

[1] The increase in pressure due to surface tension, assuming a spherical bubble, is $2\sigma/R$. It must be determined by trial and error since V is unknown. The effect of σ on p_b is of little significance.

(d) Sample Calculations for Non-Isothermal Bubble Formation

The following is a sample of the calculation of quantities pertinent to non-isothermal bubble formation:

Run H-18 (System I)

Measured quantities

$\dot{W}_i = 6.60 \times 10^{-3}$ gm/sec

$p_b = p_{atm} + h + \frac{2\sigma}{R} = 1000 + 5.4 + 0.4 = 1005.8$ cm H_2O

$T_L = 290$ K (522 R)

$T_i = 152$ K (274 R)

$t_l = 0.0326$ sec

$t_f = 0.0277$ sec

$t = 0.0603$ sec

$V_b = 0.279$ cm^3

$\bar{A} = 1.206$ cm^2

Derived quantities

terminal bubble mass

$$m_b = \dot{W}_i \times t = 3.97 \times 10^{-4} \text{ gm}$$

terminal mean bubble gas temperature

$$T_b = \frac{p_b V_b}{m_b \bar{R}} = 232 \text{ K } (418 \text{ R})$$

unaccomplished temperature ratio

$$Y = \frac{T_L - T_b}{T_L - T_i} = 0.42$$

accomplished temperature ratio

$$X = \frac{T_b - T_i}{T_L - T_i} = 0.58$$

gas properties evaluated at $T_m = \frac{T_b + T_i}{2} = 192$ C

$c_p = 0.249$ cal/gm-°C

$\alpha = 0.095$ cm²/sec

$\mu_g = 1.252 \times 10^{-4}$ gm/cm-sec

net energy transfer (equation 2.3)

$$E = m_b\, c_p\, (T_b - T_i) = 7.92 \times 10^{-3} \text{ cal}$$

average heat transfer coefficient (equation 2.4)

$$\bar{h} = \frac{m_b\, c_p}{t_f\, \bar{A}\, \ln (1/Y)} = 2.57 \times 10^{-3} \text{ cal/sec-cm}^2\text{-C}$$

unheated bubble volume (equation 2.7)

$$V_i = \frac{m_b\, \bar{R}\, T_i}{p_b} = V_b\, \frac{T_i}{T_b} = 0.188 \text{ cm}^3$$

mean mass velocity ($D_o = 0.159$ cm)

$$\bar{m} = \frac{m_b}{t_f\, A_o} = 0.723 \text{ gm/sec-cm}^2$$

mean bubble diameter

$$d_m = \left(\frac{6}{\pi} V_i\right)^{1/3} = 0.712 \text{ cm}$$

Stanton number

$$\pi_1 = \frac{Nu}{Re\ Pr} = \frac{\bar{h}}{\bar{m}\, c_p} = 0.0142$$

Reynolds number

$$\pi_2 = Re = \frac{\bar{m}\, d_m}{\mu_g} = 4126$$

Fourier number

$$Fo = \frac{\alpha\, t_f}{R_m^2} = 0.0207$$

(e) Average Heat Transfer Coefficient for Bubble Formation

The empirical correlation for the average heat transfer coefficient, equation 2.11, enables a determination of the average heat transfer coefficient for the bubble formation period in terms of parameters indicative of the mean flow into the bubble and the mean bubble size. The correlation was employed for determining the average heat transfer coefficient for the analytical computations concerning the hypothetical cases of non-isothermal bubble formation considered in Section 3.4.2 as follows:

1. The conditions for the mean flow into a bubble and the mean bubble size were determined from the experimental data pertaining to isothermal bubble formation. Thus, for run I-98: (D_o = 0.159 cm)

$$m_b = 0.802 \times 10^{-4} \text{ gm}$$

$$V_b = 0.0615 \text{ cm}^3$$

$$t_l = 0.0174 \text{ sec}$$

$$t_f = 0.0274 \text{ sec}$$

$$t = 0.0448 \text{ sec}$$

$$T_i = 300 \text{ K } (540 \text{ R})$$

2. Assuming that the flow into a bubble forming under hypothetical non-isothermal conditions was the same as determined for isothermal formation, the aforementioned values were employed in conjunction with equation 2.11 for determining $\bar{h}$ for the analytical computations. Thus,

$$\bar{m} = \frac{m_b}{t_f A_o} = 0.148 \text{ gm/sec-cm}^2$$

$$d_m = \left(\frac{6}{\pi} V_i\right)^{1/3} = 0.491 \text{ cm}$$

For a hypothetical overall temperature difference between the liquid and the gas of 167C (300 F) the properties of the gas were evaluated at a mean gas temperature estimated as

$$T_{mean} = 300 \text{ K} + \frac{1}{2} (167) = 383\text{K } (690\text{R})$$

Thus,

$$c_p = 0.25 \text{ cal/gm-}^\circ\text{C}$$

$$\mu_g = 2.13 \times 10^{-4} \text{ gm/cm-sec}$$

From equation 2.11, one obtains

$$\bar{h} = \bar{m}\, c_p \quad 26.9 \quad \left(\frac{\bar{m}\, d_m}{\mu_g}\right)^{-0.884}$$

$$\bar{h} = 5.75 \times 10^{-3} \text{ cal/sec-cm}^2\text{-}^\circ\text{C}$$

APPENDIX IV

EQUATION OF MOTION OF A SPHERICAL BUBBLE BOUNDARY

The equation of motion for an expanding and translating spherical bubble boundary can be derived by considering the motion of the liquid surrounding the bubble. Assuming the liquid to be incompressible and inviscid, the equations of continuity and motion for the liquid are, respectively

$$\nabla \cdot \bar{V} = 0 \qquad \text{(IV-1)}$$

$$\rho \frac{d\bar{V}}{dt} = -\nabla p_L \qquad \text{(IV-2)}$$

Where $\bar{V}(r,\theta,t)$ is the fluid particle velocity, $p_L(r,\theta,t)$ the pressure in the liquid. Because of the axial symmetry of the flow, the variables are functions only of r, the radial coordinate measured from the center of the bubble, θ, the angular coordinate measured from the vertical, and t, the time, for the moving coordinate system with the origin at the bubble center as previously illustrated in Fig. 44.

If it is further assumed that the liquid flow is irrotational, then

$$\nabla \times \bar{V} = 0$$

and the velocity of the liquid can be derived from a velocity potential,

$$\overline{V} = - \nabla \varphi \qquad \text{(IV-3)}$$

such that equation IV-1 becomes

$$\nabla \cdot \overline{V} = \nabla^2 \varphi = 0 \qquad \text{(IV-4)}$$

The solution for equation IV-4, for the case of an expanding and translating spherical boundary, can be obtained by a superposition of the solutions for the individual cases of an expanding spherical boundary and a translating spherical boundary, with the complete solution satisfying the boundary condition for the radial velocity component given in Section 3.2.2 as[1]

$$V_r\Big|_{r=R} = \frac{dR}{dt} + V_y \cos \theta \qquad \text{(IV-5)}$$

For an expanding spherical boundary, a spherically symmetric solution of equation IV-4 is given as

$$\varphi_1 \ (r,t) = \frac{A \ (t)}{r} + B(t) \qquad \text{(IV-6)}$$

Considering the liquid to be of infinite extent, $\varphi \to 0$ as $r \to \infty$ which therefore requires that $B(t) = 0$. Thus,

$$\varphi_1 \ (r,t) = \frac{A \ (t)}{r}$$

A solution of equation IV-4 for the case of a spherical boundary translating in an infinite liquid is given as

$$\varphi_2 \ (r,\theta,t) = \frac{B \cos \theta}{r^2}$$

A linear combination of the solutions, φ_1 and φ_2, yields a solution to equation IV-4 for the combined flow in the liquid surrounding an expanding and translating spherical boundary.

---

[1] Neglecting the effects of condensation or evaporation at the bubble wall, the velocity of the liquid at r=R can be taken equal to the wall velocity. (53)

Thus,

$$\varphi(r,\theta,t) = \frac{A\ (t)}{r} + \frac{D \cos\ \theta}{r^2} \qquad \text{(IV-7)}$$

The radial velocity component is readily obtained from equation IV-7 as

$$V_r = -\frac{\partial \varphi}{\partial r} = \frac{A\ (t)}{r^2} + \frac{2D \cos\ \theta}{r^3} \qquad \text{(IV-8)}$$

In order to satisfy the condition for the radial velocity at the spherical boundary r = R, equation IV-5, it can be seen from equation IV-8 that

$$A\ (t) = R^2\ \frac{dR}{dt}$$

$$D \quad = 1/2\ R^3\ V_y \qquad \text{(IV-9)}$$

Equations IV-7 and IV-9 combine to give the velocity potential for the flow in an infinite, incompressible, inviscid liquid surrounding an expanding and translating spherical boundary as

$$\varphi(r,\theta,t) = \frac{R^2}{r}\ \frac{dR}{dt} + \frac{1}{2}\ \frac{R^3\ V_y \cos\ \theta}{r^2} \qquad \text{(IV-10)}$$

The equation of motion for such a boundary is obtained from equation IV-2 which can be rewritten as

$$\rho \left[\frac{\partial \overline{V}}{\partial t} + (\overline{V} \cdot \nabla)\ \overline{V}\right] = -\nabla p_L \qquad \text{(IV-11)}$$

Since $\nabla \times \overline{V} = 0$, then $\nabla(\overline{V} \cdot \overline{V}) = 2(\overline{V} \cdot \nabla)\ \overline{V}$, and equation IV-11 becomes

$$\rho \left[\frac{\partial \overline{V}}{\partial t} + \nabla\left(\frac{V^2}{2}\right)\right] = -\ \nabla p_L \qquad \text{(IV-12)}$$

From equation IV-3, one obtains

$$\frac{\partial \overline{V}}{\partial t} = -\nabla \frac{\partial \varphi}{\partial t}$$

which when substituted into equation IV-12 yields

$$\nabla \left\{ - \frac{\partial \varphi}{\partial t} + \frac{V^2}{2} + \frac{p_L(r,\theta,t)}{\rho} \right\} = 0 \qquad \text{(IV-13)}$$

Integration of equation IV-13 yields the classical Bernoulli equation

$$- \frac{\partial \varphi}{\partial t} + \frac{V^2}{2} + \frac{p_L}{\rho} = F(t) \qquad \text{(IV-14)}$$

It can be seen (from equation IV-10) that the first two terms in equation IV-14 approach zero as $r \to \infty$, which gives, for a constant pressure in the liquid at infinity, p_∞

$$F(t) = \frac{p_\infty}{\rho}$$

To complete the evaluation of equation IV-14, one obtains from equation IV-10

$$\frac{\partial \varphi}{\partial t} = \frac{R^2}{r} \frac{d^2R}{dt^2} + \frac{2R}{r} \left(\frac{dR}{dt}\right)^2 + \frac{5}{2} \frac{V_y R^2 \cos\theta}{r^2} \frac{dR}{dt} + \frac{1}{2} \frac{R^3 \cos\theta}{r^2} \frac{dV_y}{dt}$$

$$+ \frac{1}{2} \frac{V_y^2 R^3}{r^3} (2\cos^2\theta - \sin^2\theta) \qquad \text{(IV-15)}$$

which accounts for the change in the coordinates of a fixed point with time due to the motion of the coordinate system.[1] Similarly, equation IV-10 is employed to evaluate

$$V^2 = V_r^2 + V_\theta^2 = \left(- \frac{\partial \varphi}{\partial r}\right)^2 + \left(- \frac{1}{r} \frac{\partial \varphi}{\partial \theta}\right)^2 \qquad \text{(IV-16)}$$

Combining equations IV-10, IV-15, and IV-16 with equation IV-14 gives the following expression for the dynamic pressure in the liquid, $p_L(r,\theta,t)$, as a function of the radius, the velocity, and the acceleration of the spherical boundary.

[1] See equation 3.3, Section 3.2.2.

$$\frac{p_L(r,\theta,t) - p_\infty}{\rho} = \left[\frac{R^2}{r}\frac{d^2R}{dt^2} + \frac{2R}{r}\left(\frac{dR}{dt}\right)^2 + \frac{5\,V_y R^2 \cos\theta}{2\,r^2}\frac{dR}{dt}\right.$$

$$\left. + \frac{R^3 \cos\theta}{2r^2}\frac{dV_y}{dt} + \frac{V_y^2 R^3}{2\,r^3}(2\cos^2\theta - \sin^2\theta)\right]$$

$$- \frac{1}{2}\left[\left\{\frac{R^2}{r^2}\left(\frac{dR}{dt}\right) + \frac{V_y R^3 \cos\theta}{r^3}\right\}^2 + \left\{\frac{V_y R^3 \sin\theta}{2\,r^3}\right\}^2\right] \quad \text{(IV-17)}$$

The pressure in the liquid at the spherical boundary, r=R, from equation IV-17, is given as

$$\frac{p_L(R,\theta,t) - p_\infty}{\rho} = R\frac{d^2R}{dt^2} + \frac{3}{2}\left(\frac{dR}{dt}\right)^2 + \frac{3}{2}V_y \cos\theta \frac{dR}{dt} + \frac{1}{2}R\cos\theta\frac{dV_y}{dt}$$

$$+ V_y^2\left(\frac{1}{2}\cos^2\theta - \frac{5}{8}\sin^2\theta\right) \quad \text{(IV-18)}$$

Equation IV-18 is the equation of motion of an expanding and translating spherical boundary which relates the velocity and acceleration of the boundary to the dynamic pressure required at the boundary (and therefore inside the boundary) to produce such motion. This equation is used further in Section 3.3.1.

APPENDIX V

LIQUID VISCOUS EFFECTS

The effects of the viscosity of the liquid upon the motion of an expanding and translating spherical bubble boundary are approximated by considering the creeping motion of a viscous liquid past a sphere. The classical solution, due to Stokes, for the uniform axisymmetric flow of a viscous liquid past a sphere, neglecting all inertia terms, is given by the following stream function

$$\Psi_1(r,\theta) = -\frac{1}{2} V_y \left(1 - \frac{3}{2}\frac{R}{r} + \frac{1}{2}\frac{R^3}{r^3}\right) r^2 \sin^2\theta \qquad (V\text{-}1)$$

Of course, equation V-1 satisfies the boundary condition of zero velocity at the surface of the sphere, r=R.

The stream function for the flow resulting from the translation of a sphere through an infinite liquid can be obtained from equation V-1 by superposing a negative uniform flow, $-V_y$, on the liquid. By so doing, one obtains from equation V-1

$$\Psi_2(r,\theta) = \frac{3}{4} V_y R r \left(1 - \frac{R^2}{3r^2}\right) \sin^2\theta \qquad (V\text{-}2)$$

The boundary condition satisfied by equation V-2 is that the velocity of the liquid at the surface of the sphere, r=R, be equal to the spherical surface velocity.

It is convenient to modify the solution for Ψ, in equation V-2, to describe the creeping flow of the liquid associated with a translating and expanding spherical boundary. The boundary condition for the velocity of the liquid at the surface of an expanding and translating spherical boundary, to be satisfied by such a modified stream function, has been previously given as (see Section 3.2.2, equation 3.2)

$$\bar{V}\Big|_{r=R} = \left(\frac{dR}{dt} + V_y \cos\theta\right) \bar{r} - V_y \sin\theta\, \bar{r}_\theta \qquad (V\text{-}3)$$

Equation V-2 has been modified to the following form in order to satisfy the aforementioned boundary condition for an expanding and translating spherical boundary.

$$\Psi(r,\theta) = \frac{3}{4} V_y R r \left(1 - \frac{1}{3}\frac{R^2}{r^2}\right) \sin^2\theta - \left(\frac{dR}{dt}\right) R^2 \cos\theta \qquad (V\text{-}4)$$

It can be readily verified that equation V-4 satisfies the boundary condition, equation V-3, at r=R and, moreover, is a solution of the equations of continuity and motion (neglecting the inertia terms). Equation V-4, therefore, describes the creeping motion of an infinite viscous liquid arising from the motion of an expanding and translating spherical boundary therein. In the subject analysis, the velocity of translation, V_y, the radial growth rate, dR/dt, and the spherical boundary radius, R, are functions of time as determined by a simultaneous solution of the conservation equations. (see Section 3.3.1) Consequently, equation V-4 represents the instantaneous stream

function in terms of the time dependent values of V_y, dR/dt, and R. The approximation of Ψ on the basis of instantaneous values of time varying parameters is of the same order as that initially neglecting the influence of the inertia terms.

Equation V-4 can be employed to evaluate the rate of work done by the spherical boundary against viscous forces by considering the tangential shear stress in the liquid at the spherical boundary, r=R. Since the velocity components are given by

$$V_r = \frac{1}{r^2 \sin\theta} \frac{\partial \Psi}{\partial \theta} \; ; \; V_\theta = - \frac{1}{r \sin\theta} \frac{\partial \Psi}{\partial r} \qquad \text{(V-5)}$$

and the tangential shear stress is given as

$$\tau_{r\theta} = \mu \left(\frac{1}{r} \frac{\partial V_r}{\partial \theta} + \frac{\partial V_\theta}{\partial r} \right) \qquad \text{(V-6)}$$

one can readily show, by means of equations V-4, V-5 and V-6, that

$$(\tau_{r\theta})_{r=R} = \frac{1}{2} \mu \frac{V_y}{R} \sin\theta \qquad \text{(V-7)}$$

The rate at which the entire spherical boundary does work against the viscous shear forces can be obtained from the following integral:

$$\left(\frac{\partial W}{dt}\right)_\mu = \int\int_{\substack{\text{spherical} \\ \text{boundary}}} (\tau_{r\theta})_{r=R} (V_\theta)_{r=R} \, d\, A \qquad \text{(V-8)}$$

Employing equations V-4, V-5, V-7, and V-8, the following expression for the viscous work rate is obtained.

$$\left(\frac{\partial W}{dt}\right)_\mu = \pi \mu V_y^2 R \left[2/3 - \cos\theta^* + \frac{1}{3} \cos^3 \theta^* \right] \qquad \text{(V-9)}$$

That expression is employed in Section 3.3.1 for evaluating the viscous work rate in the energy balance equation.

The expression for the stream function, equation V-4, can also be employed for determining the effect of the viscosity

of the liquid upon the pressure of the gas within the expanding and translating spherical boundary. The principal stress in the radial direction, for an incompressible liquid, is given by

$$\sigma_r = - p' + 2\mu \frac{\partial V_r}{\partial r} \qquad (V\text{-}10)$$

Where p' is the mean of the negative of the three principal stresses. Care should be taken not to identify the pressure of the gas within the spherical boundary with p', which exists in the liquid, but rather to identify it with the negative of the radial principal stress, $-\sigma_r$ (54).

From equations V-4, V-5, and V-10, one obtains, at r=R,

$$\sigma_r = - p' - \frac{4\mu}{R} \frac{dR}{dt} \qquad (V\text{-}11)$$

Therefore, identifying the pressure of the gas within the spherical boundary, p, with $-\sigma_r$, the increase in the pressure of the gas within the spherical boundary due to the viscosity of the liquid is, from equation V-11, given as

$$p - p' = \Delta p_\mu = 4 \frac{\mu}{R} \frac{dR}{dt} \qquad (V\text{-}12)$$

That expression is employed in Section 3.3.1 in the equation of motion for an approximate evaluation of the influence of the viscosity of the liquid upon the pressure of the gas within the expanding and translating spherical boundary.

APPENDIX VI

GEOMETRICAL RELATIONSHIPS

The instantaneous volume and surface area of the idealized bubble, as illustrated previously in Fig. 41, can be readily determined in terms of the instantaneous values for the bubble radius, R, and the limiting angle, θ^*.

The volume of the bubble, a portion of a sphere, is given by the integral

$$V = \int_{\theta=0}^{\theta^*} \int_{r=0}^{R} \int_{\varphi=0}^{2\pi} r^2 \sin\theta \, d\theta \, dr \, d\varphi + \int_{\theta=\theta^*}^{\pi} \int_{r=0}^{R\frac{\cos\theta^*}{\cos\theta}} \int_{\varphi=0}^{2\pi} r^2 \sin\theta \, d\theta \, dr \, d\varphi$$

which when evaluated gives

$$V = \frac{2\pi}{3} R^3 \left[1 - \cos\theta^* - \frac{1}{2}\cos\theta^* \sin^2\theta^*\right] \qquad \text{(VI-1)}$$

Similarily, the surface area of the bubble is given as

$$A = \int_{\theta=0}^{\theta^*} \int_{\varphi=0}^{2\pi} R^2 \sin\theta \, d\theta \, d\varphi$$

which when evaluated gives

$$A = 2\pi R^2 (1 - \cos\theta^*) \qquad \text{(VI-2)}$$

The expressions for V and A in terms of the dimensionless variable S introduced in Section 3.3.2 where

$$S = \frac{R}{R_o}$$

and therefore

$$\sin\theta^* = \frac{1}{S} \; ; \; \cos\theta^* = -\sqrt{1 - \frac{1}{S^2}} \; ; \; (\theta^* \geq \pi/2)$$

Equations VI-1 and VI-2 then become

$$V = \left(\frac{2\pi}{3} R_o^3\right) S^3 \left[1 + \frac{3}{2}\sqrt{1 - \frac{1}{S^2}} - \frac{1}{2}\left(1 - \frac{1}{S^2}\right)^{3/2}\right] \qquad \text{(VI-3)}$$

$$A = (2\pi R_o^2) S^2 \left[1 + \sqrt{1 - \frac{1}{S^2}}\right] \qquad \text{(VI-4)}$$

APPENDIX VII

LIMIT OF INDETERMINANT FORMS

In the evaluation of the derivatives $dU/d\tau$, $d\Theta/d\tau$, and $dP/d\tau$, at $\tau = 0$, by the substitution of the initial conditions, 3.28, into equations 3.24, 3.25, and 3.26, several terms involving the ratio $U/\sqrt{S^2-1}$ are indeterminant due to the initial conditions on S and U. The limit

$$\lim_{\tau \to 0} \frac{U}{\sqrt{S^2-1}} = Z \qquad \text{(VII-1)}$$

can be evaluated by a consideration of the continuity equation 3.13. At t=0,

$$\left(\frac{dm}{dt}\right)_{t=0} = \dot{W}_i - \frac{V_c}{\bar{R}\, T_c} \left(\frac{dp_c}{dt}\right)_{t=0} \qquad \text{(VII-2)}$$

The continuity equation can also be written in terms of the gas density and volumetric flow rate entering the bubble. Thus,

$$\left(\frac{dm}{dt}\right)_{t=0} = \left(\rho_g \frac{dV}{dt}\right)_{t=0} = \frac{p_o}{\bar{R}\, T_o} \left(\frac{dV}{dt}\right)_{t=0} \qquad \text{(VII-3)}$$

By differentiating with respect to time equation VI-3, Appendix VI, for the volume of the bubble, it can be easily shown that as $t \to 0$

$$\lim_{\substack{S\to 1 \\ U\to 0}} \left(\frac{dV}{dt}\right) = \frac{3}{2} \left(\frac{2\pi}{3} R_o^3\right) \frac{1}{R_o \sqrt{\rho/p_o}} \lim_{\substack{S\to 1 \\ U\to 0}} \frac{U}{\sqrt{S^2-1}} \qquad \text{(VII-4)}$$

Combining equations VII-2, VII-3, and VII-4, one obtains

$$\frac{\bar{R}\, T_o}{p_o} \left[\dot{W}_i - \frac{V_c}{\bar{R}\, T_c} \left(\frac{dp_c}{dt}\right)_{t=0}\right] = \frac{3}{2} \left(\frac{2\pi}{3} R_o^3\right) \frac{1}{R_o \sqrt{\rho/p_o}} \lim_{\substack{S\to 1 \\ U\to 0}} \frac{U}{\sqrt{S^2-1}}$$

which readily simplifies to the desired limit

$$\lim_{\substack{S\to 1\\ U\to 0}} \frac{U}{\sqrt{S^2-1}} = Z = \frac{2}{3} C \left[1 - \frac{V_c}{\overline{R}\, T_c} \frac{\left(\frac{dp_c}{dt}\right)_o}{\dot{W}_1} \right] \qquad \text{(VII-5)}$$

All terms of the form $U/\sqrt{S^2-1}$ were replaced by Z in the evaluation of the starting values of the derivatives (equations 3.24, 3.25, and 3.26) at $\tau = 0$.

In order to completely evaluate $dU/d\tau$, equation 3.24, at $\tau=0$, it was also necessary to consider separately the limit of the terms

$$\lim_{\tau\to 0} \left(Y_7 \frac{dU}{d\tau} - Y_{2o}\, U^2 \right) = Z_1 \qquad \text{(VII-6)}$$

The aforementioned terms resulted from the non-dimensionalization of the last term in equation 3.7. Thus, for the dimensional and non-dimensional forms of that term there is the identity

$$\lim_{\substack{t\to 0^+\\ r\to R_o}} \frac{1}{4} R \frac{\partial V_y}{\partial t} (1 + \cos\theta^*) = \lim_{\substack{\tau\to 0\\ S\to 1\\ U\to 0}} \frac{1}{4} \frac{p_o}{\rho} \left[Y_7 \frac{dU}{d\tau} - Y_{2o}\, U^2 \right] \qquad \text{(VII-7)}$$

The limit Z_1 can be evaluated by considering the continuity equation in the form

$$\left(\frac{dm}{dt}\right)_{t=0} = \left(\rho_g\, A_o\, V_o\right)_{t=0} \qquad \text{(VII-8)}$$

where

A_o = orifice cross-sectional area

V_o = mean velocity of the gas crossing the orifice plane

At t=0, the bubble is a hemisphere with its center, the origin of the coordinate system, in the orifice plane. If it is assumed that the density of the gas entering the bubble at t=0 is constant, then $(V_o)_{t=0}$ is equal to the velocity of translation at the start, $(V_y)_{t=0}$. Therefore, from equation VII-8

$$\left(\frac{\partial V_y}{\partial t}\right)_{t=0} = \left(\frac{\partial V_o}{\partial t}\right)_{t=0} = \frac{1}{\rho_o\, A_o} \left(\frac{d^2 m}{dt^2}\right)_{t=0} \qquad \text{(VII-9)}$$

Introducing equation 3.13 into equation VII-9, considering that $\dot{W}_1$ is constant, one obtains

$$\left(\frac{\partial V_Y}{\partial t}\right)_{t=0} = \frac{\bar{R}\, T_o}{p_o\, A_o}\left[\frac{V_c}{\bar{R}\, T_c}\left(\frac{d^2 p_c}{dt^2}\right)_{t=0}\right] \qquad \text{(VII-10)}$$

From equations VII-7 and VII-10, it follows that the limit Z_1 is given as

$$Z_1 = \lim_{\substack{S\to 1 \\ U\to 0}}\left[Y_7\,\frac{dU}{d\tau} - Y_{20}\,U^2\right] = \frac{2}{3}\,\frac{\left(R_o\sqrt{\rho/p_o}\right)^2}{p_o}\,G_1\left(\frac{d^2 p_c}{dt^2}\right)_{t=0} \qquad \text{(VII-11)}$$

Equation VII-11 was employed to complete the evaluation of $dU/d\tau$, equation 3.24, at $\tau=0$ in Section 3.3.3.